PYROLYSIS AND COMBUSTION CHARACTERIZATION OF PULVERIZED COALS FOR INDUSTRIAL APPLICATIONS

Nsakala ya Nsakala, Gary J. Goetz, Ramesh L. Patel and Tony C. Lao

Combustion Engineering, Inc., 1000 Prospect Hill Road, Windsor, CT 06095

James D. Hickerson and Harry J. Ritz

Department of Energy, Pittsburgh Energy Technology Center, Pittsburgh, PA 15236

ABSTRACT

This paper presents in-depth fundamental information obtained from a two-inch inner diameter laminar flow reactor referred to as the Drop Tube Furnace System (DTFS). This information consists of the following: (1) pyrolysis kinetic characteristics of four coals of various rank (Pennsylvania anthracite, Alabama high volatile bituminous coal, Montana subbituminous coal, and Texas lignite); and (2) combustion kinetic studies of chars produced from the foregoing parent coals. The combustion kinetic information obtained on the high volatile bituminous coal has been used in conjunction with Combustion Engineering's proprietary mathematical model to predict the combustion performance of the pilot scale (500,000 Btu/hr) Controlled Mixing History Furnace (CMHF). Comparison of the predicted data with the experimental results shows a virtually one-to-one scale-up from the DTFS to the CMHF.

INTRODUCTION

The Department of Energy's intent in sponsoring this and other related programs is to foster increased coal usage in the United States. To effectively use coal in existing and new applications requires a more definitive, quantitative understanding of coal properties vs. performance. The objective of this program is to develop the methodologies that most reliably characterize coals from a pyrolysis/combustion standpoint thereby permitting accurate performance predictions to be made. This will in turn allow intelligent use of our coal reserves for a multiplicity of industrial applications with the confidence levels required.

The quantitative fundamental data developed from this study indicate significant differences in coal/char chemical, physical, and reactivity characteristics, which should be useful to those interested in modeling coal combustion and pyrolysis processes. Coal selection is known to be one of the keys governing a successful coal conversion/utilization process. Practical applications of these data involve providing vital information to a designer in the area of carbon burnout and NO_X reduction for a large scale coal utilization scheme.

The primary research tools used in this program were CE's Drop Tube Furnace System (DTFS), a bench scale entrained laminar flow furnace and the Controlled Mixing History Furnace (CMHF), a pilot scale entrained plug flow furnace. Both the DTFS and CMHF by virtue of their ability to resolve combustion time into distance along their respective furnace lengths were used to examine carbon burnout phenomena. In addition, the CMHF by virtue of its staged-combustion capabilities was used to evaluate NO_X emissions and establish conditions conducive to low NO_X. The NO_X results obtained from this program will not be discussed in this paper. They will appear in the forthcoming final DOE report.

EXPERIMENTAL FACILITIES AND PROCEDURES

Drop Tube Furnace System (DTFS)

The DTFS (Figure 1) is comprised of a 1-inch inner diameter horizontal tube gas preheater and a 2-inch inner diameter vertical tube test furnace for providing controlled temperature conditions to study pyrolysis and/or combustion phenomena. This entrained flow reactor is capable of heating reactant gases and reacting particulates to temperatures up to 2650°F (1730°K) and obtaining particle residence times up to about one second to simulate the rapid heating suspension firing conditions encountered in pulverized coal fired boilers. The DTFS testing procedure entails the following: (1) feed the fuel at a precisely known rate through a water-cooled injector into the test furnace reaction zone; (2) allow the fuel and its carrier gas to rapidly mix with a preheated down-flowing secondary gas stream ; (3) allow combustion and/or pyrolysis to occur for a specific time (dictated by the transit distance); (4) quench the reactions by aspirating the products in a water-cooled sampling probe; (5) separate the solids from the gaseous products in a filter medium; and (6) determine on-line NO_x, O_2, CO_2, and CO concentrations in the effluent gas stream. An ash tracer technique (1, 2) is used in conjunction with the proximate analyses of a given feed sample and the chars subsequently obtained from the test furnace to calculate the pyrolysis weight losses and/or combustion efficiencies as a function of selected operational parameters (temperature, residence time, fuel type, etc.).

Controlled Mixing History Furnace (CMHF)

The pilot scale (500,000 Btu/hr) CMHF (Figure 1) is based on the principle of plug flow which resolves time into distance along the length of the furnace. It consists of a refractory-lined 1.5 foot inner diameter cylinder with an overall height of 22.6 ft. A mixture of pulverized fuel and primary air is fired downward into the furnace from a single burner centrally located at the top of the furnace. The furnace consists of four zones--preheat, combustion, water-cooled, and after-burner--proceeding downward from the fuel admission point. By sampling at different ports along the length of the furnace, it is possible to examine the carbon burnout and NO_x formation histories of a fuel. An ash tracer method is also used to determine the solids combustion efficiency as a function of operational parameters. Gaseous products aspirated in a sampling probe are analyzed on-line to determine NO_x, O_2, CO, and CO_2 concentrations.

RESULTS

Analysis of Coals

The coals selected for this study include a ligA from Wilcox seam in Texas, a subB coal from Rosebud seam in Montana, a hvAb coal from Black Creek seam in Alabama, and an anthracite from Buck Mountain seam in Pennsylvania. The proximate and ultimate analyses and higher heating values of these coals (Table 1) are consistent with their ASTM classifications.

Pyrolysis Characteristics of Coals

Size graded (200x400 mesh) coals were pyrolyzed in the DTFS in the presence of nitrogen atmosphere at five different temperatures (1450, 1600, 1900, 2400, and

TABLE 1

SELECTED ANALYSES OF COALS

ANALYSIS	TEXAS (WILCOX) ligA		MONTANA (ROSEBUD) subB		ALABAMA (BLACK CREEK) hvAb		PENN (BUCK MT.) an	
	As Rec'd	DAF	As Rec'd	DAF	As Rec'd	DAF	As Rec'd	DAF
Proximate, Wt. Percent								
Moisture (Total)	21.2	--	23.9	--	3.6	--	5.7	--
Volatile Matter	34.7	53.6	30.7	45.0	37.7	40.3	3.5	4.1
Fixed Carbon	30.0	46.4	37.6	55.0	55.8	59.7	83.3	95.9
Ash	14.1	--	7.8	--	2.9	--	7.5	--
Ultimate, Wt. Percent								
Hydrogen	3.5	5.5	3.6	5.3	4.9	5.3	1.7	1.9
Carbon	45.6	70.5	51.6	75.5	78.5	84.0	82.7	95.3
Sulfur	0.6	0.9	0.7	1.0	0.7	0.7	0.4	0.5
Nitrogen	0.8	1.3	0.9	1.3	1.6	1.7	0.7	0.8
Oxygen (Diff)	14.2	21.8	11.5	16.9	7.8	8.3	1.3	1.5
Ash	14.1	--	7.8	--	2.9	--	7.5	--
Higher Heating Value, Btu/lb	7845	12130	8800	12080	13935	14910	12740	14675

2650°F) and residence times ranging up to 0.9 sec. Results, Figure 2, show that: (1) pyrolysis weight loss depends significantly on temperature and time for each coal; (2) and pyrolysis is virtually complete within 0.2 sec. for the lignite, subbituminous, and high volatile bituminous coals. The lignite and subbituminous coal showed, respectively, 12% and 14% volatile matter enhancements over their proximate ASTM volatile matter yields; the high volatile bituminous coal and anthracite, on the other hand, showed no volatile matter enhancements over ASTM results.

Results in Figure 2 were used to derive the pyrolysis kinetic parameters for each coal. The derivation method used by Nsakala et al. (1), Scaroni et al. (3), and Walker et al. (4) was also used here. That is, briefly:

$$C = Co \exp(-kt) \qquad 1)$$

where Co is the maximum obtainable weight loss referred to as ΔW_∞, and C is the remaining pyrolyzable material weight at time t ($C = \Delta W_\infty - \Delta W$, where ΔW is the pyrolysis weight loss at time t), and k is a pyrolysis rate constant. Plugging these values into and manipulating Equation 1 yields

$$\ln (1 - \Delta W/\Delta W_\infty) = -kt \qquad 2)$$

Plotting the left hand side of Equation 2 vs. t yields straight lines (Figure 3) from which the k values can be obtained from the slopes of the least squares fits.

Now, the k values can be used in conjunction with a first order Arrhenius law to obtain

$$k = ko \exp(-E/RT) \qquad 3)$$

where ko, E, R, and T are, respectively, the pyrolysis frequency factor, the apparent activation energy, the universal gas constant, and the reaction temperature.

Plotting ln k vs. 1/T yields straight lines (Figure 4) from which the values of ko and E can be obtained from the intercepts and slopes of the least squares fits. Results from this study are given in Table 2.

TABLE 2

KINETIC DATA FOR PYROLYSIS OF 200X400 MESH COALS IN NITROGEN ATMOSPHERE AND 1450-2650°F(1060-1730°K) TEMPERATURE RANGE

FUEL TYPE	E(cal/mole)	ko(sec^{-1})	γ
Texas LigA	7980	50.8	-0.95
Montana subB	4740	13.5	-0.93
Alabama hvAb	7825	32.5	-0.98
Pennsylvania Anthracite	7755	38.7	-0.79

γ = Correlation Coefficient

The low activation energies (4.7-8.0 kcal/mole) encountered here seem to indicate that a physical, rather than a chemical, control mechanism does control the thermal decomposition process. Various investigators (2, 3, 4, 5) employing dilute-phase reactors similar to the present DTFS have also encountered relatively low activation energies (generally less than 20 kcal/mole) for thermal decomposition of coals of various rank.

Combustion Characteristics of Coal Chars

A commercial grind (~70%-200 mesh) of each coal was pyrolyzed in the DTFS in nitrogen atmosphere at 2650°F. The resultant char was subsequently size graded to obtain a 200x400 mesh size fraction. The proximate and pore structural analyses of each coal char is given in Table 3. It is noteworthy that: (1) all the chars are virtually volatile matter-free; and (2) while the BET surface areas follow the

TABLE 3

PROXIMATE AND PORE STRUCTURAL ANALYSES OF 200X400 MESH DTFS-GENERATED CHARS

QUANTITY	TEXAS ligA	MONTANA subB	ALABAMA hvAb	PENN. an.
Proximate, Wt.%.				
Volatile Matter	2.3(3.5)*	2.3(2.8)*	1.5(1.6)*	1.3(1.4)*
Fixed Carbon (Diff)	64.3	80.3	94.6	92.1
Ash	31.2	14.9	3.9	5.9
$S_{BET}, m^2/g, daf$	191.3	89.9	16.4	2.6
$S_{CO2}, m^2/g, daf$	210.9	162.9	16.3	1.6
$\rho_{Hg}, g/cm^3, daf$	0.79	0.69	0.86	1.62
$\rho_{He}, g/cm^3, daf$	1.71	2.01	1.75	1.86
$V_T, cm^3/g$	0.681	0.952	0.591	0.080
Porosity, %	53.8	65.7	50.9	12.9

*Dry-ash-free-basis

trend ligA > subB > hvAb > anthracite, the total open porosity trend is subB > ligA > hvAb > anthracite.

Each char was burned in the DTFS in 0.03 atm. O_2 (in nitrogen balance) at five temperatures (1600, 1900, 2150, 2400, and 2650°F) and residence times ranging up to 0.85 sec. Results show: (1) a strong temperature and time dependence of combustion efficiencies of the ligA, subB, and hvAb chars; and (2) a relatively weak temperature and time dependence of the anthracite char combustion efficiency.

Results in Figure 5 were used to determine for each char the overall rates of carbon removal per unit external surface area (K) assuming that the reaction proceeds by a shrinking core mechanism. The K values were then used in conjunction with classically calculated corresponding diffusional reaction rate coefficients (K_D) to derive the surface reaction rate coefficients (K_S) according to

$$1/K=1/K_D+1/K_S \qquad 4)$$

First order Arrhenius Equations is then applied to the data as follows

$$K_S=A \exp(-E/RT) \qquad 5)$$

where A, E, R, and T are, respectively, the frequency factor, apparent activation energy, gas constant, and reaction temperature.

Plotting ln K_S vs. 1/T yields straight lines (Figure 6) from which the values of A and E can be obtained from the intercepts and slopes of the least squares fits. This calculation procedure is given in detail by Field (6, 7) and Goetz et al. (8).

Two methods were used in this derivation. The first method used the bulk gas temperatures (T_g). The second method entailed calculating particle surface temperatures (T_s) by a heat balance method (7) as follows

$$H_g = H_c + H_r \qquad 6)$$

Where H_g, H_c, and H_r are, respectively, the rate of heat generation per unit area, the rate of heat loss by conduction, and the rate of heat loss by radiation. Differences between T_s and T_g ranged from 20 to 197°F. These differences are reflected in the reaction kinetic parameters given in Table 4. These results depict the importance of specifying the method used in deriving combustion kinetic parameters.

TABLE 4

SENSITIVITY OF COMBUSTION KINETIC PARAMETERS OF VARIOUS 200X400 MESH CHARS TO THE METHOD OF DERIVATION

	E(CAL/MOLE)		A($g/cm^2 sec. O_2 atm.$)	
FUEL TYPE	METHOD 1	METHOD 2	METHOD 1	METHOD 2
Texas Lignite	21050	20350	57	35.6
Montana subB	26730	25400	593	271
Alabama hvAb	23320	22550	80	50
Pennsylvania Anthracite	17900	17840	4.3	3.7

Method 1: Using measured gas temperature (T_g)
Method 2: Using calculated particle surface temperature (T_s)

DTFS to CMHF Scale Up Studies

The combustion and NO_x characteristics of the Alabama hvAb coal were also determined in the CMHF at 500,000 Btu/hr firing rate. The DTFS-derived kinetic parameters of this coal char were used in conjunction with other coal data and an in-house mathematical model to simulate the CMHF combustion processes under various conditions. This mathematical model is essentially based upon the formulation of Field and co-workers (9), whereby the following differential equation is solved

$$du_j/dt = -S_j q_j \qquad 7)$$

where u_j, S_j, and q_j are, respectively, the weight of a particular residual char fraction at time t per unit initial weight of char, the geometric surface area of each particular fraction per unit weight of char and the rate of carbon removal per unit geometric surface area. Equation 7 assumes that the volatile matter is instantaneously released and burned. As such, the pyrolysis process is not modeled. It is noteworthy that the pyrolysis information presented in this paper can be used in developing coal pyrolysis models for incorporation in overall combustion models.

Results obtained from the present simulation study will be explained in detail in the final DOE report. Figure 7 depicts two cases: (1) a base line (no air staging, 20% excess air, commercial fuel grind); and (2) an optimum NO_x reduction (50% primary stage stoichiometry, 20% excess air, fine grind). A very good agreement exists between theoretical and experimental results, indicating a virtually one-to-one DTFS-to-CMHF scale-up. CE is beginning to use this technique for predicting carbon heat losses in utility and industrial boilers. This technique is therefore of practical uses.

CONCLUSIONS

- The apparent activation energies for coal pyrolyses are so low (4.7-8.0 kcal/mole) that they seem to indicate a physical rather than a chemical control of the pyrolysis process.
- The apparent activation energies for coal char combustion are in the 17.9-26.7 kcal/mole range, indicating a very significant temperature dependence of coal char combustion.
- Pore structure plays an important role during char combustion. The higher the total open porosity, generally, the greater is the char reactivity.
- Combustion performance as predicted from DTFS kinetic data and use of a mathematical model agrees very well with combustion performance as directly measured on the CMHF using the same coal.
- The fundamental data presented here have significant practical value as inputs to computer models to predict carbon heat losses.

ACKNOWLEDGEMENTS

We appreciatively acknowledge the Department of Energy for the financial support of this program under Contract No. DE-AC22-81PC 40267.

REFERENCES

1. Nsakala, N., Essenhigh, R. H., and Walker, P. L., Jr., Combustion Science and Technology, 16, 153 (1977).
2. Badzioch, S., and Hawksley, P. G. W., In. Eng. Chem. Process Des. Develop., 9, 521 (1970).
3. Scaroni, A. W., Walker, P. L., Jr., and Essenhigh, R. H., Fuel, 60, 71 (1981).
4. Maloney, D. J., PhD Thesis, The Pennsylvania State University, University Park, PA, 1983.
5. Walker, P.L., Jr., Jenkins, R. G., Vastola, F. J., and Spackman, W.,DOE Final Technical Report DE-AC01-79ET14882, January 1983.
6. Field, M. A., Combustion and Flame, 13, 237 (1969).
7. Field, M. A., Combustion and Flame, 14, 237 (1970).
8. Goetz, G. J., Nsakala, N., Patel, R. L., and Lao, T. C., EPRI Final Report AP-2601, September 1982.
9. Field, M. A.,Gill, D. W., Morgan, B. B., and Hawksley, P. G. W., Combustion of Pulverized Coal, BCURA, Leatherhead, England, 1967, p. 211.

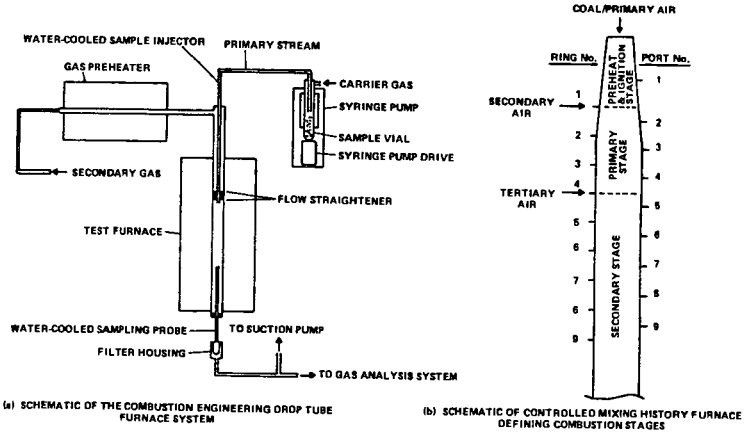

FIGURE 1 PRINCIPAL EXPERIMENTAL EQUIPMENT USED

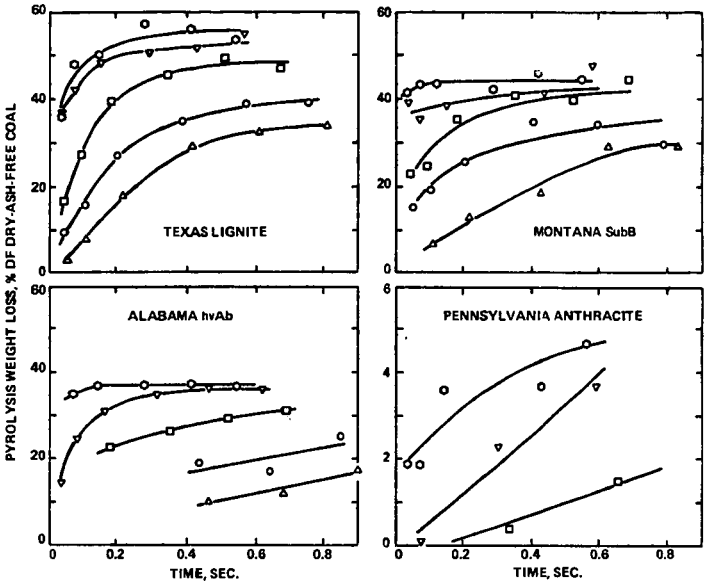

FIGURE 2 DTFS PYROLYSIS WEIGHT LOSSES OF 200 x 400 MESH COALS IN NITROGEN ATMOSPHERE AT VARIOUS TEMPERATURES (△ 1450°F, ○ 1600°F, □ 1900°F, ▽ 2400°F, ◇ 2650°F)

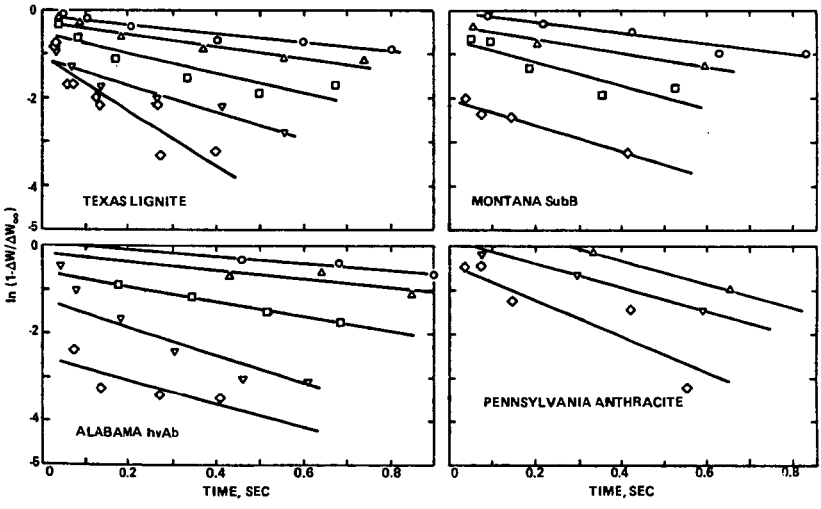

FIGURE 3 VARIATION OF ln (1-ΔW/ΔW$_\infty$) WITH DTFS RESIDENCE TIME FOR PYROLYSIS OF 200 x 400 MESH COALS IN INITROGEN ATMOSPHERE AT VARIOUS TEMPERATURES (○ 1450°F, △ 1600°F, □ 1900°F, ▽ 2000°F, ◇ 2650°F)

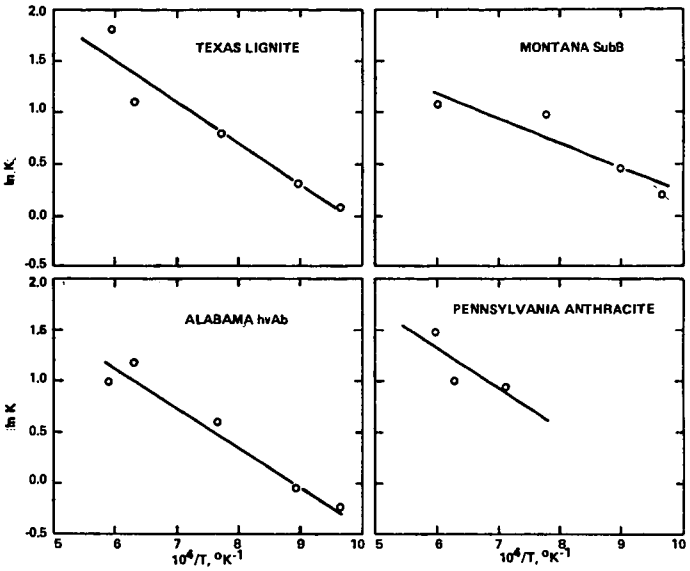

FIGURE 4 ARRHENIUS PLOTS FOR DTFS PYROLYSIS OF VARIOUS 200 x 400 MESH COALS

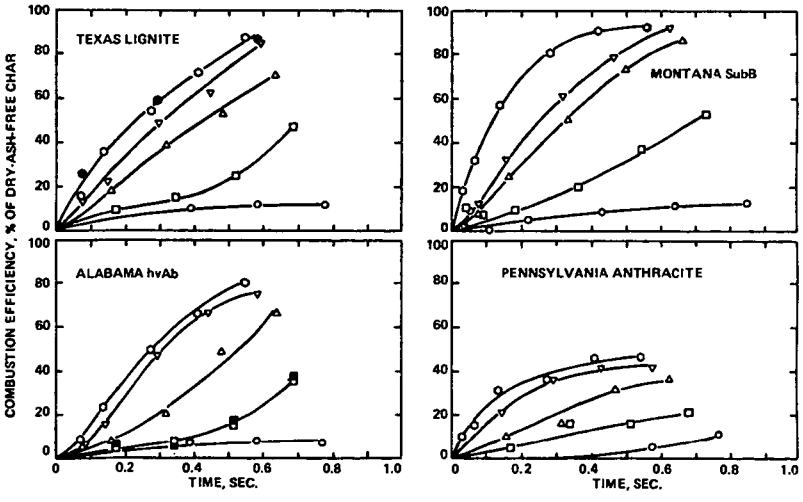

FIGURE 5 DTFS COMBUSTION EFFICIENCIES OF 200 x 400 MESH COAL CHARS IN 3% O_2 / 97% N_2 MEDIUM AT VARIOUS TEMPERATURES (○1600°F,□■1900°F, △ 2150°F, ▽ 2400°F,○●2650°F)

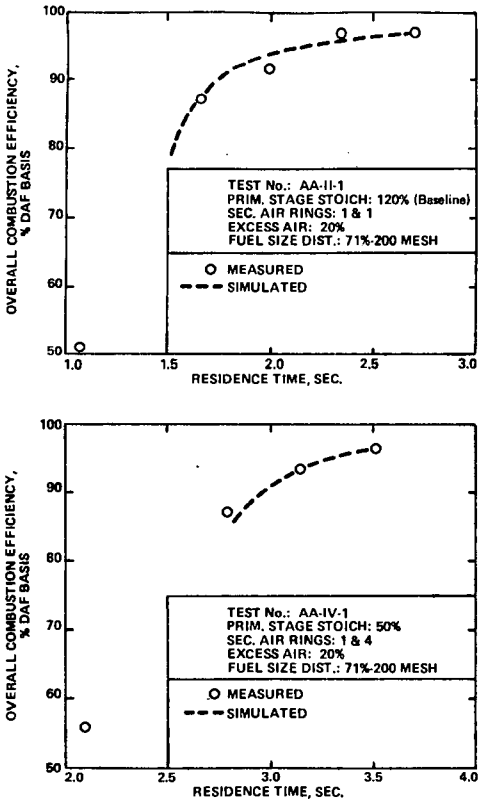

FIGURE 7 SIMULATED CMHF COMBUSTION PERFORMANCE FOR ALABAMA hvAb COAL USING DTFS KINETIC INFORMATION

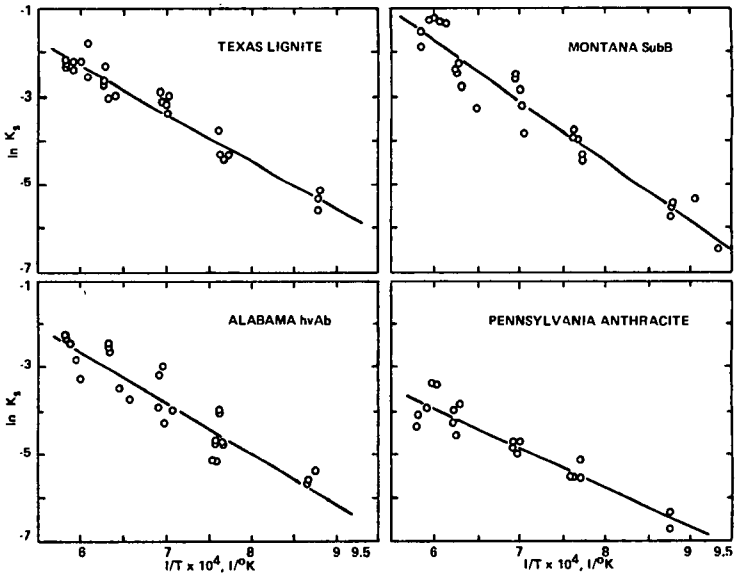

FIGURE 8 ARRHENIUS PLOTS FOR OTFS COMBUSTION OF VARIOUS 200 x 400 MESH COAL CHARS

FLASH PYROLYSIS OF COAL IN NONREACTIVE GASES

Muthu S. Sundaram*, Meyer Steinberg, and Peter T. Fallon
Process Science Division
Department of Applied Science
Brookhaven National Laboratory
Upton, N.Y. 11973

ABSTRACT

Coal pyrolysis experiments were carried out with a New Mexico subbituminous coal in the presence of nonreactive He, N_2, and Ar gases in an entrained downflow tubular reactor. The percent carbon conversions to CH_4, C_2H_4, BTX, CO and CO_2 were determined as a function of temperature and residence time at 50 psi. In helium atmosphere, the yields of methane and CO_x reached asymptotic values in about 1 sec and ethylene was produced thourghout the length of the BNL reactor corresponding to a coal particle residence time of 1.7 sec. The relative yields of individual products were influenced by the pyrolysis atmosphere but the total carbon conversion remained almost unaffected. A reduction in the cationic content of coal by acid treatment enhanced the production of CO and CO_2 but inhibited the formation of ethylene.

INTRODUCTION

Devolatilization plays an important role in the conversion of coal to gases and liquids. It is generally agreed that combustion and gasification of coal is preceded by the release of volatile matter from the coal particle. Under rapid heating conditions ($>10^4$ °K/sec), volatile yields in excess of those from proximate analysis ($<10^2$ °K/sec) have been obtained (Budzioch, 1970). Other reaction parameters which affect the volatile yields during pyrolysis of coal are: reaction temperature, particle residence time, and gas pressure. In addition, the pyrolysis product composition also depends on the nature of the entraining gas medium.

Previous research at Brookhaven mainly focused on the yields, distribution, and kinetics of formation of products in reactive hydrogen and methane atmospheres (Sundaram, 1982; Steinberg, 1982; Sundaram, 1984). An investigation was, therefore, inititated with special emphasis on determination of flash pyrolytic behavior of coal in nonreactive gases and their mixtures. This paper is specifically concerned with the effect of gaseous atmosphere on the pyrolysis product yields.

(FPC:1.3:1)

EXPERIMENTAL

Figure 1 presents the schematics of the entrained downflow isothermal tubular reactor. A detailed description of the design, construction, and operation of the reactor is available (Sundaram, 1982). The reactor is heated electrically by four clamshell-type heaters and designed for operation at temperatures up to 1050°C and pressures up to 4000 psig. Particle heatup rates in the range 10^4 to 10^5 °K/sec are attainable in this reactor. Other carbonaceous materials such as biomass and oil shale have also been successfully run in the unit.

Coal ($\leq$150 μm in diameter) is mixed with 10 to 30% by weight of Cab-O-Sil, an inert fumed silica powder, to prevent agglomeration, and is fed by gravity into the preheated gas stream at an average flow rate of about 400 to 600 g/hr. The preheated gas is injected at an average volumetric flow rate of about 40 to 45 l/min. At the beginning of the run, the coal and gas flow rates are so adjusted that a constant solid-to-gas feed ratio of 0.15 to 0.25 g coal/l gas is maintained in order to be able to continue a dilute phase operation. The residence time of the coal particles is determined from the free-fall velocity of the solid particles using Stoke's law and from the velocity of the entraining gas molecules.

The proximate and ultimate analyses of coal used in the study are shown in Table 1. The acid-washed New Mexico subbituminous coal was prepared by treating the original coal with large excess of 1 N HCl at room temperature followed by washing with deionized water until the filtrate was free of chloride ions. All coal samples were dried in a vacuum oven for at least 24 hours before feeding into the reactor. The gases used were of 99% or higher purity. The density, heat capacity, and thermal conductivity data for experimental gases are listed in Table 2. 50-50 gas mixtures of helium and argon were prepared from pure gases on a volume percent basis.

The principal pyrolysis products were methane, ethylene, BTX, CO, and CO_2. Product gas samples, corresponding to coal particle residence times variable up to 2 sec, are taken from any of the four sample taps located at 2-ft intervals throughout the length of the reactor and analyzed via on-line GC. Products heavier than BTX are formed only at low temperatures (<800°C) and collected in water-cooled condensers during isothermal runs and analyzed separately. Char containing coal ash, Cab-O-Sil, and unreacted carbonaceous material is collected in a char pot. The yields of individual carbon-containing products are reported as percent of carbon contained in the feed coal.

RESULTS AND DISCUSSION

The product distibutions from pyrolysis of coal in nonreactive gaseous atmospheres of helium, nitrogen, and argon were obtained as a function of temperature, residence time, and pressure (Steinberg, 1983). A specific purpose of this work was to find whether the heat transfer characteristics of these gases had any influence on the pyrolytic product distibution and if so, to what extent.

The yield versus coal particle residence time curves for various products obtained from the flash pyrolysis of New Mexico subbituminous coal in helium are shown in Figure 2 for different isothermal temperatures, from 700° to 1000°C. Although the total carbon conversion to hydrocarbon gases, BTX, and CO_x tends to increase with coal particle residence time, one may note that most of the conversion occurs within 1 sec, and further increase in residence time does not cause significant increase in total carbon conversion. For instance, at 800°C, a carbon conversion equivalent to 10% is achieved at 1 sec and increasing the residence time by 0.6 sec increases the total carbon conversion by only 1.6%.

This is expected because the hydrogen required for stabilization of free radicals generated from coal and from pyrolysis tar is "donated" by coal itself, and the amount of "donatable" hydrogen, present mostly in the hydroaromatic rings in coal, is a fixed quantity. The extent of cracking of hydroaromatic rings to release hydrogen is probably not influenced by coal particle residence time alone. The hydroaromatic rings are connected to other units and functional groups in coal by chemical bonds of different strengths. As the temperature is increased, bonds with higher dissociation energy are thermally broken and additional hydrogen can be released from the hydroaromatic portion of coal. Initial acceleration in the reaction rate, especially during the early stages of pyrolysis, has been attributed to the occurrence of simultaneous reactions and/or to the resistance of intraparticle mass transfer (Kobayashi, 1977).

The product curves show that ultimate asymptotic yields have been obtained for methane and CO_x within the residence time employed. The production characteristic of ethylene appears to be considerably different from that of methane and CO_x. Polymethylene moieties present in coal are considered to be main precursors for ethylene production (Calkins, 1983). At low temperatures, ethylene is produced only at long residence times. (Similar behavior is noticed in CO_x production.) At higher temperatures, ethylene is continously produced throughout the length of the reactor and no maximum in its yield is visible from the curves. Extrapolation of the 900°C curve indicates a maximum of about 5.8% at about 2-sec coal particle residence time. At temperatures above 900°C, ethylene undergoes decomposition as can be clearly seen in Figure 3 in which the product yields are plotted as a function of temperature for various residence times. Because of lack of hydrogen, only part of the decomposed ethylene results in the formation of methane. It is seen from this Figure that at 1.5 sec ethylene yield decreases from 4.9% at 900°C to 2.3% at 1000°C (a reduction of 2.6% in absolute yield), whereas methane yield increases from 3.4% at 900°C to 5.0% at 1000°C (1.6% increase in absolute yield). The increase in the BTX yield from 1.5% at 900°C to 2.2% at 1000°C (Table 3) might be attributed to the secondary reactions of ethylene unaccounted for as above.

It appears that cracking of polymethylene groups is catalyzed by in situ mineral matter in coal. When an acid-treated New Mexico subbituminous coal containing 6.2% ash was pyrolyzed, ethylene yields

were 25 to 30% lower than those from original coal containing 22.8% ash. An increase in the temperature from 900° to 1000°C decreased the ethylene yields by approximately 50% in both cases (Table 3). The presence of coal mineral matter, however, seems to favor the formation of methane and BTX at the expense of ethylene. For example, in the case of untreated coal, the combined yields of methane and BTX increase by 2.3% C against a 2.6%C decrease in the yield of ethylene. On the other hand, in the case of acid-treated coal, ethylene formed at low temperature seems to undergo secondary thermal cracking reactions at high temperature resulting in the formation of char.

As can be see in Table 3, reduction of cationic content of coal by acid treatment increased the yields of CO and CO_2 gases. The decrease in ethylene and BTX yields were more than compensated by increase in CO_x yield in that the overall carbon conversion to hydrocarbon gases plus BTX and CO_x actually increased. From studies based on model compounds (Cypres, 1975) and coal (Schafer, 1979), it is known that phenolic functional groups in coal are mainly responsible for the production of CO. On this basis, it is suggested that coal mineral matter might catalyze the polymerization reactions involving phenolic groups or their precursors during early stages of devolatilization, thereby inhibiting the evolution of CO. In situ mineral matter seems to catalyze the dimerization of solvent radicals under coal liquefaction conditions (Sundaram, 1983-1); caution should, however, be exercised in extending these results to coal pyrolysis because of drastic changes in reaction severity.

In addition, it is also possible that the acid treatment could have caused changes in pore structure and/or chemical structure of coal, which may have influenced the pyrolysis behavior. A more thorough and systematic study is required before an acceptable mechanism can be advanced.

In any case, the preliminary results from the present study are different from recent findings by Franklin of MIT (Franklin, 1981) who pyrolyzed coal via an extensively used captive sample technique with reported heating rates of about 1000°K/sec and holding times up to 5 sec. In the later study, an acid-demineralized Pittsburgh No. 8 coal was spiked with various inorganic additives such as calcite, quartz, kaolinite, montmorillinite, etc., and calcium minerals were found to be particularly effective in cracking oxygen functional groups to produce CO. It is not clear whether the differences between the two studies are due to their experimental techniques (BNL: entrained flow, short residence time, high heating rate; MIT: captive sample, long holding time, slow heating rate) or to coal rank (BNL: subbituminous coal; MIT: bituminous coal). We intend to pursue this subject matter in more detail in the future.

The results of pyrolysis experiments in other nonreactive gases are shown in Figure 4. The total conversion includes the yields of methane, ethylene, BTX, and CO_x. Because of analytical limitations in measuring CO in the presence of nitrogen or argon, CO yield data from helium pyrolysis experiments were used to determine total conversion under nitrogen and argon atmospheres. Examination of Figure 4 with

this assumption suggests that the total carbon conversion is almost unaffected by pyrolysis atmosphere under the conditions reported. An increase in total conversion in the order of He>N_2>Ar was reported earlier (Sundaram, 1983-2). In that study, coal was pyrolyzed at a higher pressure (200 psi) and the results obtained from experiments employing somewhat nonuniform residence time conditions (3.5 to 4.7 sec) were compared, whereas in this paper results from more uniform, narrow range residence time (1.5 to 1.7 sec) experiments are compared. Pyrolysis experiments under other conditions are in progress, and the results will be published in a future report.

Even though the total carbon conversion remained almost unaffected by pyrolysis atmosphere, the relative yields of pyrolysis products seem to be altered by different nonreactive gases. A clear-cut trend in product yields, however, is not revealed in Figure 4. Nevertheless, some generalizations on product yields could be made. Conversion to methane followed the increasing order of He>50%He/50%Ar>N_2>Ar. The yield of ethylene was lower in helium atmosphere than in N_2 or Ar and the ethylene yield maximized at 900°C in all gaseous atmospheres. A slightly larger amount of BTX was produced in Ar and He/Ar than in He or N_2 up to 900°C; at 1000°C, the BTX yield is almost the same in all gaseous atmospheres.

The gas-film heat transfer coefficient and hence the heat-up rate of the coal particles were found to follow the order He>N_2>Ar. It appears that the magnitude of difference in the particle heat-up rate is not large enough to significantly affect the total volatiles yield under the conditions reported herein. The effect of nonreactive gases on the physical and chemical characteristics of the resulting char is not known at present. In one investigation, the surface area of pyrolysis char was found to be affected by the pyrolysis atmosphere and it was reported to follow the order, He>Ar>N_2 though for unexplained reasons (Thakur, 1982).

CONCLUSIONS

When a New Mexico subbituminous coal was pyrolyzed in different nonreactive gases, the relative yields of volatile products were altered but the total carbon conversion remained almost unaffected. Acid treatment of the coal enhanced the production of CO_x gases but inhibited the formation of ethylene. This suggests that the in situ mineral matter might catalyze polymerization reactions involving oxygen functionalities in coal.

ACKNOWLEDGMENT

This research was supported by the U.S. Department of Energy under Contract No. AC02-76CH00016.

REFERENCES

Budzioch, S., and Hawksley, P.G.W., Ind. Eng. Cham. Proc. Deg. Dev., 9, 521 (1970).

Calkins, W.H., ACS Fuel Div. Prepr., 28, 85 (1983).

Cypres, R., and Bettens, P., Tetrahedron, 31, 359 (1975).

Franklin, H.D., Peters, W.A., and Howard, J.B., ACS Fuel Div. Prepr., 26 (37, 35, (1981).

Kobayashi, H., Howard, J.B., and Sarofim, A.F., Proc. 16th Intnl. Symp. on Comb., 411 (1977).

Schafer, H.N.S., Fuel, 59, 302 (1980).

Steinberg, M., and Fallon, P.T., Hydrocarb. Proc., 61, 92 (1982).

Steinberg, M., Fallon, P.T., and Sundaram, M.S., "Flash Pyrolysis of Coal with Reactive and Non-Reactive Gases", Ann. Tech. Rep. to U.S. DOE, Rep. No. DOE/CH/00016-1402 (DE83011264), 1983.

Sundaram, M.S., Steinberg, M., and Fallon, P.T., "Flash Hydropyrolysis of Coal for Conversion to Liquid and Gaseous Fuels: Summary Rport", DOE/METC/82-48 (1982).

Sundaram, M.S., and Given, P.H., ACS Fuel Div. Prepr., 28(5), 26 (1983-1).

Sundaram, M.S., Steinberg, M., and Fallon, P.T., ACS Fuel Div. Prepr., 28, 106 (1983-2).

Sundaram, M.S., Steinberg, M., and Fallon, P.T., ACS Fuel Div. Prepr., 29(2), 129 (1984).

Thakur, S., and Brown, L.E., Carbon, 20, 17 (1982).

TABLE 1. ANALYTICAL DATA FOR NEW MEXICO SUB-BITUMINOUS COAL

Ultimate Analysis	(wt % dry)	Ultimate Analysis	(dry)
Carbon	55.9	Volatile Matter	34.9
Hydrogen	4.3	Fixed Carbon	42.4
Nitrogen	1.1	Ash	22.8
Sulfur	1.0		
Oxygen (by diff.)	14.9		

TABLE 2. PHYSICAL PROPERTIES OF GASES AT 900°C AND ATM. PRESSURE

	Helium	Nitrogen	Argon
ρg (gm/cc)	2.80×10^{-3}	1.96×10^{-2}	2.81×10^{-2}
μg (CPS)	5.78×10^{-2}	5.56×10^{-2}	7.29×10^{-2}
Kg (Cal/cm^2°K sec)	9.78×10^{-4}	1.68×10^{-4}	1.13×10^{-4}
C_p (Cal/Mole °K)	7.57	4.97	4.97

TABLE 3. FLASH PYROLYSIS OF NEW MEXICO SUB-BITUMINOUS COAL IN HELIUM ATMOSPHERE AT 50 PSI TOTAL PRESSURE

Particle Residence Time : 1.3 - 1.5 sec.

Percent Carbon Conversion to Designated Products

	Untreated Coal*		Acid-Washed Coal**	
Run No.	756	754	770	770
Temperature, °C	900	1000	900	1000
Product Yields:				
CH_4	3.4	5.0	3.7	3.8
C_2H_4	4.9	2.3	3.4	1.7
BTX	1.5	2.2	2.4	1.9
CO	2.7	5.6	5.8	8.1
CO_2	1.1	1.8	2.0	2.5
Total	13.6	16.9	17.3	18.0

* Ash Content: 22.8%
** Ash Content: 6.2%

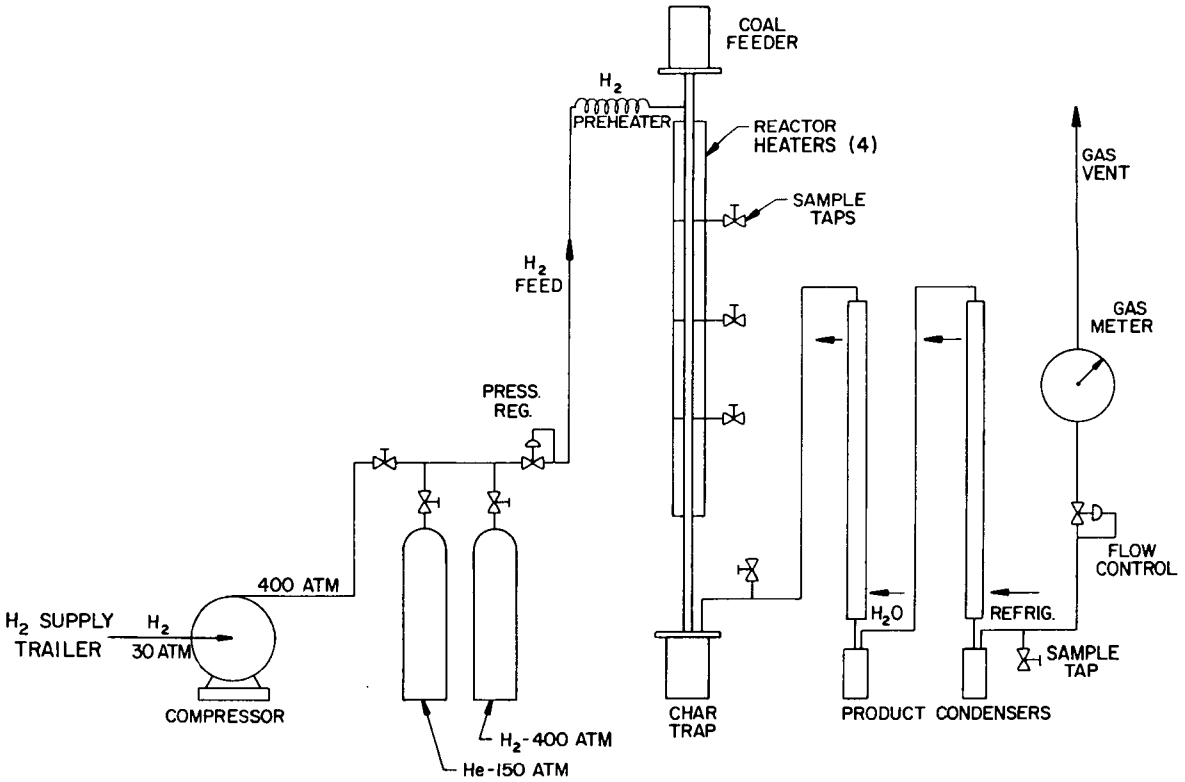

Figure 1. Schematic Representation of Pyrolysis Reactor.

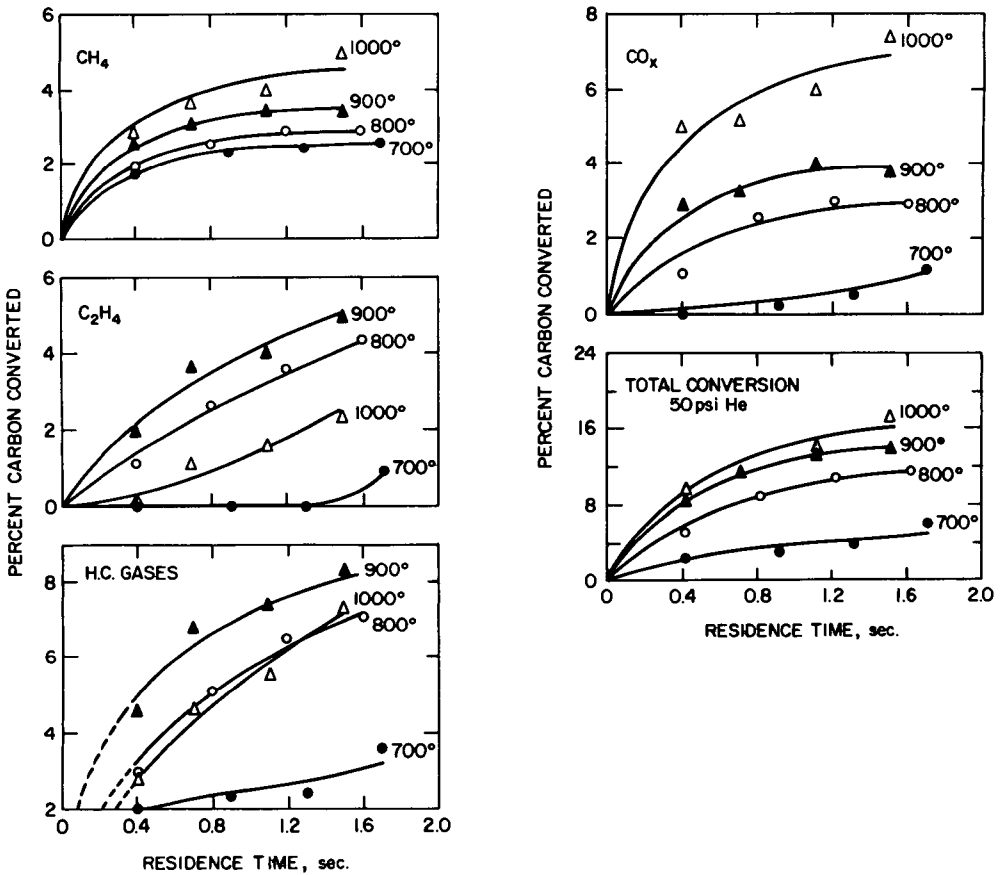

Figure 2. Flash Pyrolysis of New Mexico Sub-Bituminous Coal in Helium. Effect of Coal Particle Residence Time on Product Yields.

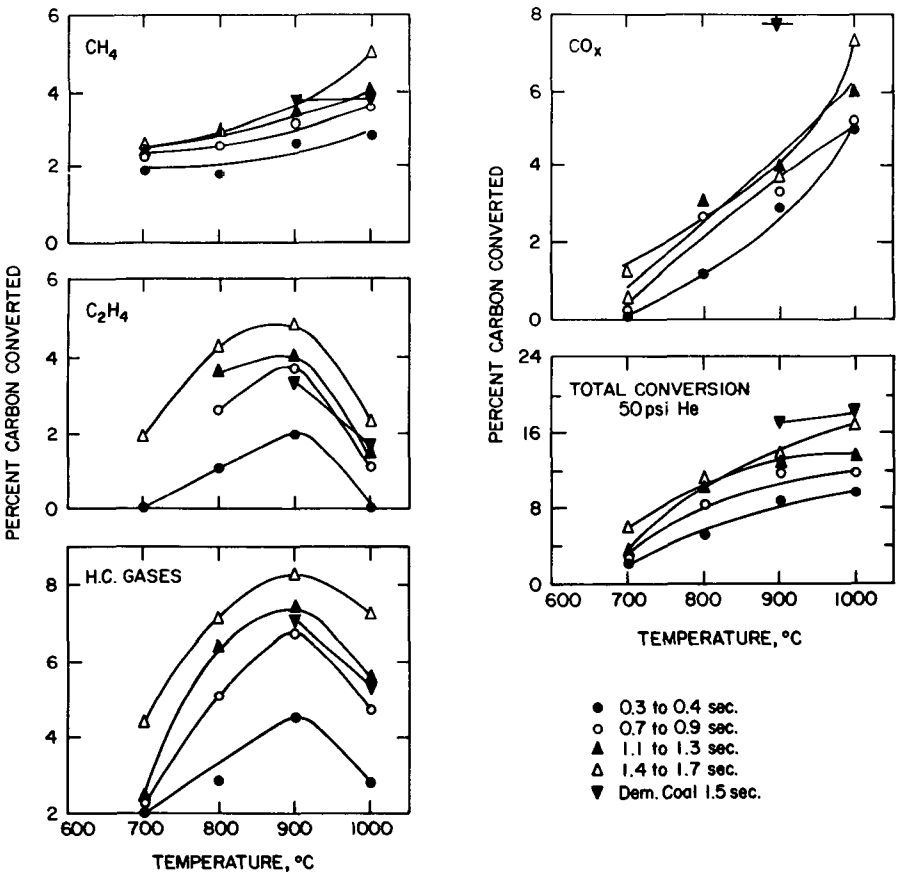

Figure 3. Flash Pyrolysis of New Mexico Sub-Bituminous Coal in Helium. Effect of Coal Temperature on Product Yields.

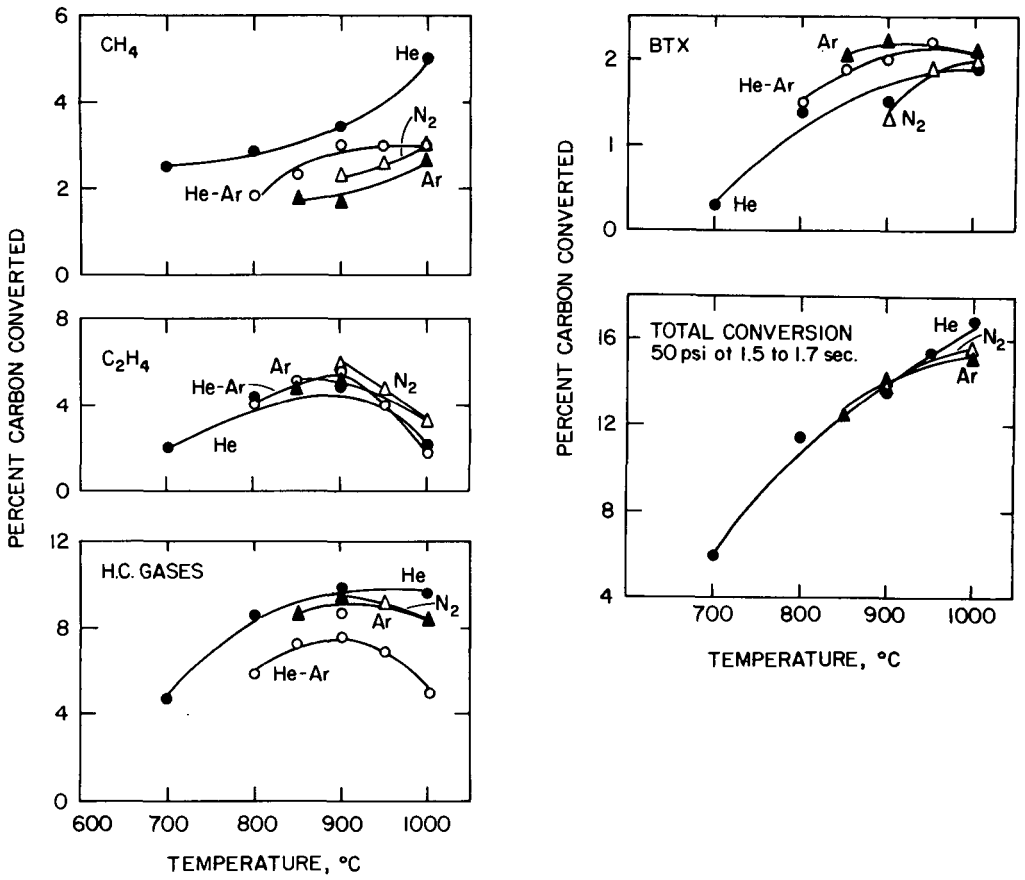

Figure 4. Flash Pyrolysis of New Mexico Sub-Bituminous Coal in He, N_2, and Ar. Effect of Temperature on Product Yields.

EVOLUTION OF TARS AND GASES DURING DEVOLATILIZATION OF COAL IN A FIXED BED REACTOR

Gokhale, A.J., Vasudevan, T.V., and Mahalingam, R.
Department of Chemical Engineering
Washington State University
Pullman WA 99164-2710

ABSTRACT

Devolatilization of a subbituminous coal has been investigated in a laboratory fixed bed gasifier, by contacting the coal with a reactive gas mixture similar to that entering the devolatilization zone of a commercial gasifier. Two particle sizes of feed coal PSOC-241 (-2,+1 and -4,+3 mm) at a single reactor pressure (30 psig) were evaluated, in the temperature range 350 to 550 C. The tars evolved were characterized by capillary gas chromatography and gel permeation chromatography. The tar and gas evolutions are described in terms of concentration and pressure profiles, through considerations involving diffusion and pore structure. The overall devolatilization rates are evaluated through the unreacted shrinking core model.

INTRODUCTION

In coal gasification, the objective is to increase the calorific value of the original raw fuel by removing the unwanted constituent, viz., ash, and also to produce a fuel which is cheaper to transport, handle and utilize. The present discussion will be limited to a Lurgi type fixed bed coal gasifier. Figure 1 [1] shows a schematic diagram of a Lurgi fixed bed gasifier. At the present state of technology, reliable engineering data are available on the gasification and combustion zones and can be readily applied to the design of a fixed bed gasifier. This is not the case with the devolatilization zone and no systematic study of the devolatilization phenomenon in the range of operating parameters for a fixed bed gasifier, has been reported in literature. Thus, it becomes necessary to conduct experimental and modelling work on the devolatilization behavior of coals, as influenced by particle size, pressure, temperature and a reactive gas environment [2]. Such devolatilization studies on a laboratory scale fixed bed gasifier form the main objective of the work described here [3]. The operating conditions for these studies are selected based on whatever data are available in the literature on fixed bed gasifiers, the approach being to simulate the conditions existing in the devolatilization zone of a fixed bed gasifier. The composition of the reactive gases entering the reactor is approximated to that entering the devolatilization zone of a fixed bed gasifier in practice. The residence time for the flow of reactive gases through the coal bed is

selected to be maintained at 5 seconds for all the runs. The results obtained from the devolatilization of a subbituminous coal, PSOC-241, at 30 psig (0.308 MPa) reactor pressure are presented here. Two particle sizes of feed coal were evaluated: (-2,+1) mm and (-4,+3) mm. Reaction temperatures used were 350, 450 and 550 C. The H2/CO mole ratio in the feed gas was maintained at 2.5. The duration of a devolatilization run was 5, 10, 20 or 30 minutes.

EXPERIMENTAL

A schematic representation of the experimental set-up is shown in Figure 2. The fixed bed reactor used for conducting the devolatilization studies was a 4.1 cm i.d. x 72 cm long 316 stainless steel tube provided with a wire mesh grid(0.25 mm opening), located 4 cm from the bottom, to hold the coal and char in the reactor. The reactor was placed vertically inside a furnace body. The graded coal sample was introduced into the reactor from the top under gravity by means of a Swagelok-type nut and feed pipe arrangement. Based on the reported gasification rates in a Lurgi type air blown gasifier [1,4] it was calculated that the entering gas environment in the devolatilization reactor should approximately have the following composition by volume:

Gas	H2	CO	CO2	CH4	N2	O2	Steam	Total
Volume%	18	7	14	4	25	2	30	100

Individual gases were drawn from compressed gas cylinders and mixed together with steam in a steam tube. The role of the steam tube was to convert feed water into steam, mix and preheat the steam-gas mixture to the desired devolatilization temperature. The steam tube was a 316 stainless steel tube(1.5 cm i.d. X 30 cm long), filled with inert catalyst support beads (3 mm diameter, alumina content=99% by wt. min; silica content =0.2% by wt. max; surface area=0.3 sq.m/gm; Norton Chemical Company) and was placed inside a small electric furnace. The feed gas stream entered the coal bed through a gas distributor located at the bottom of the reactor. A high pressure back pressure regulator after the condensers was used to maintain the desired pressure in the reactor system. The hot gases leaving the reactor from the top were laden with the tar generated inside the reactor; in order to quantitatively collect the tar and steam condensate, a double pipe heat exchanger was used as a condenser. Cooling water was circulated through the outer annulus and the tar laden gases were passed through the inner tube. Three such condensers (6mm i.d. X 40 cm long) were used in series to condense most of the tars. A high pressure glass fiber filter was used after the condensers as a final trap for the tar particles. After the completion of a run, methylene chloride was used as a solvent to wash down the condensers and the lines; dissolved tars and water phase were then collected from the bottom of the condensers. The yield of tar was measured in gm of tar per 100 gm of coal fed to the reactor. A Hewlett Packard 5840A gas chromatograph (with a 30 m long SE type 30 glass capillary column and a flame ionization detector (FID)) was used to quantitatively determine the species present in the tar samples. Area vs concentration curves for 30 standard species in methylene chloride were prepared. The species for standardization were selected

based on the published literature [5]. The molecular weights of tar samples were determined with a Waters Associates HPLC system. The columns used were 100 A and 500 A Ultrastyragel, made by Waters (columns: 7.8 mm i.d. X 30 cm long). The carrier solvent was tetrahydrofuran (THF) and a UV detector was used for absorption measurements. Polystyrene standards of known molecular weights were used to prepare a molecular weight vs elution volume curve.

The gas samples collected at 5, 10, 20 and 30 minutes from the sampling cylinders during the devolatilization run were analyzed for individual components. The permanent gases - CO2, CO, and O2 - were analyzed on a CARBOSIEVE S3 column and the hydrocarbon gases were analyzed on a PORAPAK R column. Both the columns were fitted on to a Hewlett Packard gas chromatograph 5840A equipped with an ECD detector. A MOLECULAR SIEVE 5A column was used on a Carle gas chromatogarph 111H, equipped with a TCD detector to analyse the H2 in the gas samples. N2 was obtained by difference. At the end of a 5, 10, 20 and 30 minute run, the reactor was quenched in water and the char was removed and weighed.

RESULTS AND DISCUSSION

Chemical Analyses of Coal Sample

Table 1 gives the proximate and ultimate analyses of the subbituminous coal, PSOC-241. The coal sample was ground to minus 200 mesh U.S. sieve size and equilibrated to room conditions. The analyses were performed by the Continental Testing and Engineering Company, Vancouver, B.C., Canada. From these analyses, the value for the ultimate yield of volatiles was obtained as 50.07% of coal, to be used later in the kinetic models. In order to determine the effect of the duration of the devolatilization run on the total weight loss, some selected devolatilization runs were conducted for durations of 60 minutes and it was observed that there was no additional weight loss after 30 minutes from the start of the run. At 550 C, the maximum weight loss occured equal to 49% of feed coal sample weighing 100 gm.

A. Devolatilization

Effect of Temperature

The principal effect of temperature on the devolatilization phenomenon is the decomposition of the organic structure of coal to yield water, hydrogen, methane, oxides of carbon and hydrocarbons. Consider the data on weight loss and tar/gas yields for the (-2,+1) mm and (-4,+3) mm size coal as shown in Tables 2 and 3. The weight loss is maximum at 550 C and is the least at 350 C. This confirms the earlier observation reported in literature about the nature of pyrolysis of

coal. At 350 C, the free moisture in the coal is removed and a small amount of tar is produced, which indicates that at this temperature, the majority of the coal chemical structure is still intact. At 550 C, most of the devolatilization is completed around 30 minutes as indicated by no additional weight loss during some runs conducted upto 60 minutes duration.

A plot of the distribution of molecular weights of tar samples is shown in Figure 3. From this it is clear that the fraction of evolving tar having molecular weight of about 300 units decreases as the run is continued. This can be attributed to the physical depolymerization of similar structures or the chemical cracking of a species to lower molecular weight as it is exposed to temperature for longer times.

The volumetric rate of evolution for all gases (Figures 4 and 5) shows a peak around 5 minutes from the start of a run and the rate then tapers off to zero around 30 minutes. In general, the rate of evolution for all gases is higher at higher temperature of reaction, i.e. 550 > 450 > 350 C, for all particle sizes.

Effect of Particle Size

The runs at 30 psig reactor pressure in the reactive gas atmosphere did not exhibit any difference in the total weight loss for the two particle sizes of coal studied, at 550 C. For the (-2,+1) mm coal, the yield of tar at 30 minutes increased with temperature as shown in Table 3; whereas for the (-4,+3) mm coal, the yield of tar showed a maximum at 450 C, as shown in Table 2. This can be attributed to the cracking of tar at 550 C, resulting in reduced yield of tar at 550 C as compared to that at 450 C. Figure 6 shows the total weight loss and tar yield data for the two particle sizes. The tar molecules have longer residence time within the larger coal particles and hence the former are amenable to dissociation by cracking. The next section shows how the internal pressure build-up and tar concentration within the coal particle also increase with the particle size.

B. Mathematical Models for Devolatilization

Single First Order Reaction Model

The earliest approach to the mathematical description of the devolatilization phenomenon was that of Pitt (1962) [6] who proposed a simple first order rate expression for the overall rate of evolution of volatiles:

$$\frac{dV}{dt} = -kV \qquad (1)$$

Anthony and Howard (1976) [7] have pointed out that this is an over simplified description and the literature values for the activation

energy vary from as low as 4 kcal/mol to as high as 55 kcal/mol. This observation can be explained partly as being dependent on the type of the experimental set-up and operating variables, but mainly stems from the fact that when a series of parallel first order reactions are forced to be represented by a single reaction, very low values for the activation energy are bound to be obtained. In that respect, this representation is purely arbitrary but sometimes it has the ability of describing the observed rate process. Also, since there is often a limitation on analyzing the different chemical species quantitatively, such a simplified approach does have some merit. The values of activation energy and frequency factor for the subbituminous coal studied were: 11.4 kcal/mol and 0.554 1/sec for the (-2,+1) mm size coal; and 3.9 kcal/mol and 0.005 1/sec for the (-4,+3) mm size coal respectively. These indicate that although primary devolatilization involves organic reactions which have activation energy of the order of 50 kcal/mol, the first order approximation yields a very low overall value. Thus, it will be inappropriate to conclude from these low values that the devolatilization phenomenon is purely diffusion controlled. Of course there is a significant resistance to diffusion of volatiles through the ash layer, which will be evaluated later. A cross reference to the literature indicates that Shapatina et al., (1960) [8] have reported very low values for activation energy, viz., between 1 and 4 kcal/mol.

Unreacted Shrinking Core Model

This model was tested with the experimental data from the PSOC-241 subbituminous coal. The runs were conducted at 30 psig reactor pressure and in a reactive gas atmosphere. Two particle sizes of coal were used: (-4,+3) and (-2,+1) mm. The governing equation for this model is:

$$\alpha C_A'(\text{gas}) + S(\text{solid}) \longrightarrow \text{gas} + \text{solid} \qquad (2)$$

Fluid film resistance control

Equation (3) gives the necessary relation for fractional conversion of coal, for this case:

$$t/t^* = X, \qquad t^* = R_p C_{SO}/3k_{mA'CA'0}, \quad X = 1 - r_c^3/R_p^3 \qquad (3)$$

Based on equation (3), X, the fractional conversion of coal to volatiles was plotted against the reaction time. Figure 7 shows the data for (-2,+1) mm particle size, at 30 psig and reaction temperatures of 350, 450 and 550 C. The data points fall on straight lines, but since these lines do not pass through the origin, it is logical to assume that there is not significant resistance to diffusion in the gas film around the particles. Similar conclusions are arrived at for (-4,+3) mm size coal, as shown in Figure 8.

Ash layer diffusion control

Equation (4) gives the necessary relation in this case:

$$t/t^* = [1-3(1-X)^{2/3} + 2(1-X)], \quad t^* = \alpha R_p^2 C_{so}/6 D_{eA'} C_{A'0} \quad (4)$$

Based on equation (4), [1-3(1-X) + 2(1-X)] was plotted against time, as shown in Figures 9 and 10. It appears that there is some resistance to diffusion within the ash layer and this will be examined further through equation (6).

Chemical reaction control

Equation (5) gives the necessary relation in this case:

$$t/t^* = [1-(1-X)^{1/3}], \quad t^* = R_p/k_s C_{A'0} \quad (5)$$

Based on equation (5), [1-(1-X)] was plotted against time, as shown in Figures 11 and 12. These curves also indicate that there could be some reaction control on the progress of the coal devolatilization. This will also be further examined through equation (6).

Ash layer diffusion versus chemical reaction control

Equation (6) gives the modified version of equation (4) as:

$$t/t^* = [1-(1-X)^{1/3}]^2, \quad t^* = \alpha C_{so} R_p^2/2 C_{A'0} D_{eA'} \quad (6)$$

ln[1-(1-X)] was plotted against ln[t] as shown in Figures 13 and 14. Since the slopes of these lines are greater than two, it can be concluded that the ash layer offers the most of the resistance to the progress of coal devolatilization. This is further confirmed from Figure 15, where r_c/R_p is plotted against t/t* as suggested by Levenspiel (1972) [10]. From this figure it is seen that the curve shows a point of inflection on the 135 degree dotted line (joining the points (0,1) and (1,0)), indicating that ash layer controls the progress of the reaction.

It must be pointed out at this stage that the above model is only 'phenomenological' and does not take into account the actual intrinsic chemical reactions. The numerous chemical species involved in devolatilization have been lumped into one hypothetical specie for the sake of mathematical simplicity and due to lack of detailed information on chemical structure. Thus this model is more qualitative in nature for this type of gas-solid system; it, however is quite informative.

Intraparticle Diffusion Model for Subbituminous Coal [11]

This model has been described by Gavalas (1982) [11]. It describes the concentrations of tar and gas inside the coal particle as a function of radial position, temperature, pressure and experimental

yields of tar and gas. The principal equations describing this model are:

$$\frac{dC_G}{dr} = -\frac{\beta}{\mu}\frac{C_G}{D_{GK}}\frac{dp}{dr} - \frac{r}{3}\left[\gamma_G\left(\frac{x_T}{D_{GT}} + \frac{1}{D_{GK}}\right) - \gamma_T\frac{x_G}{D_{GT}}\right] \quad (7)$$

$$\frac{dC_T}{dr} = -\frac{\beta}{\mu}\frac{C_T}{D_{TK}}\frac{dp}{dr} - \frac{r}{3}\left[\gamma_T\left(\frac{x_G}{D_{GT}} + \frac{1}{D_{TK}}\right) - \gamma_G\frac{x_T}{D_{GT}}\right] \quad (8)$$

The analytical solution of these equations gives the dimensionless pressure build-up as:

$$W(0) - 1 = \frac{(-1 + A)}{A}\left\{\left[1 + \frac{A_{at}(1 + \delta\varsigma_T)\,B}{(1 + A)^2}\right]^{1/2} - 1\right\} \quad (9)$$

where

$$\xi = r/a,\ V_i = C_i/(p_0/RT),\quad (i = G, T),\ W = p/p_0$$

$$\delta = \gamma_T/\gamma_G,\ \varsigma_T = D^*_{GK}/D^*_{TK},\ A = 3\beta p_0/\varepsilon\mu D^*_{GK}$$

$$B = RTa^2\gamma_G/\varepsilon p_{at} D^*_{GK}$$

The parameter 'A' in this model depends on bulk pressure outside the particles and on the temperature of the reaction. The parameter 'B' depends on the square of the particle radius. The differential equations describing the variation of tar and gas concentrations within the coal particle were solved on ACSL (Advanced Computer Simulation Language) and the following plots were made: The dimensionless pressure build-up, within the coal particle is plotted against the parameter A in Figure 16. This plot indicates that the pressure build-up is higher for larger particles. A plot of tar mole fraction within the particle against the radial position is shown in Figure 17. A plot for the tar concentration at the center of the coal particle with respect to parameter A (which is a measure of the total pressure on the system), is shown in Figure 18. This figure shows that for the pressure range investigated in the runs (30 - 375 psig) [3], the tar concentration is less sensitive to pressures upto 300 psig. Also, from these plots it can be seen that at a given pressure, the tar concentration increases with particle size.

CONCLUSIONS

The coal devolatilization experimentation reported herein involves realistic sizes of coal, and a reactive gas environment, as postulated to be present in the devolatilization zone of a Lurgi fixed bed gasifier, operating at a given pressure and temperature. No such work has been reported on a macrosample of coal and hence the results from the present work should be more meaningful. The conclusions to be drawn from the results presented are:

1. Devolatilization of coal is influenced by the operating variables.
2. The peak in molecular weight for the tar generated is around 300.
3. A first order approximation of the overall rate of devolatilization does not adequately describe the phenomenon.
4. The resistance to diffusion of tar out of the coal particle in the ash layer constitutes a major controlling mechanism in coal devolatilization.
5. Pressure build-up and tar concentration inside the coal particle both increase with particle size.

ACKNOWLEDGEMENT

This work has been carried out as part of a United States Department of Energy contract # DE-AC21-82MC 19208.

NOTATION

a	radius of coal particle, cm
A	dimensionless parameter
A'	component in the gas phase
B	dimensionless parameter
$C_{A'0}$	bulk concentration of A', gmol/cm^3
C_G	concentration of gas evolved, gmol/cm^3
C_{S0}	initial concentration of S, gmol/cm^3
C_T	concentration of tar evolved, gmol/cm^3
$D_{eA'}$	effective diffusivity of A', cm^2/sec
D_{GT}	binary diffusivity, cm^2/sec
D_{iK}^*	Knudsen diffusivity of the ith component, cm^2/sec
D_{iK}	effective Knudsen diffusivity of the ith component, cm^2/sec
E	activation energy, kcal/mol
k, k_s	reaction rate constant, 1/sec
k_0	frequency factor, 1/sec
$k_{mA'}$	gas film mass transfer coefficient, cm/sec
p	pressure, atm
P_0	total bulk presssure, atm

p_{at}	atmospheric pressure, atm
r	radial position within the coal particle, cm
r_c	radius of unreacted core, cm
R	gas constant, cal/gmol. K
R_p	radius of coal particle, cm
S	component in the solid phase
t, t^*	time, sec
T	temperature, K
V	yield of volatiles, gm
W	fractional pressure build-up
x_T	mole fraction of tar evolved
x_G	mole fraction of gas evolved
X	fractional conversion
α	stoichiometric coefficient
γ_T	rate of evolution of tar, gm/gm.sec
γ_G	rate of evolution of gas, gm/gm.sec
β	permeability of coal
μ	viscosity of gaseous mixture, cm^2/sec
ε	voidage

REFERENCES

[1] Denn, M., J. Wei, W.C. Yu and R. Cwiklinski, 'Detailed simulation of a moving-bed gasifier', a research report prepared for the Electric Power Research Institute, AP-2576 (1982).

[2] Talwalkar, A.T., 'A topical report on coal pyrolysis', prepared for the Morgantown Energy Technology Center of the U.S. Department of Energy, WV, Contract # DE-AC21-82MC19316 (1983).

[3] Gokhale, A.J., 'Devolatilization behavior of coals in a fixed bed reactor', Ph.D. dissertation, Chemical Engineering, Washington State University, Pullman, WA (1985).

[4] Probstein, R.F. and R.E. Hicks, 'Synthetic Fuels', McGraw-Hill Book Company, N.Y. (1982).

[5] Gangwal, S.K. and D.G. Nichols, 'Coal conversion and the environment', U.S. Department of Energy- Battelle NorthWest Symposium, Richland, WA, DOE-Symp. Series 54 (1981).

[6] Pitt, G.J., 'The kinetics of the evolution of volatile products from coal', Fuel, 41, 267 (1962).

[7] Anthony, D.B. and J.B. Howard, 'Coal devolatilization and hydrogasification', A.I.Ch.E.J., 22, 625 (1976).

[8] Shapatina, E.A., V.A. Kalyuzhnyi and Z.F. Chukhanov, 'Technological utilization of fuel for energy: thermal treatment of fuels (1960)', reviewed in the B.C.U.R.A. Monthly Bulletin, 25, 285 (1961).

[9] Wen, C.Y., 'Noncatalytic heterogeneous solid fluid reaction models', Industrial and Engineering Chemistry, 9, 34-54 (1968).

[10] Levenspiel, O., Chemical Reaction Engineering, John Wiley & Sons Inc. (1972).

[11] Gavalas, G.R., Coal Pyrolysis, Vol 4, Elsevier Scientific Publishing Company (1982).

Table 1. Chemical Analyses of Coal Sample

Subbituminous Coal (PSOC-241)			
Proximate Analysis		Ultimate Analysis	
% Moisture	10.81	% Carbon	66.17
% Ash	6.24	% Hydrogen	4.53
% Volatiles	39.26	% Nitrogen	1.09
% Fixed Carbon	43.69	% Chlorine	0.01
	100.00	% Sulphur	0.39
		% Ash	6.25
		% Oxygen	21.54
Btu/lb	9941		100.00
free swelling index = 0			

Table 2. Volatiles, Tar and Gas Yields: PSOC-241 coal, (-4,+3) mm;reactor @ 30 psig;reactive gas + steam mixture

Total Volatile Yield, gm				
min	30	20	10	5
550 C	43.0	41.7	38.0	36.3
450 C	36.4	34.9	29.8	26.7
350 C	26.0	22.2	20.7	15.7
Tar Yield, gm				
min	30	20	10	5
550 C	1.75	1.07	0.77	0.31
450 C	2.17	0.89	0.80	0.74
350 C	0.75	0.53	0.45	0.28
Gas Yield, gm				
min	30			
550 C	13.7			
450 C	18.3			
350 C	6.3			

Table 3. Volatiles, Tar and Gas Yields: PSOC-241 coal, (-2,+1) mm;reactor @ 30 psig;reactive gas + steam mixture

Total Volatile Yield, gm				
min	30	20	10	5
550 C	42.9	42.2	37.1	35.8
450 C	37.0	36.8	33.5	31.9
350 C	24.0	23.8	23.4	21.5
Tar Yield, gm				
min	30	20	10	5
550 C	1.90	1.3	0.85	0.64
450 C	1.47	1.17	1.05	0.55
350 C	0.82	0.65	0.4	0.3
Gas Yield, gm				
min	30			
550 C	19.7			
450 C	7.3			
350 C	N.A.			

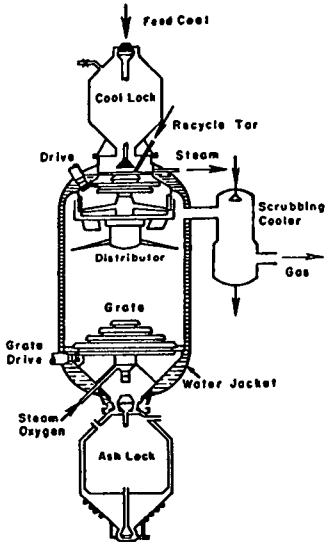

FIG. 1 - LURGI PRESSURIZED GASIFIER [1]

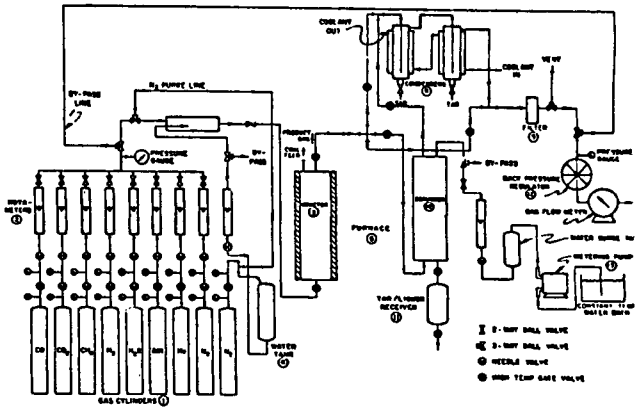

FIG. 2 - EXPERIMENTAL SET-UP [3]

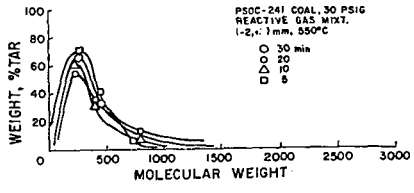

FIG. 3 - MOLECULAR WEIGHT DISTRIBUTION OF TAR

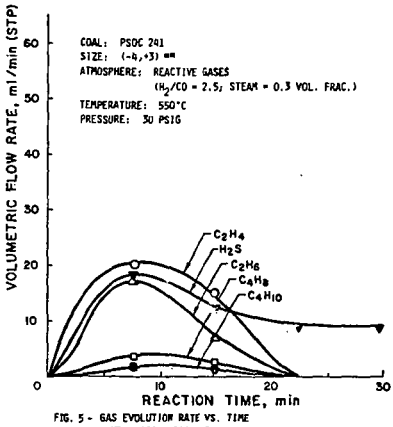

FIG. 5 - GAS EVOLUTION RATE VS. TIME
(HYDROCARBON GASES EXCL. METHANE AND INCL. H_2S)

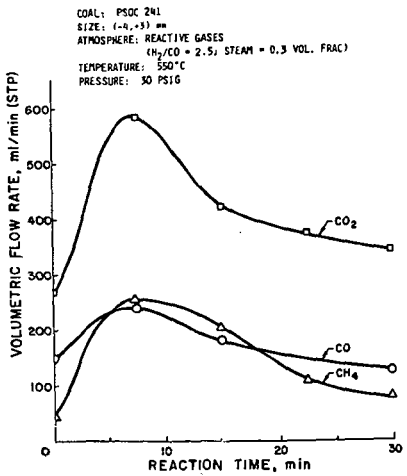

FIG. 4 - GAS EVOLUTION RATE VS. TIME
(PERMANENT GASES INCL. METHANE)

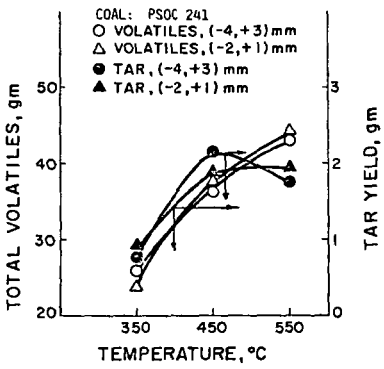

FIG. 6 - EXPERIMENTAL DATA

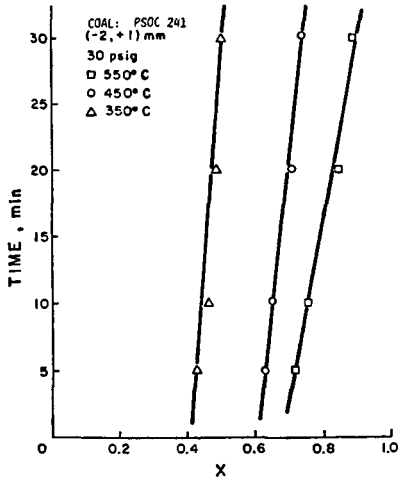

FIG. 7 - FLUID FILM RESISTANCE CONTROL, TYPE I

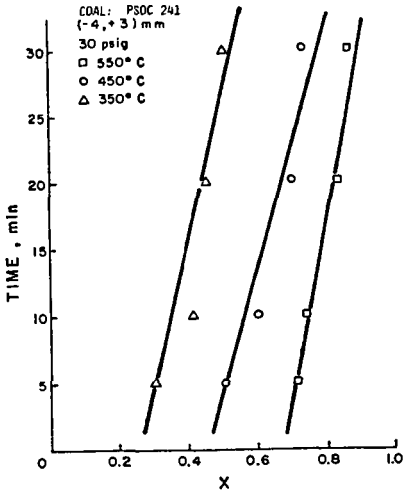

FIG. 8 - FLUID FILM RESISTANCE CONTROL, TYPE I

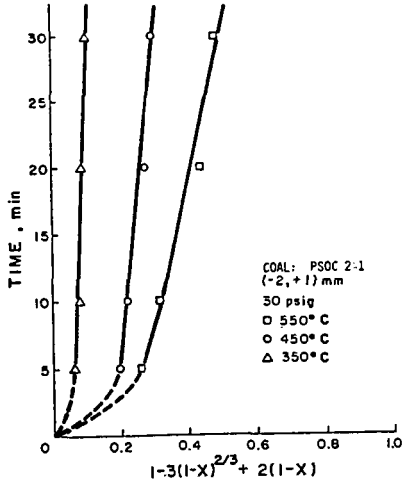

FIG. 9 - ASH LAYER RESISTANCE CONTROL, TYPE II

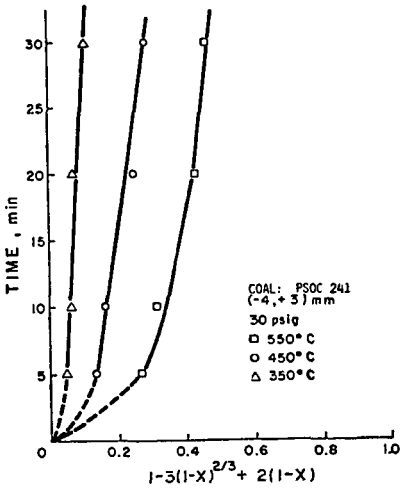

FIG. 10 - ASH LAYER RESISTANCE CONTROL, TYPE II

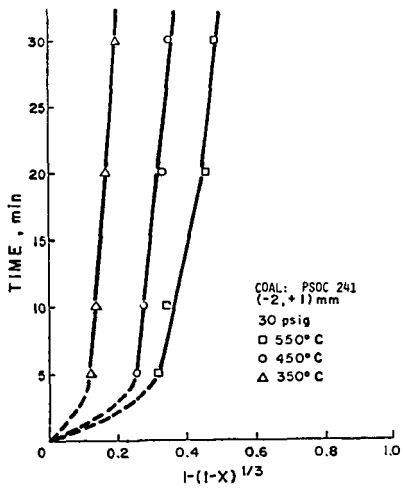

FIG. 11 - CHEMICAL REACTION CONTROL, TYPE III

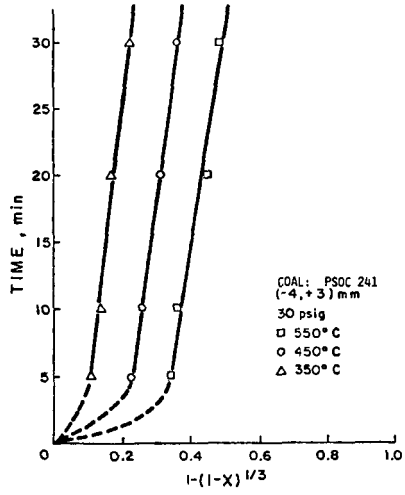

FIG. 12 - CHEMICAL REACTION CONTROL, TYPE III

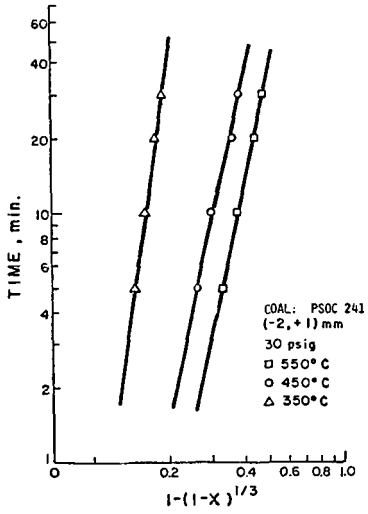

FIG. 13 - ASH LAYER RESISTANCE CONTROL, TYPE II'

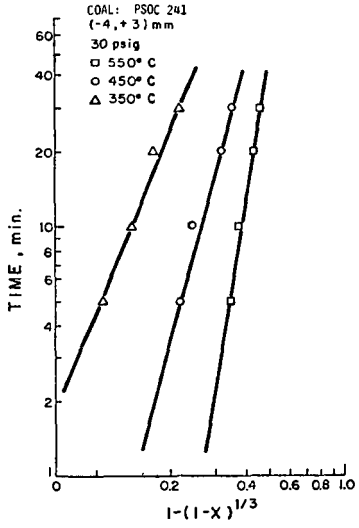

FIG. 14 - ASH LAYER RESISTANCE CONTROL, TYPE II'

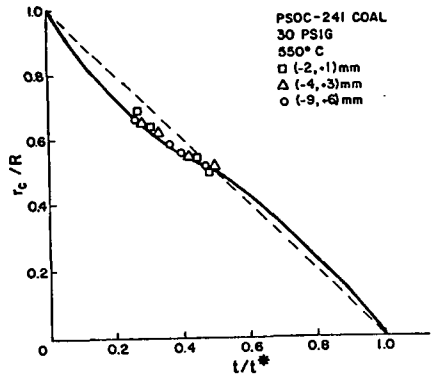

FIG. 15 - UNREACTED SHRINKING CORE MODEL

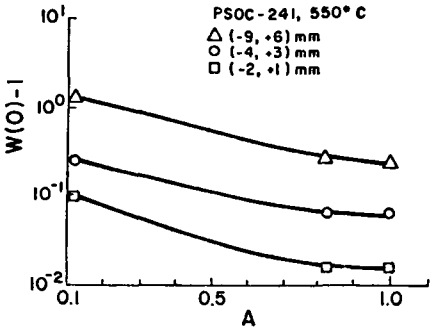

FIG. 16 - DIMENSIONLESS PRESSURE BUILD-UP AT 550°C

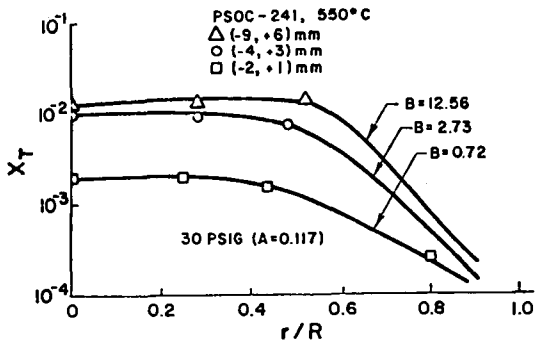

FIG. 17 - TAR MOLE FRACTION INSIDE COAL PARTICLE

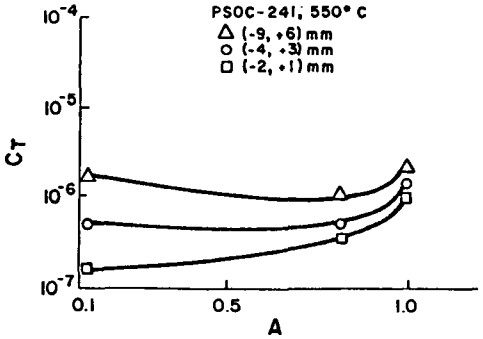

FIG. 18 - TAR CONCENTRATION AT THE CENTER OF COAL PARTICLE

HYDROXYL FUNCTIONAL GROUP DETERMINATION IN COAL TARS AND PYROLYSIS OF O-METHYLATED COAL

Susan A. Cannon, C. Judith Chu, Robert H. Hauge and John L. Margrave

Department of Chemistry, William Marsh Rice University
P. O. Box 1892, Houston, Texas 77251

INTRODUCTION

The objective of this investigation was to study the hydroxyl functional groups of tar molecules and to determine their involvement in the mechanism of tar evolution during coal pyrolysis processes. Strong similarities exist between the infrared spectra of coals and their respective tars suggesting that the tar molecules are similar in structure to the parent coal and contain similar functional groups characteristic of the parent coal.(1) Clarification of the structure of tar molecules should lead to a better understanding of the parent coal structure. Our main concern has been centered on the identification of tar hydroxyl functional groups and the determination of their role in the mechanism of tar evolution. Whether hydrogen bonding through the hydroxyl functional groups is an important factor in tar evolution will be investigated through the pyrolysis studies of methylated coals. The process of methylation replaces most of the phenolic and carboxylic hydrogens in coal with methyl groups.(2,3) Thus hydrogen bonding via the phenolic or carboxylic hydrogens should be largely eliminated.

The experiments were designed so that tar molecules and other gaseous products of coal pyrolysis could exit the reaction zone rapidly and be trapped with inert nitrogen gas on a cold matrix surface. Matrix isolation studies of tar molecules produce better resolved FTIR spectra than those in a coal matrix, making structural characterization of the tar molecules a more definite possibility.

EXPERIMENTAL

The Rice University multisurface matrix isolation apparatus was used in the pyrolysis studies of four different ranks of coal and their respective methylated products. The four coal samples studied were Pittsburgh bituminous, Illinois #6, Rawhide sub-bituminous and Texas lignite. The samples were ground and sifted under inert nitrogen atmosphere to prevent oxidation. Only the -500 mesh size coal particles were used in the experiments.

The matrix isolation FTIR apparatus possessses 60 deposition surfaces which are useful for pyrolysis studies over a wide range of temperatures. Small changes occuring as a result of variations in reaction temperature can be readily detected. Gaseous pyrolysis products including the tar molecules were trapped in a nitrogen matrix at 12°K. One surface was used for every 40-100°C increment rise in temperature over a 10 minute trapping period. The frozen matrice were later analyzed off-line with an integrated IBM-FTIR spectrometer. Tar evolution was observed to occur within the same temperature range (150-600°C) for the four coals studied. Therefore the experimental temperature range studied was from room temperature to approximately 620°C. Detailed descriptions of the MI-FTIR apparatus and the pyrolysis reactor can be found elsewhere.(4,5)

Methylation of the coal samples was performed according to the procedures described by R. Liotta in "Selective Alkylation of Acidic Hydroxyl Groups in Coal".(2) The general reaction procedure may be described using the following equations:

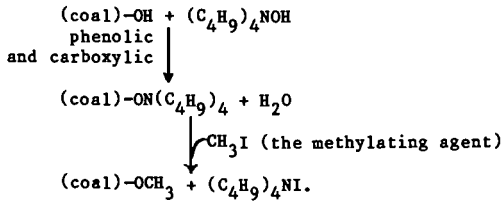

Only -500 mesh coal particles were used in our methylation reactions. The experimental procedure for the pyrolysis of the methylated coals was identical to that of the original coal in order to determine if methylation in any way alters the pyrolysis behavior of the original coal.

RESULTS AND DISCUSSION

Determination of Hydroxyl Functional Groups in Tar

Hydroxyl functional group determination in coals has been undertaken both spectroscopically (6) as well as through a combination of chemical and spectroscopic means.(7) The spectroscopic method of hydroxyl determination relied on the measurement of the broad infrared absorption region between 3600-2000 cm^{-1}. This broad absorption range was complicated by the presence of KBr water absorptions as well as absorptions attributed to hydrogen bonded OH. The second method of hydroxyl functional determination involved the measurement of intensities of infrared bands (carbonyl stretching at 1770 and 1740 cm^{-1}) assigned to products of acetylation reactions of coal. Both methods involved indirect determination of OH functional groups in the parent coal matrix. Studies of coal pyrolysis processes using matrix isolation techniques have the advantage of actually isolating the individual tar molecules and other gaseous products in an inert matrix. Isolation of the individual tar molecules in an inert gas matrix at 12°K produced well resolved infrared spectra not observed in the FTIR spectra of tars in a coal matrix, thus making structural characterization of the tar molecules highly feasable. The matrix isolated tar should also be free of hydrogen bonding thus facilitating the identification of hydroxyl functional groups.

Figure 1 shows the matrix isolated FTIR spectra of the gaseous pyrolysis products of Pittsburgh bituminous from r.t. to 621°C. The evolution of tar molecules was initiated at temperatures as low as 130°C and continued until maximum evolution was reached at 470°C. Absorptions characteristic of tar molecules were broad bands at 3000-2800 cm^{-1} due to CH stretching, and 1550-1100 cm^{-1} due to CH bending and CO stretching. Study of the OH stretching region of the matrix isolated tar spectra should provide information concerning the hydroxyl functional groups present in the tar molecules. The presence of water OH stretching modes and absorptions due to water-tar complexes in this region complicated the identification of tar OH functional groups. Co-deposition of water (0.5 H_2O/100 N_2) with tar molecules resulted in noticeable increases in absorptions due to water-tar complexes. This is shown in Figure 2 which compares the matrix isolated FTIR spectra of Illinois #6 tar molecules with the results obtained from tar-water co-deposition experiments. As can be seen, two distinct broad absorptions at 3626.5 and 3580.9 cm^{-1} remained unaffected by the addition of water molecules. These were assigned to tar hydroxyl functional groups. The OH stretching frequencies of all four of the coal tar molecules studied are shown in Figure 3. Considerable amounts of hydroxyl functional groups were found in the tars of the two higher rank coals, Pittsburgh bituminous and Illinois #6, with Illinois #6 possessing greater amounts of hydroxyl functional groups. Considerably less hydroxyl absorption was observed for the two lower rank coal tars, Rawhide sub-bituminous and Texas lignite. The

observation of less hydroxyls for the lower rank coals is in accordance with lower rank coals possessing less aromatic character.

Comparison of OH stretching frequencies of phenol, 2-napthol and cyclohexanol in nitrogen matrix with those of matrix isolated tar is shown in Figure 4. The broad tar OH absorption at 3626.5 cm^{-1} compares favorably with the OH stretching frequencies of phenol and 2-napthol but not with cyclohexanol. In general, the less acidic alcoholic hydroxyls have OH absorptions at frequencies higher than 3630 cm^{-1} (OH stretching frequency of nitrogen matrix isolated methanol is 3664 cm^{-1}). The peak at 3626.5 cm^{-1} is thus assigned to a phenolic hydroxyl. One also concludes that alcoholic hydroxyls are not present in matrix isolated tar molecules. The less intense tar OH absorption at 3580.9 cm^{-1} is still under investigation. Since this absorption is lower in frequency than the phenolic OH, it is probably due to a more acidic OH functional group than the phenolic hydroxyl. Possibilities are carboxylic hydroxyls or phenolic hydroxyls with an adjacent thiophene group (hydroxy-benzothiaphene).(8)

Pyrolysis of O-Methylated Coal

The role of hydroxyl functional groups in the mechanism of tar evolution is of great interest. Hydrogen bonding through the hydroxyl functional groups could be an important intermolecular bond in the structure of coal. If hydrogen bonding through the hydroxyl functional groups were the predominant factor in determining the volatility of the coal (determined by the ease of tar evolution and percent weight loss), then replacing the hydroxyl hydrogens with methyl groups should eliminate this hydrogen bonding and make the coal more volatile. Hydroxyl functional groups can also undergo water elimination reactions to form new C-O-C cross linkages. The formation of these new cross linkages would also act to reduce the volatility of coal and thus increase the tar evolution temperature. Methylation of the coal would eliminate the formation of these new cross linkages. More tar might also be evolved due to the increased volatility and decreased decomposition of the O-methylated coal.

If the evolution of tar during coal thermal decomposition occured primarily through the cleavage of weak linkages such as methylene linkages, then methylation should not effect the volatility of the coal or the tar evolution temperature.

Slow pyrolysis studies of methylated coals were performed to determine if O-methylation in any way has altered the pyrolyis behavior of the original coal. Figure 5 shows the matrix isolated FTIR spectra of the pyrolysis products of methylated Pittsburgh bituminous from r.t. to 604^{o}C. Comparison of pyrolysis results of the methylated coal (Figure 5) with those of the original coal (Figure 1) showed several differences indicative of coal structural changes after methylation. Tar evolution temperature has been reduced by approximately 150-200^{o}C, indicating a more volatile coal after methylation. This was observed for all four ranks of coal studied. An increase of approximately 10% volatility was also observed for all four coals after methylation. Comparisons of the matrix isolated tars with their respective methylated tars are shown in Figure 6. For all four coals, O-methylation has changed the relative intensities of CH_3 to CH_2 groups in the tar molecules in favor of greater CH_3 absorptions as is to be expected since CH_3 groups have replaced all hydroxyl hydrogens in the methylated tar. Phenolic hydroxyl absorptions at 3626.5 cm^{-1} are also absent in the methylated tar molecules.

The increased volatility and the lowering of tar evolution temperature of the O-methylated coal suggest that methylene linkages are not involved in the mechanism of tar evolution. Our results from the pyrolysis of O-methylated coal suggest two possible mechanisms of tar evolution. The first involves breaking only hydrogen bonding of the hydroxyl groups as tar is evolved. A second mechanism envisions the formation of new cross linkages through decomposition of tbe hydroxyl groups at lower temperature. The temperature at which tar evolves in then set by the temperature at which the new cross linkages decompose. Isotopic enrichment studies are currently in progress to assist in distinguishing between the above mechanisms.

In any case, the large increase in volatility of the tar component of all four coals is quite remarkable and suggests a common bonding mechanism in all coals.

ACKNOWLEDGEMENT

The authors greatfully acknowledge support of this work by the Department of Energy, Morgantwon, West Virginia. We also thank Exxon Research and Engineering at Baytown, Texas for supplying our coal samples.

REFERENCES

1. Solomon, P.R., "Relation Between Coal Structure and Thermal Decomposition Products", Coal Structure, Adv. in Chem. Series, 192, eds. Gorbaty, M.L. and Ouchi, K., Am. Chem. Soc., p. 95, 1981.
2. Liotta, R., "Selective Alkylation of Acidic Hydroxyl Groups in Coal", Fuel, vol. 58, 724, 1979.
3. Liotta, R. and Brons, G., "Coal. Kinetics of O-Alkylation", J. Am. Chem. Soc., 103, p. 1735-1742, 1981.
4. C.J. Chu, L. Fredin, R.H. Hauge and J.L. Margrave, "Studies of Pyrolysis Processes of Illinois #6 and its Tar Using Matrix Isolation FTIR Spectroscopy", High Temperature Science, 1984, in press.
5. C.J. Chu, L. Fredin, R.H. Hauge and J.L. Margrave, "Pyrolysis Studies of Illinois #6 and its Tar using Matrix Isolation FTIR Spectroscopy", ACS, Div. Fuel Chemistry, Preprints, 29, (2), 49, 1984.
6. Solomon, P.R., and Carangelo, R.M., "FTIR Analysis of Coal. 1. Techniques and Determination of Hydroxyl Concentrations", Fuel, vol. 61, p. 663, 1982.
7. Snyder, R.W., Painter, P.C., Havens, J.R., and Koenig, J.L., "The Determination of Hydroxyl Groups in Coal by Fourier Transform Infrared and ^{13}C NMR Spectroscopy", Applied Spectroscopy, vol. 37, no. 6, p. 497, 1983.
8. Spiro, C.L., Wong, J., Lytle, F.W., Greegor, R.B., Maylotte, K.H., and Lampson, S.H., "X-ray Absorption Spectroscopic Investigation of Sulfur Sites in Coal: Organic Sulfur Identification", Science, vol. 226, p. 48, 1984.

Figure 1: Pittsburgh Bituminous Slow Pyrolysis

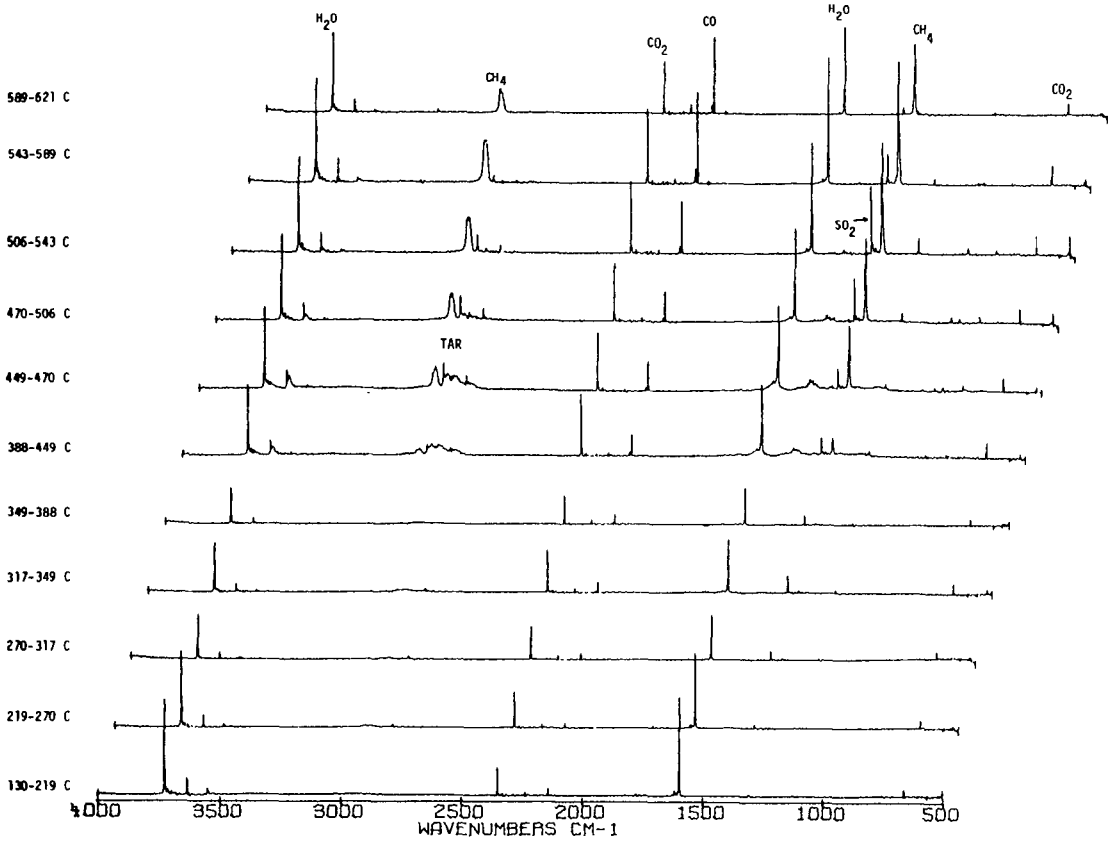

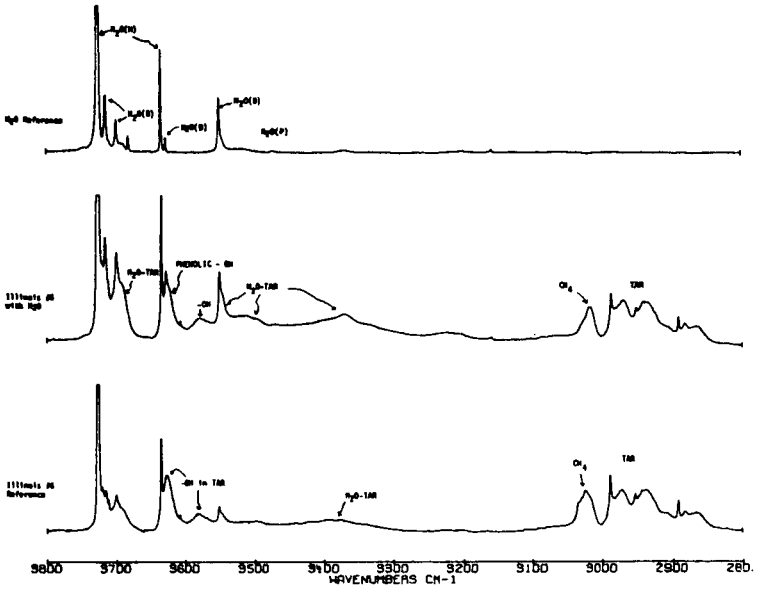

Figure 2. Co-Deposition of Illinois #6 Tar and H_2O in N_2 Matrix

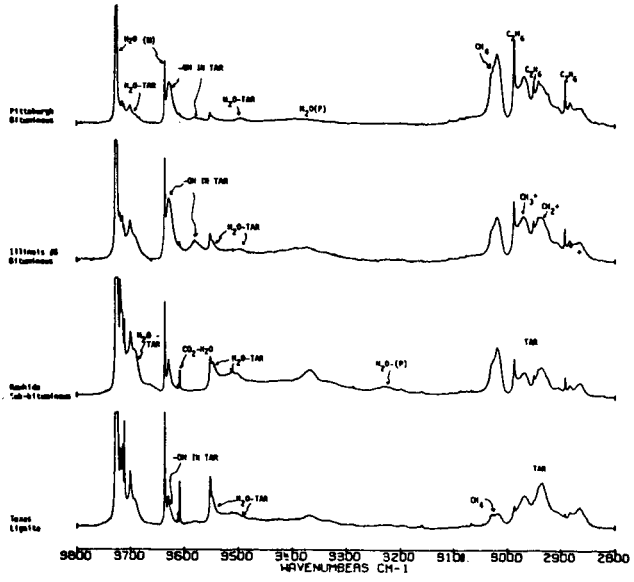

Figure 3. MI-FTIR Spectra of Four Coal Tars

Figure 5: O-Methylated Pittsburgh Bituminous Slow Pyrolysis

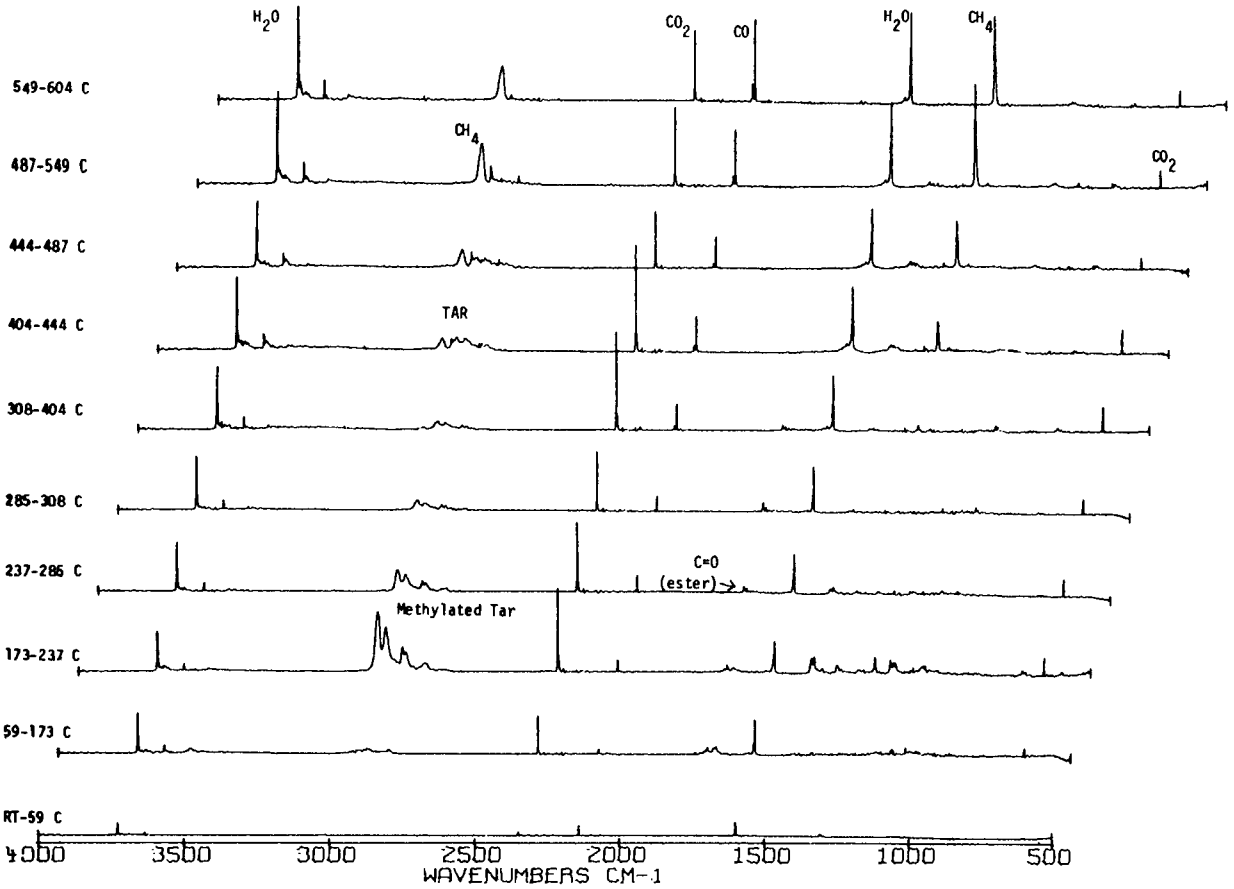

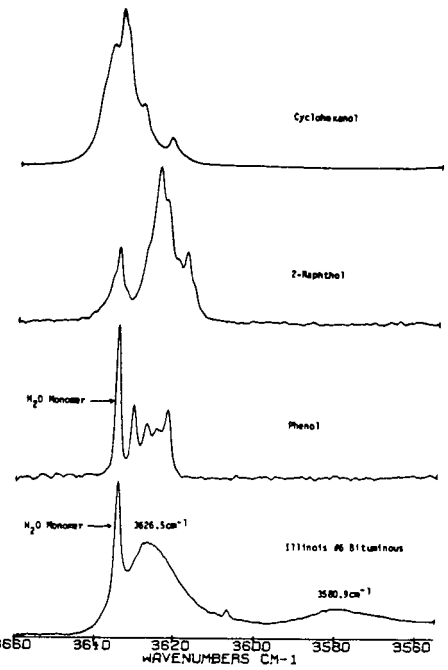

Figure 4. Comparison of Hydroxyl Stretching Frequencies in N_2 Matrix

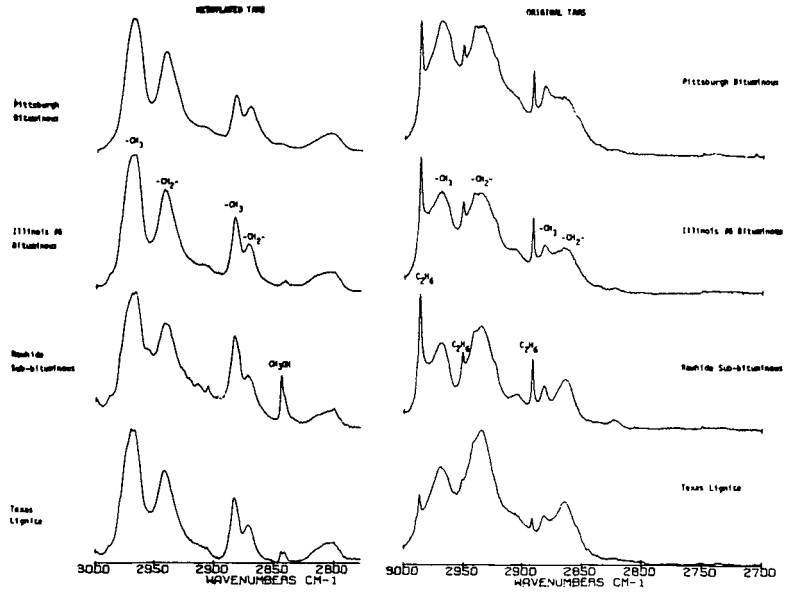

Figure 6. Comparison of CH Stretching Region of Tar and O-Methylated Tar

DISC #52

VERY RAPID COAL PYROLYSIS

Peter R. Solomon, Michael A. Serio, Robert M. Carangelo and James R. Markham

Advanced Fuel Research, Inc., 87 Church St., East Hartford, CT 06108 USA

INTRODUCTION

Considerable controversy exists concerning the rate of coal pyrolysis. For example, at 800°C, rates reported in the literature (derived assuming a single first order process to define weight loss) vary from a low of around 1 sec^{-1} (1-4) to a high near 100 sec^{-1} (5-8), with values in between (9,10). The discrepancies cannot be explained by differences in sample composition because experiments in which coal rank alone was varied typically show no more than a factor of 5 variation in rate (11). One problem is that if the higher rate is correct, then any experiment which attempts to obtain isothermal rate data at 800°C must heat the coal in a time short compared with the pyrolysis time, i.e. on the order of 100,000°C/sec. At higher temperatures the heating rate to obtain isothermal data must be even faster. But for most experiments at temperatures of 800°C or higher, calculations of heat up rates for pulverized coal suggest that if the higher rate is correct, pyrolysis will typically be occurring during heat up, even assuming zero heats of reaction. Under these circumstances it is necessary to know the coal particle temperature to derive kinetic rates. Coal particle temperatures during rapid pyrolysis have not generally been measured.

In an attempt to resolve this controversy, a new pyrolysis experiment was designed which provided for high heating rates and a geometry which simplified the prediction of particle temperatures (12). It used a small diameter electrically heated tube into which coal and helium carrier gas were injected. The reaction distance was varied by moving the electrode positions. The particle temperatures and the particle residence times were calculated from the measured tube wall temperatures and the gas flow rates, respectively. Even allowing for the uncertainty in these estimated values, the rates measured at asymptotic tube temperatures of 700°C, 800°C and 900°C agreed with the highest reported rates and were inconsistent with the low rates.

These heated tube experiments therefore, lent support to the high rate advocates but suffered in conclusiveness as did the other experiments in this temperature range in not having a direct measure of particle temperature (2-10,12) and reaction time (2,5,7-9,12). The tube reactor experiment was modified to eliminate these drawbacks. Temperatures of the solids were determined at the tube exit using FT-IR emission and transmission spectroscopy (13,14) and the transit time for the coal was measured using photo transistors at the top and bottom of the tube. Temperature measurements were also made inside and outside the tube with a thermocouple.

Measurements were made of the amount and composition of the tar, char and gases evolved as a function of the measured reaction time and temperature. We focus on primary pyrolysis, during which the initial rapid weight loss, the evolution of tar and lighter hydrocarbons, and the disappearance of the aliphatic (or hydroaromatic hydrogen) in the coal/char all happen at similar rates. For a 200 x 325 mesh fraction of a dry North Dakota lignite in a 115 cm long tube having an asymptotic tube temperature of 800°C, primary pyrolysis was completed in a period of 14 milliseconds based on the mean particle residence times. The extent of axial dispersion was small. During this period, the maximum coal temperature was increasing from 600 to 740°C. These data, as well as data obtained at equilibrium tube temperatures of 700°C and 935°C, are in agreement with the high pyrolysis rate originally reported (12).

This paper describes the experimental apparatus and measurement technique, and presents the results for a lignite at temperatures between 600°C and 935°C. The results are compared to the predictions of a pyrolysis model and to the literature data. Reasons for the discrepancies are discussed.

EXPERIMENTAL

The reactor is illustrated in Fig. 1. It consists of a 0.2" i.d. Inconel 702 tube which is heated electrically. Coal entrained in cold carrier gas is injected at the top of the tube. The coal is fed using a previously described entrainment system (7,8). The coal-gas mixture enters the heated section of tube and heats rapidly. The heat transfer rate is large because of the small tube diameter, the high thermal conductivity of the helium carrier gas, and the fact that the particles collide with the hot walls of the tube. After a variable residence time, the reacting stream is quenched in a water cooled section of tube. The product collection train consists of a cyclone to separate the char followed by a collection bag to collect the gas, tar and soot. The gas from the bag is analyzed by FT-IR and the solids and liquids are collected on the bag surface and in a filter.

Temperature Measurements

The temperature of the gas-coal mixture and outside tube temperature has been measured with a thermocouple. At constant current, the tube will reach an equilibrium temperature such that the external power loss by radiation and convection is equal to the electrical power input. With gas and coal flowing in the tube, the tube is initially cooler than the equilibrium temperature, since heat is used to raise the temperature of the gas and coal. The heat absorbed by the coal and gas can be calculated from the measured tube temperature. When the reactants reach the equilibrium temperature, the outside of the tube reaches a constant temperature.

The results for one set of measurements with coal present are presented in Fig. 2. The measurements include: a) thermocouple measurements inside and outside the tube; b) FT-IR measurements at the center of the gas/solid stream 0.75 cm below the end of the hot tube; c) thermocouple measurements at the position of the FT-IR measurement; and d) thermocouple measurements inside a water cooled tube attached to the hot tube to measure the quenching rate.

Heat transfer calculations suggest that inside the tube the thermocouple reads 10-20°C higher than the gas due to radiation from the wall. The bead temperatures at the FT-IR focal point was calculated to be lower by approximately the same amount outside the tube. The measurements of the external tube wall temperature are low due to heat loss from the thermocouple bead to the surroundings. However, the maximum effect of this error can be determined by comparing the asymptotic values of the external wall temperature and the internal gas temperature, which come to thermal equilibrium for sufficiently long distances. The knowledge of this temperature difference along with the apparent wall temperature can be used to determine the error at each measured wall temperature, which gets lower as the tube gets cooler. For example, in the 800°C experiment, the corrections ranged from +35°C at 800°C to +10°C at 500°C when using a 0.002" diameter thermocouple bead. The corrections scaled with bead diameter, as expected. The wall profile shown in Fig. 2 has been corrected for radiation errors. The temperature difference between the outside and the inside of the tube was calculated to be negligible.

Measurements of coal particle temperatures were made using FT-IR emission and transmission spectroscopy. As described in a previous publication (13), the transmittance measurement is used to determine the total emitting surface of the coal particles so that a normalized emission, (emission/(1-transmittance)) can be compared

in both shape and amplitude to a theoretical black-body. The FT-IR measurement can provide a direct measurement of the coal particle temperature during heat up. A simple case is illustrated in the insert of Fig. 2. For this case sufficient time was allowed for the coal to reach the asymptotic tube temperature of 935°C (1208 K) and for pyrolysis to have occurred. For a grey-body (such as shown here for char) the shape of the normalized emission spectrum gives the temperature and the amplitude gives the emittance. The normalized emission spectrum is in good agreement with a theoretical black-body at 1190 K with an amplitude corresponding to an emissivity of 0.9. The measured temperature is in excellent agreement with the tube temperature as a 10°C drop in temperature is expected between the end of the tube, and the measuring point at 0.75 cm below the end. The measurement of temperature before and during pyrolysis is not as simple, since for the size of coal particles used here only specific bands (corresponding to the absorbing bands in coal) provide sufficient absorbance for the spectral emittance to reach 0.9. Then, only these regions can be used to compare to the black-body. The measurement technique, the problems encountered, their solutions and the results are discussed in another paper at this meeting (14). The results at 800°C are presented as the triangles in Fig. 2.

Calculations of the temperature of the gas, the thermocouple bead, and the coal particles were performed given the tube wall temperature as a boundary condition. The calculations assume the temperature dependent heat capacity for coal derived by Merrick (15) which agrees with the measurements of Lee (16), an average spectral emittance of 0.5 for the 200 x 325 mesh particles of coals in agreement with recent FT-IR measurements (14) and zero heat of reaction. The calculations assume convective heat transfer between the tube wall and gas and between the gas and coal particle or thermocouple bead and radiative heat transfer between the wall and the coal particle or thermocouple bead. The heat transfer coefficient between the wall and the gas, which was determined from the Sieder-Tate equation (17), was validated by equating the electric power input to the power radiated and convected outside the tube (determined from the tube temperature and emissivity) plus the heat transfer to the gas inside the tube.

In order to match the measured particle temperatures in the early part of the tube (e.g., $<$ 50 cm at 800°C) it was necessary to include a term to account for heat transfer due to collisions of relatively cold particles with the hot walls. This phenomenon, known as wall-contact heat transfer, has been described by Boothroyd (18). A heat transfer coefficient was defined by analogy to a conventional convective coefficient, i.e. $Q_{wc} = h_{wc} (T_{wall} - T_{coal})$.

The predicted results (lines in Fig. 2) are in good agreement with the measured temperatures. The agreement between the actual thermocouple measurements and the predicted values is a good indication that the corrected wall temperature profile is accurate. The measured particle temperatures are slightly below the predicted values in agreement with a 10°C drop from the tube end to the measuring point. Possible values for the heat of reaction were considered. A value of 250 K cal/gram of total volatile material results in a predicted temperature which is too low although the shape of the temperature vs distance curve matched the FT-IR data better than the zero heat of reaction case. Additional data are needed to determine the possible values for the heat of reaction and the chemical reactions to which it applies (e.g. tar loss, overall weight loss, etc.).

Particle Residence Time

The heated tube reactor was modified for particle velocity measurements. The passage of a pulse of coal through the system was measured for each electrode position by recording signals from photo transistors mounted on glass sections at the top and bottom of the reactor tube on a dual channel oscilloscope. Photographs of the oscilloscope traces allow an assessment of the mean particle residence time and the extent of axial dispersion.

A technique was developed where short, well-defined pulses could be introduced by using an electrically activated solenoid to inject the contents of a tube containing the coal charge and gas at 10 psig. In addition, the reactor was set up over the FT-IR bench in preparation for hot tests with temperature measurements. This configuration has the added advantage of using a laser from the FT-IR beam as the light source for the lower photo transistor, which improved the signal to noise significantly. It also eliminated the lower glass tube which tended to be obscured with tar after a few hot runs. The only problem was a slight spreading of the particle stream as it emerged from the tube, which meant that the measured dispersion was in excess of what actually occurred in the tube.

The photographs enabled an assessment of the particle residence time and of the particle dispersion, which impacts on the kinetic analysis. Some representative traces from cold and hot tests are shown in Fig. 3. Figure 3a indicates a transit time of approximately 60 milliseconds for the coal in the cold tube. The average transit time in the cold experiments was determined from a number of measurements to be 56 milliseconds. The particles, therefore, travel at about 80% of the gas velocity of 28 m/sec. Figures 3b-3d show the transit time when the tube is heated over increasing distances (75, 100 and 115 cm). The transit time is reduced to about 32 milliseconds when 115 cm is heated (Fig. 3d).

The extent of axial dispersion was small and was typically almost symmetrical, which would lead to a slight (approximately 10%) underestimation of the rate constant. It was neglected in the analysis of results for this paper.

Data are presented in Fig. 4 for the mean particle transit times for hot experiments. The hot data are adjusted so that the transit time in the cold part of the tube is not included. This was done by subtracting the heated length from the distance between the detectors (125 cm) and using the cold data to determine the transit time which should be subtracted from the observed transit time for the hot experiment. The adjusted data then reflect the amount of time it takes to traverse the hot zone.

The particle residence time data definitely indicate that the particles are accelerating in the hot experiments at close to the same rate as the gas except for a slowdown in the region where pyrolysis begins ($\sim$50 cm). This is reasonable in light of the small value of the characteristic drag time, 1.5 milliseconds, (which indicates the relaxation time for a particle for a step change in gas velocity) for the size fraction used in the hot experiments (-200, +325 mesh) (17). The data were fit by a model which assumes the particles are moving at 80% of the average gas velocity until primary pyrolysis is 1% complete, at 40% of the gas velocity between 1% and 75% pyrolysis, and back to 80% of the gas velocity after pyrolysis is 75% completed. The reason for the slow down during pyrolysis is not yet clear but is probably associated with evolution of gas from the coal or swelling which has been observed for this lignite under these extremely high heating rates.

Additional confirmation of the particle velocities was obtained from comparing the particle feed rate with the density of particles exiting the tube determined by FT-IR transmittance measurements, where the density of particles in the focus is inversely proportional to their velocity.

RESULTS

The results are shown in Fig. 5 for isothermal tube temperatures of 700°C, 800°C, and 935°C. Figures 5a-c present the weight % char, tar, and gas (the sum of measured individual gas species) as a function of the reaction distance. The mass balance was between 96.5 and 101%.

The measured and calculated particle temperatures and times as functions of distance are shown in Figs. 5d-f. The calculated particle temperatures match FT-IR temperature data obtained at 800°C and 935°C and the particle times match transit time data obtained at 800°C. Confidence can be placed in the calculated temperature at 700°C because the calculations use the same heat transfer coefficients which give the validated calculations at 800°C and 930°C. The time calculations at 700°C and 935°C employ the same relative velocity between gas and particles that was measured at 800°C. For all three temperatures, pyrolysis occurs during particle heat up, even though heating rates are in excess of 40,000°C/sec.

The solid lines in Figs. 5a-5c are generated using a previously presented pyrolysis theory (8) which calculates the evolution of individual species using a distributed activation energy of the form introduced by Anthony et al. (1) for each species. The rates for tar and hydrocarbon gases are shown in Fig. 6. The gas rate is five times higher than the rate for the same species in Ref. 8. This is to account for the factor of 5 higher rates observed for lignites compared to bituminous coals, discussed in (11). An error was discovered in the calculation of tar evolution in Ref. 8. The rate in Fig. 6 is for the corrected calculation. As a further comparison, the reciprocals of the times required to achieve 63% tar yield are plotted (solid circles) in Fig. 6 as a function of the reciprocal of the average absolute temperature during this period. A single pyrolysis experiment at 600°C gave a rate constant of 6.3 sec^{-1}. These data fall close to the line defining the tar rate.

The theory is in excellent agreement with the data. At all three temperatures the observed weight loss is a result of rapid evolution of tar and slower evolution of the gases. The increase in total weight loss with increasing final temperature is the result of gas evolution (primarily CO and H_2O) due to loss of tightly bound functional groups.

For comparison with previous weight loss data, a single first order weight loss has been calculated (dashed lines) using a rate $k = 4.28 \times 10^{14} \exp(-55{,}400/RT)$ sec^{-1}. This is one half k_{tar} (see Fig. 6) and represents a compromise between the rapid evolution of tar and the slower rate for gas evolution. The single first order rate does not fit the data as well. It gives a steeper weight loss than is observed and the yield does not increase with temperature. Given these limitations inherent in a single first order model, the theory is in good agreement with the data.

DISCUSSION

The measured rate for primary pyrolysis weight loss is therefore higher than the high rates originally measured by Badzioch and Hawskley (5). The activation energy of 55 kcal is what is expected from thermochemical kinetics for ethylene bridges between aromatic rings and agrees with pyrolysis rates for model compounds and polymers where these bonds are the weak links (19). The rate is also in agreement with data obtained at much lower temperature (~450°C) at a heating rate of 30°C/sec.

What are the reasons for the discrepancies between these rates and rates reported by many other investigators (1-4,9,10,20-22)? There are two reasons for the discrepancies, interpretation of the rate and knowledge of the particle temperatures. Consider first the grid experiments. The data and analysis by Anthony et al. (1) illustrates the first reason. They presented two kinetic interpretations for their data, a single first order process and a set of parallel processes with a Gaussian distribution of activation energies. Both interpretations fit the data using Arrhenius expressions for kinetic rates. The single first order process which uses an activation energy of 11 kcal/mole requires two parameters, while the distributed rated model which uses a mean activation energy of 56 kcal/mole requires a third parameter to describe the spread in rates. Niksa et al. (3) used a single first

order model with its low activation energy. Suuberg et al. (6) rejected the low activation of the two parameter fit as being chemically unreasonable, and settled for a less accurate fit but with appropriate activation energies. The problem is that a variety of interpretations may provide good fits to the data over a limited range of temperature and heating rates. The grid experiments do not provide sufficient information to choose between the possibilities, some of which lead to highly inaccurate extrapolations. It is only by performing additional experiments at higher heating rates and therefore higher pyrolysis temperatures that the ambiguities can be eliminated. The data presented in this paper indicate that the distributed activation energy model was the better choice to produce $k \approx 100$ sec^{-1} at 800°C. Additional discrepancies are probably due to inaccurate assumptions regarding particle temperatures which have not been measured in the grid experiments.

If the high activation energy rate is the better choice, what about the data of Kobayashi et al. (2) which give a rate on the order of 1 sec^{-1} at 800°C and only 100 sec^{-1} at 1700°C? There was no direct measurement or confirmation of the particle temperature in these experiments. Instead, an assumption was made that the particles were at the gas temperatures at the longest residence time (200 milliseconds) for a nominal furnace temperature of 1260 K where a weight loss of 26 wt. % was observed. It was assumed that the 26 wt.% point was always reached at a temperature of 1260 K in the higher temperature experiments. These assumptions were used to determine a parameter, θ, defined as the ratio of the momentum shape factor to the energy shape factor. The particle temperature calculations were performed assuming: a value of $\theta = 3$, although a value closer to unity would be more likely; a smaller value of particle heat capacity than is now believed (15,16); a higher value for the absorption of radiation than recent data would indicate for small coal particles (13) and zero heat of pyrolysis. The resulting calculation gives a heatup time of approximately 18 milliseconds at 1260 K, in conflict with the observation that no weight loss has occurred at 70 milliseconds. Furthermore, the initial assumption is in conflict with the data presented in this paper which suggest that had the coal been at 1260 K for even 10 milliseconds, substantially more than 26% weight loss would have occurred. We believe that the particle temperatures at which pyrolysis was occurring were significantly overestimated by Kobayashi et al. (2), leading to underestimation of the kinetic rates.

There are other data which do not agree with our rates and where two color temperature measurements were made (20-22). These measurements suggest a high solids temperature. But these measurements may indicate the temperature of a hot cloud of soot surrounding the particle or hot spots on the particle surface and not reflect the temperature in the region of the particle where pyrolysis is occurring. It is also true that the assumption of constant emissivity used in interpretation of two-color data can be erroneous in some cases (13,14).

CONCLUSION

An experiment has been performed to determine pyrolysis rates for a lignite in which both the transit time and temperature of particles have been measured. The measured rate for weight loss is greater than 100 sec^{-1} at 800°C. The results suggest a reinterpretation of heated grid data which have given rates much lower than this at comparable temperatures. The results also suggest that lower rates obtained in entrained flow reactors were due to heat transfer limitations.

ACKNOWLEDGEMENT

This work was supported by the Morgantown Energy Technology Center of the U.S. Department of Energy under Contract No. DE-AC21-81FE05122, Holmes A. Webb, Contractor Monitor.

REFERENCES

1. Anthony, D.B., Howard, J.B., Hottel, H.C. and Meissner, H.P., 15th Symposium (Int) on Combustion, The Combustion Institute, Pittsburgh, PA pg. 1303 (1975) and Anthony, D.B., Sc.D. Thesis, M.I. T., Dept. of Chemical Engineering, Cambridge, MA (1974).
2. Kobayashi, H., Howard, J.B. and Sarofim, A.F., 16th Symposium (Int) on Combustion, The Combustion Institute, Pittsburgh, PA, pg. 411, (1977). and Kobayashi, H., Ph. D. Thesis, M.I.T. Dept. of Mechanical Eng., Cambridge, MA (1976).
3. Niksa, S., Heyd, L.E., Russel, W.B. and Saville, D.A., On the Role of Heating Rate in Rapid Coal Devolatilization, 20th Symposium (Int) on Combustion (to be published).
4. Solomon, P.R. and Colket, M.B., 17th Symposium (Int) on Combustion, The Combustion Institute, Pittsburgh, PA pg. 131 (1978).
5. Badzioch, S. and Hawksley, P.G.W., Ind. Eng. Chem. Process Design Develop., 9, 521, (1970).
6. Suuberg, E.M., Peters, W.A. and Howard, J.B., Ind. Eng. Process. Design Develop., 17, #1, pg. 37 (1978).
7. Solomon, P.R. and Hamblen, D.G., Measurement and Theory of Coal Pyrolysis Kinetics in an Entrained Flow Reactor, EPRI Final Report for Project RP 1654-8 (1983).
8. Solomon, P.R., Hamblen, D.G., Carangelo, R.M. and Krause, J.L., 19th Symposium (Int) on Combustion, The Combustion Institute, Pittsburgh, PA, pg. 1139 (1982).
9. Maloney, D.J. and Jenkins, R.G., Coupled Heat and Mass Transport and Chemical Kinetic Rate Limitations during Coal Rapid Pyrolysis, 20th Symposium (Int) on Combustion, to be published.
10. Freihaut, J.D., A Numerical and Experimental Investigation of Rapid Coal Pyrolysis, Ph.D. Thesis, Pennsylvania State University, (1980).
11. Solomon, P.R. and Hamblen, D.G., Finding Order in Coal Pyrolysis Kinetics, DOE Topical Report for Contract No. DE-AC21-81FE05122 (1983) and Progress Energy Combustion Science, 9, 323 (1984).
12. Solomon, P.R., Hamblen, D.G., Carangelo, R.M., Markham, J.R. and DiTaranto, M.B., ACS Div. of Fuel Chem. 29, 83, (1984).
13. Best, P.E., Carangelo, R.M. and Solomon, P.R., ACS Division of Fuel Chem., 29, 249 (1984).
14. Solomon, P.R., Hamblen, D.G., Carangelo, R.M., Markham, J.R. and Chaffee, M.R., Application of FT-IR Spectroscopy to Study Hydrocarbon Reaction Chemistry, ACS Div. of Fuel Chemistry Preprints 30 (1985).
15. Merrick, D., Fuel, 62, 540 (1983).
16. Lee, A.L., ACS Div. of Fuel Chem. Preprints, 12 (3), 19 (1968).
17. Perry, R.H. and Green, D., Chemical Engineers' Handbook, 6th Edition, McGraw-Hill, NY (1984).
18. Boothroyd, R.G., Flowing Gas-Solids Suspensions, Chapman and Hall, Ltd., London (1971).
19. Solomon, P.R. and King, H.H., Fuel, 63, 1302, (1984).
20. Ballantyne, A., Chou, H.P., Orozvo, N. and Stickler, D., Volatile Production during Rapid Coal Heating, Presented at the DOE Direct Utilization AR&TD Contractors Review Meeting, Pittsburgh, PA (1983).
21. Seeker, W.R., Samuelsen, G.S., Heap, M.P. and Trolinger, J.D., 18th Symposium (Int) on Combustion, The Combustion Institute, pg., 1213, (1981).
22. Witte, A.B. and Gat, N., Effect of Rapid Heating on Coal Nitrogen and Sulfur Releases, Presented at the DOE Direct Utilization AR&TD Contractors Review Meeting, Pittsburgh, PA, (1983).

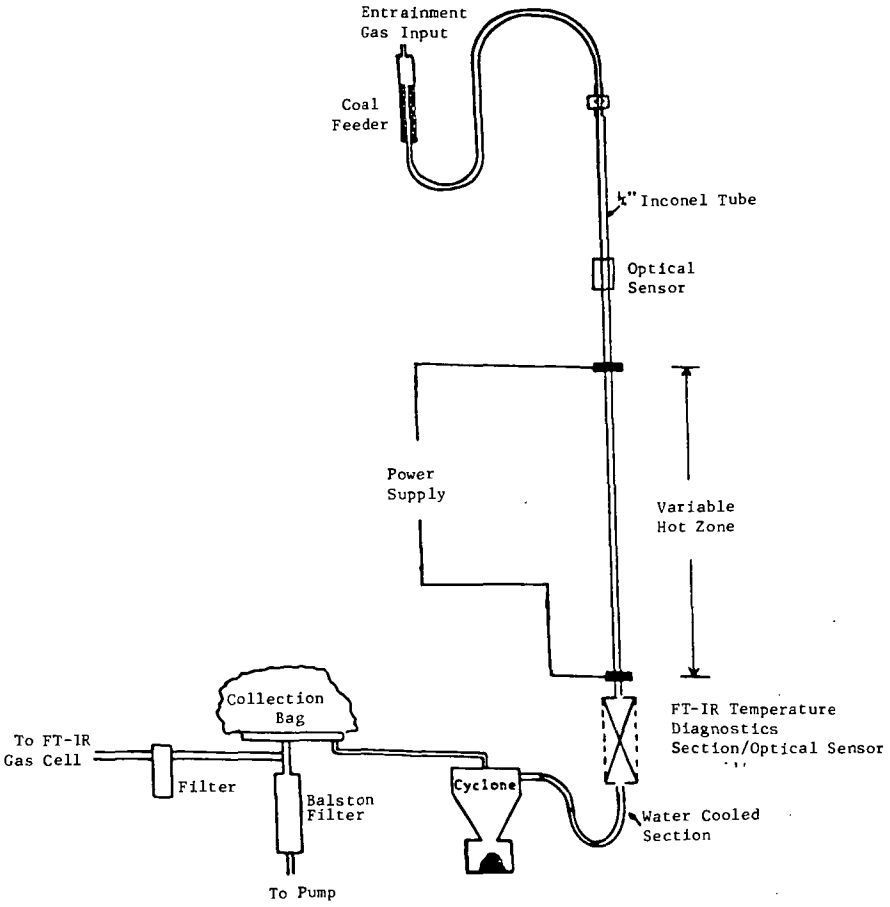

Figure 1. Schematic of Heated Tube Reactor.

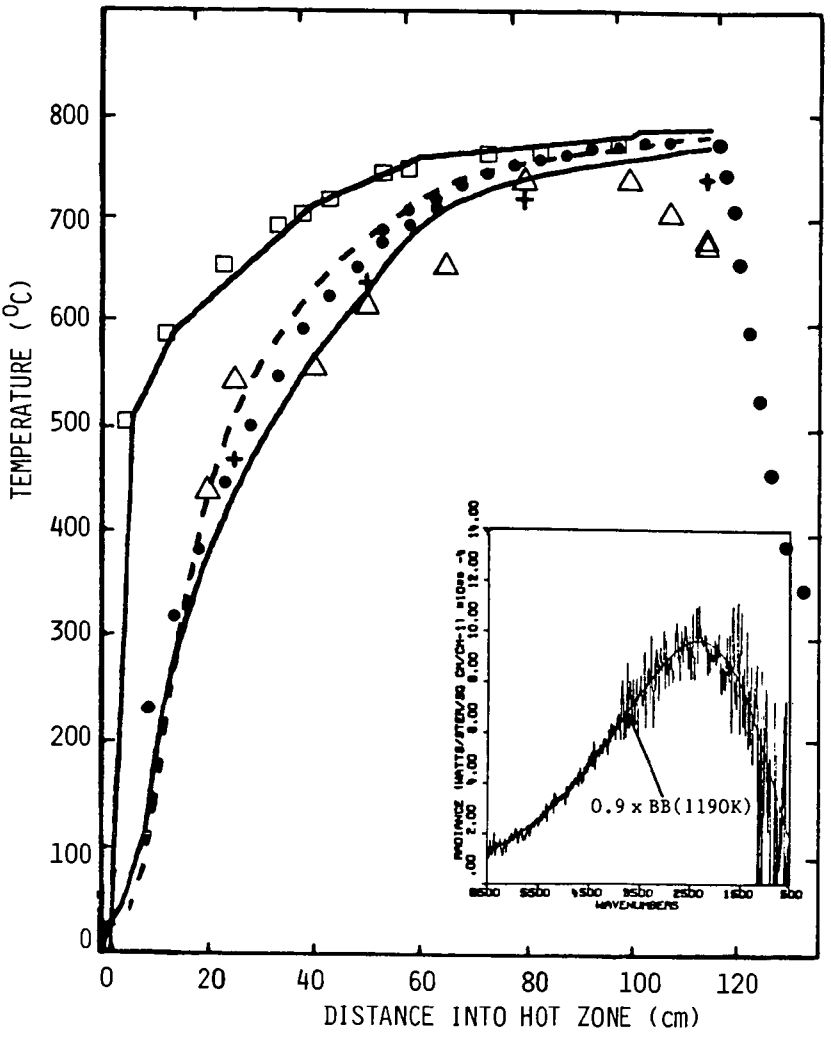

Figure 2. Measured and Calculated Temperatures in the Tube Reactor with Coal and Helium. □ Outside Tube Temperature Corrected for Heat Loss. ● Thermocouple Temperature Inside the Tube. ✚ Thermocouple Temperature at FT-IR Focal Point. △ FT-IR Temperature of Coal Particles. Upper Line is the Wall Temperature used as Input. Lower Line is the Calculated Coal Particle Temperature. Dashed Line is the Calculated Thermocouple Temperature. Insert is a Comparison of an FT-IR Normalized Emission Spectrum with a Theoretical Black-body Assuming ϵ = 0.9.

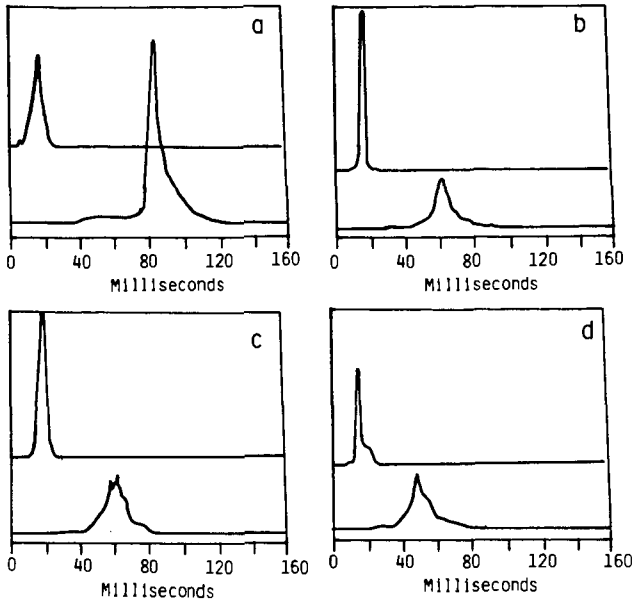

Figure 3. Phototransistor Signals Indicating Coal Particle Transit Times for 4 Electrode Positions. a) 125 cm Cold, b) 50 cm Cold, 75 cm Hot, c) 25 cm Cold, 100 cm Hot, and d) 10 cm Cold, 115 cm Hot.

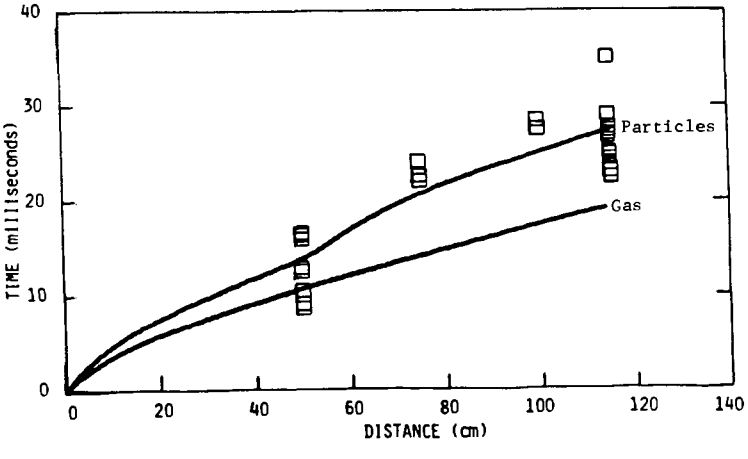

Figure 4. Measured and Calculated Particle Residence Time and Calculated Gas Residence Time in the Heated Tube Reactor. The Calculation Assumes the the Particles are at 80% of the Gas Velocity before and after Primary Pyrolysis and at 40% between 1% and 75% Weight Loss.

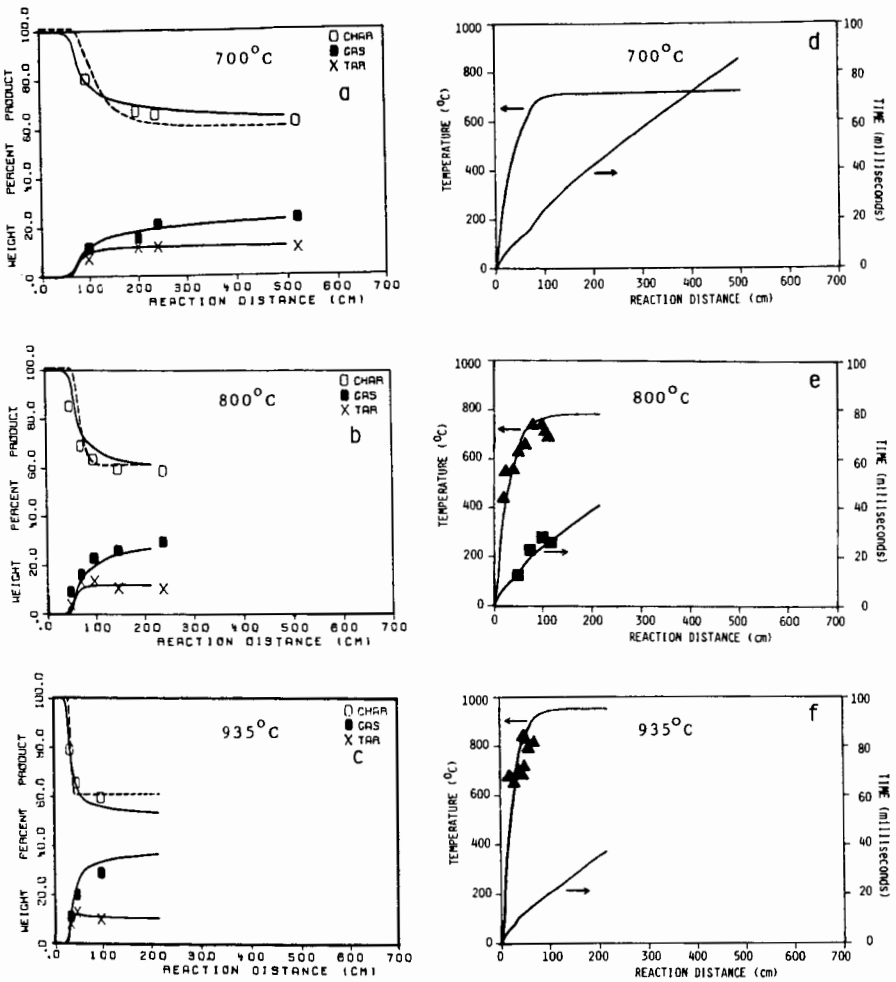

Figure 5. Pyrolysis Results Comparing the Theory and Data for Yields and Particle Time Temperature Histories. Symbols are Data, Solid Lines in a-c are from the Functional Group Model (8). The Dashed Lines are a Single Rate First Order Model. Lines in d-f are from a Heat Transfer Model.

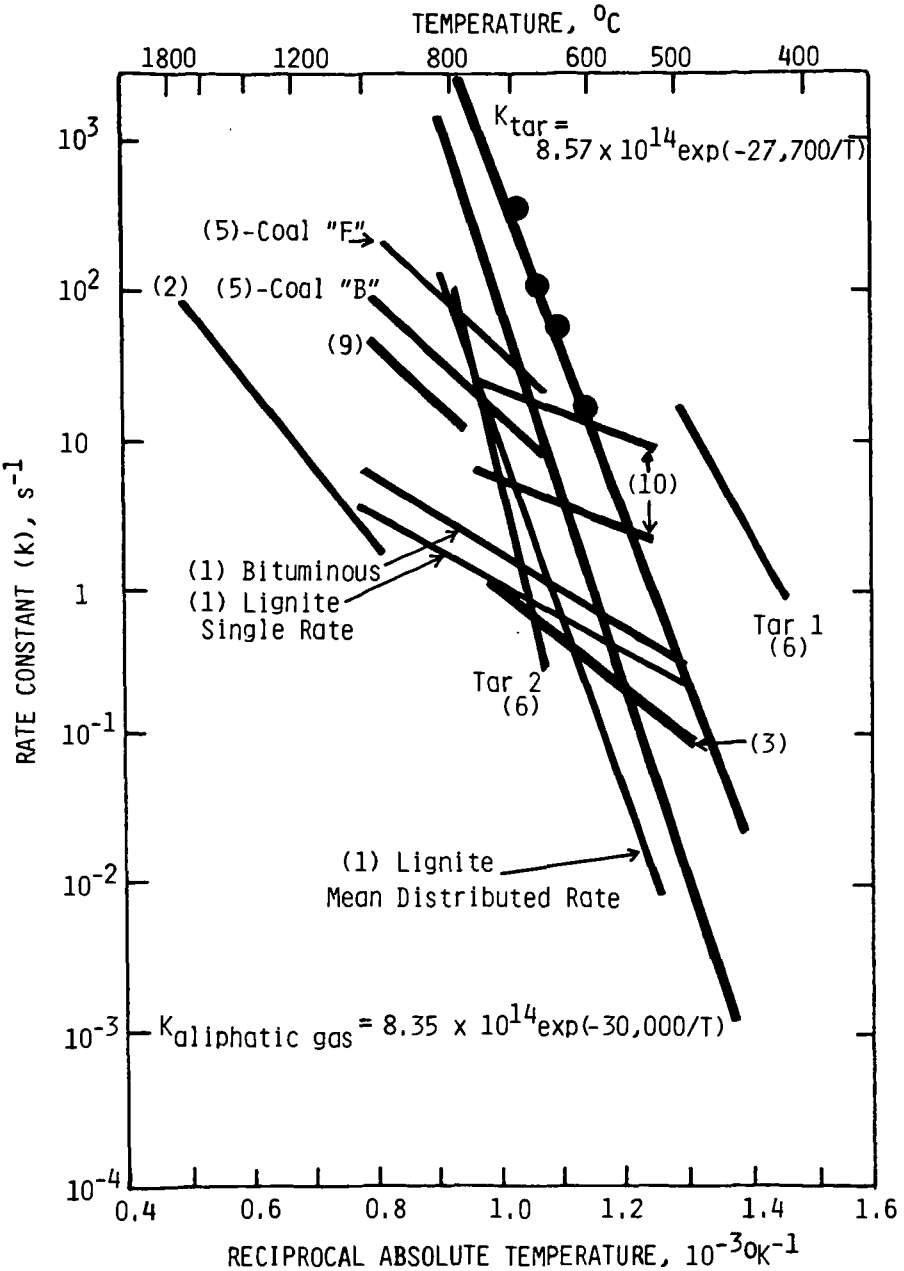

Figure 6. Comparison of Kinetic Rates for Weight Loss (or Tar Loss) from Several Investigations. The Numbers in Parentheses Indicate the Reference from which the Rates were Obtained. The Upper Lines for Reference 10 was for 53-106 μm dia. Particles, the Lower Lines was for 850-1000 μm dia. Particles. The Rates for Tar and Aliphatic Gas are those used in the Theoretical Calculation. Note that the Number in the Exponent is Roughly 1/2 the Activation Energy.

REACTIVITY IN AIR OF CHARS PRODUCED FROM A LIGNITE CONTAINING VARIOUS CATIONS

Alan W. Scaroni and Bruce A. Morgan

Fuel Science Program
Department of Materials Science and Engineering
The Pennsylvania State University
University Park, PA 16802

The combustion of coal is practiced widely throughout the world. In the United States in 1982, for example, almost 600 million tons of coal were burned for electricity production (1). Nevertheless, many fundamental aspects of coal combustion are not well understood. It has been established, however, that at least two general processes occur during combustion: pyrolysis or devolatilization of the coal due to an applied thermal stress and heterogeneous combustion of the remaining char according to carbon-oxygen reactions. The relative importance of each process to the overall combustion of a particular coal is not easy to measure experimentally and is even more difficult to predict a priori.

In the sequence of events that is coal combustion, heterogeneous char combustion, which is usually referred to as char burnout, necessarily occurs last. This has lead to the deduction that the char burnout is the rate determining step in the overall process. This argument then provides that to burn coal more effectively and efficiently, it is necessary to understand the mechanism, and thereby be able to affect the rate of the char-oxygen reaction.

While it is true that the rate of release and combustion of the volatiles in most practical systems are fast compared to the rate of the $C-O_2$ reactions, the yield of volatiles, which determines the amount of char which must be burned heterogeneously, is equally important in determining the char burnout time. Hence, an alternative to increasing the rate of the $C-O_2$ reaction is to decrease the required extent of the $C-O_2$ reaction by reducing the yield of char. Both aspects of the combustion of a range of coals have been addressed in the current project, but coverage in this paper is restricted to the properties of lignites which affect the yield of volatiles and the char reactivity, both of which may affect the overall combustion rate of lignites.

The heterogeneous reaction rate of a coal char with a reactant gas is influenced by such parameters as the inherent char reactivity, which is related to the number of carbon active sites, the rate of transport of the reactant gas to the active surface area and the presence of potentially catalytic inorganic species. Jenkins et al. (2,3) have shown that the air reactivity of coal chars is dependent upon the pyrolysis conditions under which the chars were prepared. As the severity of the pyrolysis conditions was increased, the number of carbon active sites in the char was found to decrease, hence, the reactivity decreased. In addition, coal char reactivity was shown to be rank dependent; chars produced from lignites being more reactive than those from higher rank coals.

The high reactivity of lignite chars has been attributed, in part, to the presence of ion exchangeable cation on the original coals. These are predominantly alkali and alkaline earth metals (4), some of which are excellent catalysts for the $C-O_2$ reaction (5,6). Their presence on low rank coal chars, as distinct from discrete mineral phases, has been shown to increase reactivity (7). However, as the severity of the pyrolysis or reaction conditions increases, the metals lose their catalytic activity due primarily to a loss of dispersion via sintering. This occurs as the holding time at temperature or the reaction temperature itself

increases (8). The objective of the current work was to determine the effect of the presence of cations, namely calcium and magnesium, on the pyrolysis of a lignite under combustion conditions and on the subsequent reactivity of partially burned chars.

Experimental

The ion exchangeable cations on a Texas lignite, PSOC 623, were removed by acid washing in 0.04 N HCl. Alkaline earth metals, Ca and Mg, were back exchanged onto the acid washed samples using 1 M metal acetate solutions. Details of the exchange procedure have been outlined previously (9). Cation contents of the prepared samples were measured by atomic absorption spectrosopy.

The raw and modified lignite samples were pyrolyzed and partially combusted in an entrained-flow reactor at an initial reactor (gas and wall) temperature of 1173 K. A description of the reactor and its mode of operation have been provided elsewhere (10).

Reactivity data were generated on chars produced under either a N_2 or air atmosphere at various residence times in the entrained flow reactor using a Fisher Thermogravimetric Analyzer (Model 260 F). The reactivities were obtained isothermally in air at atmospheric pressure and a temperature of 533 K.

For these conditions and by using only 2 mg of char spread thinly on a Pt pan, heat and mass transfer effects should not mask the reaction rate. Hence, the reported reactivities are believed to be intrinsic, chemically controlled rates. The gasification reactivities are taken from the maximum slope of the TGA recorder plot, normalized to the initial weight of dry ash free char.

Results and Discussion

The ultimate analysis of the raw lignite and the proximate analyses of the raw and modified samples are shown in Table 1. The raw lignite contained 1.8 wt% cations on a dry basis, predominantly Ca (1.4%) and Mg (0.26%) with trace quantities of Na, K, Ba and Sr. The acid washing reduced the cation content to less than 0.01 wt%. The two cation-loaded samples chosen for comparison in the present study contained 1.9 wt% Ca and 1.6 wt% Mg, respectively.

Weight Loss Rate Data

Weight loss rate data for pyrolysis in N_2 and combustion in air at 1173 K are shown in Figure 1 for raw and acid washed lignite. The same data for the Ca and Mg loaded lignite are shown in Figure 2. Details of the model for predicting residence times have been provded by Tsai and Scaroni (10). In addition, an analysis is provided which estimates particle and gas temperature excursions from the initial furnace temperature of 1173 K due to the superimposition of endothermic heats of pyrolysis and exothermic heats of combustion. The essence of the analysis is that the lignite particles are being heated to the furnace (gas and wall) temperature for at least 0.1 s. Upon ignition, particle temperatures exceed gas temperatures for a short period (< 0.1 s) by in excess of 200 K. Hence, the weight loss rate data in Figures 1 and 2 are for nonisothermal pyrolysis and combustion for about 0.15 s.

The data shown in Figures 1 and 2 have been discussed previously (9) and can be summarized as follows. The presence of ion exchangeable cations suppresses the evolution of volatiles during pyrolysis. This is attributed to an increase in secondary char forming reactions primarily involving tars. Such reactions are catalyzed by Ca and Mg (11). In an air atmosphere, however, catalysis of the $C-O_2$

reaction by Ca for a short time increases the weight loss by the Ca loaded lignite to above that of the acid-washed sample. No such rapid rate of weight loss occurs for the Mg-loaded coal since Mg is not a good catalyst for the $C-O_2$ reaction. At longer residence times, weight loss rates are similar for the raw, acid-washed and Ca-loaded samples, and sightly larger for the Mg loaded sample. This implies that catalysis of the $C-O_2$ reaction is no longer occurring. Loss of catalytic activity by Ca at high temperature has been ascribed to loss of dispersion due to sintering (7). Hence, comparing the behavior of the raw and acid washed samples, the increased weight loss due to short-lived but significant catalysis of the $C-O_2$ reaction by the presence of cations on the raw lignite simply compensates for the reduced yield of volatiles because of their presence.

TGA Reactivity Data

Maximum reactivities in air at 533 K of partially combusted chars are shown in Figure 3 as a function of weight loss in the entrained flow reactor. For each form of the lignite, reactivities decrease with increasing weight loss in the reactor up to about 85-90%. For higher weight losses, reactivities are low and approximately constant at < 0.1 mg/mg h. A decreasing reactivity indicates a loss of carbon active sites, whereas a constant reactivity may indicate a constant active site concentration or control of the reaction rate by oxygen diffusion to the active surface area though an ash barrier formed from the mineral matter in the coal.

Maximum char reactivities at 50, 75 and 90% weight loss and the time required to reach each level of weight loss for the variously treated lignites are given in Table 3. Note that 50% weight loss exceeds the level reached by pyrolysis in N_2. For residence times less than 0.10-0.13 s, reactivities at each level of weight loss decrease in the order Ca > Raw > Mg > acid-washed. This is in accordance with the order predicted by catalysis of the $C-O_2$ reaction. For residence times greater than 0.10-0.13 s, reactivities are low and approximately the same. This implies an absence of significant catalysis, possibly due to temperature induced sintering of the metals. Ignition of the particles with an attendant temperature increase occurs within this time range.

The significance in relating TGA reactivity data to weight loss in the entrained flow reactor is seen by comparing the data in Table 3 for the cation containing samples. After a weight loss of 50%, reactivities decrease in the order Ca > Raw > Mg while the additional time required to reach 90% weight loss in the entrained flow reactor increases in the order Ca < Raw < Mg. In this region of the weight loss curve where heteogeneous char combustion is occurring, catalysis of the $C-O_2$ reaction may be important implying that chemical reactivity controls the weight loss rate. Although different conditions prevail, TGA data may give a qualitative indication of behavior in this region. It is difficult to interpret the data for the acid washed lignite in this manner, however. Work is continuing to explain this apparent anamoly.

For residence times greater than 0.13 s in the entrained low reactor, which correspond to weight losses in excess of 85-90%, weight loss rates are low and approximately constant at 3.8×10^{-4} g/cm^{2}s (expressed per unit external surface area). There is no apparent effect of the presence of cations in this region of the weight loss curve. It has been suggested previously that this may indicate physical rate control of the reaction mechanism (9). The TGA reactivity data can now be used to help determine the reaction Zone.

TGA reactivities at 533 K for these chars were approximately constant at 6.1×10^{-9} g/cm^{2}s. Extrapolating these data to the entrained-flow reactor operating temperature of 1173 K using the Zone II Activation Energy of 21.7 kcal/mole as determined by Young (12), produces a reactivity of 4.4×10^{-4} gm/cm^{2}s. This is

similar to the experimentally measured reactivity of 3.8×10^{-4} g/cm^{2}s, and is considerably less than the value calculated for Zone III control, 7.7×10^{-2} g/cm^{2}s.

Arrhenius parameters are currently being generated in the TGA for the C-O_2 reactions appropriate for the current chars. This will eliminate the need to use Arrhenius parameters generated by others. However, if the data of Young are appropriate for use in this situation, the implication is that the same reaction zone does not exist in the TGA and entrained flow reactor, the former being Zone I, and the latter Zone II.

Summary

TGA reactivity data of partially combusted chars have been used to elucidate the char burnout stage of pulverized coal combustion. The absence of a significant effect of cations on char reactivity at high levels of burnoff implies the absence of catalysis of the C-O_2 reaction. This was ascribed to sintering of the metal cations following ignition. The char particles then burn out slowly under Zone II control, the chars having relatively low inherent reactivities.

Acknowledgments

The lignite was supplied by W. Spackman from the PSU-DOE Coal Sample Bank and Data Base. Financial support for Bruce Morgan was obtained from the Coal Cooperative Program and MRI Fellowship Program at Penn State.

Literature Cited

1. Annual Energy Review, 1983, Energy Information Administration, DOE/EIA-0384(83), April 1984.

2. Jenkins, R. G., Nandi, S. P., and Walker, P. L., Jr., Fuel, 52, 288, 1973.

3. Radovic, L. R., Walker, P. L., Jr., and Jenkins, R. G., Fuel, 62, 849, 1983.

4. Morgan, M. E., Jenkins, R. G., and Walker, P. L., Jr., Fuel, 60, 189, 1981.

5. McKee, D. W., Fuel, 62, 170, 1983.

6. Walker, P. L., Jr., Matsumoto, S., Hanzawa, H., Muira, T., and Ismail, I. M. K., Fuel, 62, 140, 1983.

7. Radovic, L. R., Ph.D. Thesis, The Pennsylvania State University, 1982.

8. Radovic, L. R., Walker, P. L. Jr., and Jenkins, R. G., J. Catal., 82, 382, 1983.

9. Morgan, B. A. and Scaroni, A. W., in "The Chemistry of Low Rank Coals," Amer. Chem. Soc. Symposium Series 264, 255, 1984.

10. Tsai, C. Y. and Scaroni, A. W., AIME-SME Preprints, 336, 1984.

11. Tanabe, K., "Solid Acids and Bases," Academic Press, NY, 1970.

12. Young, B. C., in "The Chemistry of Low Rank Coals," Amer. Chem. Soc. Symposium Series, 264, 243, 1984.

Table 1
ULTIMATE AND PROXIMATE ANALYSES FOR THE RAW AND MODIFIED LIGNITE

Ultimate Analysis

	C	H	N	S	O (by diff)
% (daf)	70.1	5.0	1.7	1.4	21.8

Proximate Analysis

	% H_2O	% Ash (dry)	VM(daf)
Raw	10.8	15.9	59.7
Acid Washed	7.8	10.7	54.9
Ca Loaded	5.3	13.7	57.6
Mg Loaded	6.8	12.0	57.1

Table 2
CATION CONTENTS OF THE RAW AND MODIFIED LIGNITE

Raw	Ca	Mg	Na	K	Ba	Sr	Total	Acid Washed	Ca Loaded	Mg Loaded
wt % (dry)	1.4	0.26	0.03	0.03	0.03	0.02	1.8	<0.01	1.9	1.6
meq/g (dry)	0.7	0.2	0.01	0.01	0.002	0.002	0.9	~0	1.0	1.3

Table 3

TIME TO REACH AND MAXIMUM CHAR REACTIVITIES AT VARIOUS LEVELS OF WEIGHT LOSS IN ENTRAINED FLOW REACTOR AT 1173 K

Weight Loss in Entrained Flow Reactor at 1173 K	Maximum Char Reactivity, mg/mg h (daf) (Time to reach weight loss, ms)			
	Ca-loaded	Raw	Mg-loaded	Acid-washed
50	2.1 (80)	0.8 (65)	0.6 (90)	0.4 (50)
75	1.2 (95)	0.7 (85)	0.4 (125)	0.3 (70)
90	<0.1 (110)	<0.1 (145)	<0.1 (290)	0.1 (140)

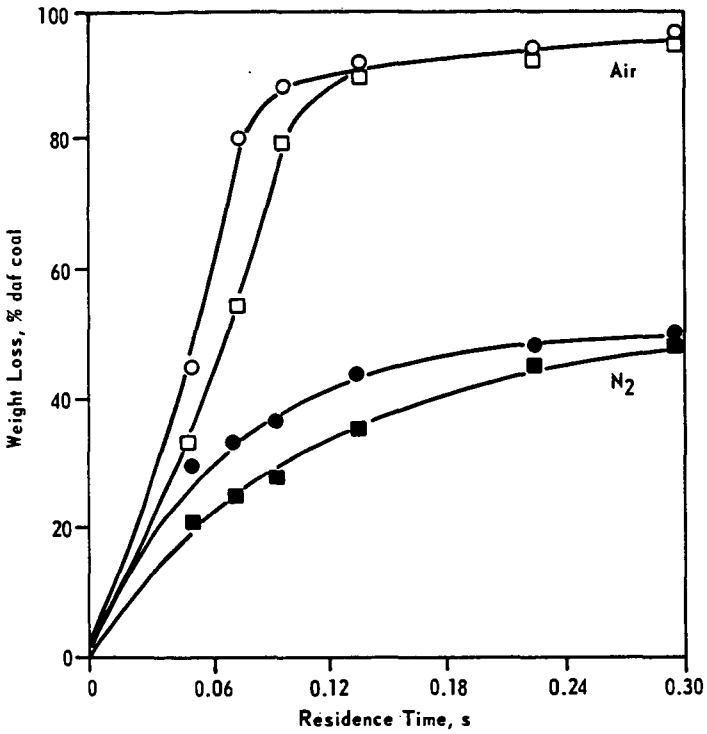

Figure 1. WEIGHT LOSS RATE IN AIR AND N_2 FOR RAW (□,■) AND ACID-WASHED (○,●) LIGNITE IN ENTRAINED FLOW REACTOR AT 1173 K

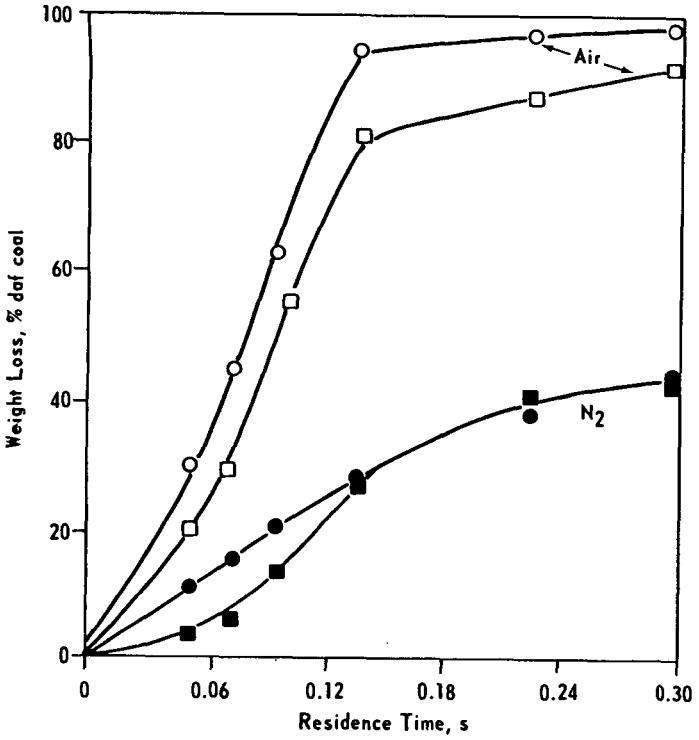

Figure 2. WEIGHT LOSS RATE IN AIR AND N_2 FOR Ca (○,●) AND Mg (□,■) LOADED LIGNITE IN ENTRAINED FLOW REACTOR AT 1173 K

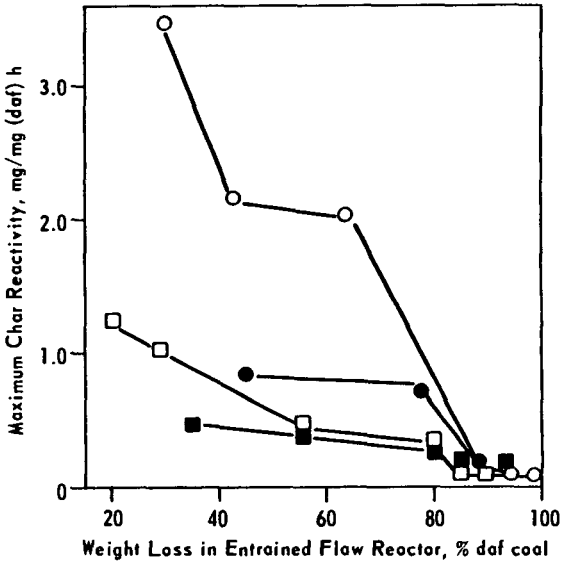

Figure 3. TGA REACTIVITIES IN AIR AT 533 K OF CHARS PRODUCED FROM Ca-LOADED (○), RAW (●), Mg-LOADED (□) AND ACID WASHED (■) LIGNITE AS A FUNCTION OF WEIGHT LOSS BY PARTIAL COMBUSTION IN ENTRAINED FLOW REACTOR AT 1173 K

A COMPARISON OF CO_2 AND O_2 GASIFICATION OF GLASSY CARBON

S. R. Kelemen
H. Freund
Exxon Research and Engineering Company
Clinton Township
Route 22 East
Annandale, New Jersey 08801

Abstract

O_2 is known to be much more reactive then CO_2 toward carbon. We have separated and studied with surface spectroscopies the dissociative adsorption step from the CO formation step in the O_2 and CO_2 gasification of glassy carbon. The reactive adsorption probabilities decreased with increased coverage. At high coverage the derived activation energy for O_2 dissociation was 33 kcal/mole and 50-60 kcal/mole for CO_2. The CO formation energy decreased from 90 kcal/mole at very low coverage to 70 kcal/mole at high coverages. The steady state oxygen coverage during CO_2 gasification corresponded to these high coverages with a measured activation energy of 67 kcal/mole. CO formation energetics limit the rate of CO_2 gasification. The increased gasification activity for O_2 is associated with a more facile gaseous dissociation step causing higher oxygen coverages which in turn generates lower energy CO formation sites.

I. INTRODUCTION

It is widely recognized that O_2 has a much higher reactivity than CO_2 toward carbon; this difference has been kinetically quantified to be 10^5 greater at 800K and 0.1 atm pressure (1). Despite this large reactivity difference the responsible elementary processes on the carbon surface are not well understood. Oxidation and gasification reactions of carbon are a class of very difficult reactions to characterize and quantify. Gasification reactions are sensitive to the type of carbon being gasified (2). A better understanding of these systems could be achieved by detailed physical characterization of the external surface of a given carbon coupled to adsorption and reactivity studies of the reactant gases (2-4). The application of surface sensitive probes to this area is an essential component to approach the problem. These results are used to interpret observations of steady state reactivity.

II. EXPERIMENTAL

Experiments were performed in an ultra-high-vacuum spectroscopy chamber with a base pressure lower than 2×10^{-10} Torr. Auger electron spectroscopy (AES) was performed with a double-pass cylindrical mirror analyzer using a 2.2 keV primary beam energy and 2V peak to peak voltage modulation.

The amount of oxygen was determined using AES. The overall amplitude of the dN(E)/dE oxygen (510 eV) to carbon (272 eV) was taken as the measure of oxygen surface concentration. A linear absolute coverage scale which corresponds to the AES O/C ratios was previously estimated and used in other studies on carbon surfaces (5-7). A coverage of one oxygen per surface carbon atom $\Theta_{oxygen} = \Theta = 1$ gives a AES O/C value of 0.25. We will self consistently apply this same coverage scale throughout the course of this study.

The glassy carbon samples were cut from plates obtained from Atomergic Chemetals and were outgassed at 1300°C in UHV prior to use. The presence of small amounts of very strongly bound oxygen could be reduced further by heating to higher temperatures, but this did not significantly effect the CO_2 and O_2 chemistry at high oxygen coverages. Further details of the characterization of the glassy carbon substrates can be found elsewhere (6). This procedure removed oxygen which was the principal contaminant measured by AES. The initial AES carbon to oxygen ratio was near 0.01. This represents a small amount of very strongly bound oxygen.

III. RESULTS

We have characterized the glassy carbon surface using ultraviolet photoemission spectroscopy following oxygen uptake from O_2 and CO_2 at 300°C. Previous UPS studies of atomically clean glassy carbon surfaces show enhanced electron emission near the Fermi level (6). This is associated with the presence of unsaturated surface carbon valences, "dangling bonds". These levels are removed upon chemically bonding to oxygen. Emission within 3 eV of the Fermi level decreases on glassy carbon as these levels become involved in bonding to oxygen (6). The emission from oxygen 2p levels was found between -4 and -11 eV following exposure to either O_2 or CO_2. Features which could be identified with molecularly adsorbed O_2 or CO_2 were absent. The similarity between O_2 and CO_2 suggest that the dissociation of CO_2 gives rise to surface oxygen and gaseous CO at 300°C. UPS thus gives us an indication that O_2 and CO_2 dissociation predominates under our conditions in these adsorption systems. This agrees with the conclusion reached for O_2 adsorption on graphon based on thermal desorption and isotope labeling studies (8).

XPS was also used to characterize the oxidized carbon surface. The O(1s) XPS signals following 300°C oxidation by O_2 and CO_2 showed a peak at 532 eV binding energy. The carbon (1s) peak for clean glassy carbon occurred at 284.2 eV. Following oxygen uptake from either O_2 or CO_2, there was a slight increase in emission at lower binding energies. The carbon (1s) peak did not, however, possess a 288.5 eV binding energy component which is associated with carbon coordinated to multiple oxygen atoms as in a carboxylic functionality (9-12). These results also indicate that similar oxygen functionalities were produced by CO_2 and O_2 at 300°C, and these are likely to be surface carbon atoms coordinated to one oxygen.

We have measured the increase in the oxygen AES signal following CO_2 and O_2 exposures at 300°C. We used a maximum temperature of 300°C in order to achieve high oxygen surface coverages but also to limit complications introduced by in situ gasification of carbon (13). The maximum oxygen coverages generated from O_2 and CO_2 corresponded to θ_o = 0.85 and 0.45 respectively. The adsorption processes were placed in quantitative terms. The efficiency of reactive adsorption as a function of the amount of oxygen already present was obtained from the incremental changes of oxygen coverage with the interval of exposure to either CO_2 or O_2 at 300°C. The efficiencies were calculated for increasing intervals of one decade of exposure. Figure 1 shows these results on glassy carbon as a function of oxgyen coverage. The adsorption process is characterized by relatively rapid initial uptake on the order of 10^{-4} efficiency for both gases up to approximately θ_o = 0.1 oxygen coverage. Above this coverage, there is a rapid decrease to 10^{-10}. Further exposure to O_2 will increase the oxygen coverage. The adsorption coefficient declines with coverage from 10^{-10} to 10^{-12} from θ_o = 0.25 to θ_o = 0.85. At higher coverages the behavior of O_2 and CO_2 begin to depart. CO_2 was limited in the amount of oxygen which could be deposited under these conditions. The decline in the coefficient for CO_2 was more rapid with coverage and decreased to below 10^{-14} near half monolayer coverage. Presumably, the coefficient declines further for CO_2 at higher coverages, but we were unable to measure slower processes.

The AES oxygen thermal stability profile was measured on glassy carbon following O_2 and CO_2 oxidation at 300°C. Figure 2 shows that the surface oxygen concentration remains nearly constant up to 600°C in both cases. Between 600 - 700°C, the surface oxygen coverage begins to decrease for the O_2 oxidized surface, yet for CO_2 the coverage still remains almost constant. Above 600°C CO was the dominant desorption product. Above 800°C there were similar reductions in oxygen coverage in both cases. CO evolves from the surface over a very wide range of temperature.

The CO formation energies were determined from the rate of change of oxygen coverage with time during heating in UHV by assuming first order kinetics and a frequency factor of 10^{13}. This formalism provides a framework to estimate the desorption energy. The results are shown in Figure 3. They are plotted as a function of oxygen coverage based on the common AES coverage scale as previously defined. The oxygen coverage dependency of the formation energy is similar for the surface oxgyen derived from O_2 and CO_2 adsorption. At low oxygen coverages, θ_o = 0.25, the energy decreases from 95 to 80 kcal/mole. The formation energy exhibited much smaller changes with coverage at the higher coverages. O_2 adsorption produced higher oxygen coverages. The energy ranged between 80 - 70 kcal/mole between θ_o = 0.25 to 0.85. CO_2 coverage was limited to θ_o = 0.4 but between θ_o = 0.25 , and 0.4 the energies were similar as with O_2. The CO formation energy decreases with increasing oxygen coverage.

IV. DISCUSSION

The adsorption of O_2, and CO_2 on glassy carbon surfaces were examined using AES. The study was restricted to carbon surfaces that had been previously outgassed in UHV at elevated temperature and characterized with surface sensitive techniques. In this way we were able to directly compare two gases which have widely different gasification activities.

There have been few adsorption studies on well-characterized, clean carbon surfaces. Original studies of oxygen adsorption on clean "paracrystalline" carbon (15) and sputter-damaged graphite surfaces (16) have shown complex adsorption behavior. The rate of uptake was characterized by coverage regions having a linear dependence with the log of exposure. This was interpreted as evidence for many discrete types of adsorption sites. It is believed that different oxygen adsorption sites exist on carbons with different thermal stabilities (2). Unfortunately these early studies did not relate adsorption to subsequent reactivity. A more recent study of O_2 on the edge surface of graphite has shown a strong oxygen coverage dependence on the reactive adsorption efficiency (7) similar to these original studies even though the edge surface of graphite has a limited amount of site heterogenity (14). Corrolated thermal stability studies of oxygen enabled estimates of the energetics of product formation. The values that were obtained on the edge graphite surface were dependent on the oxygen coverage (10). The thermal stability of oxygen on carbon for a given site is then sensitive to the amount of nearby oxygen already present. In this study we have compared the rate of oxygen uptake from O_2 and CO_2 at 300°C on glassy carbon and have measured the thermal stabilities of the resultant oxidized surfaces.

The maximum oxygen uptake from O_2 at 300°C on glassy carbon represented adsorption over a majority of the surface. A high absolute oxygen coverage was achieved. We observed a similar pattern of oxygen uptake on the edge surface of graphite 300°C (7) as on the glassy carbon samples. The similarity of the high coverage oxygen chemisorption results on the edge surface of graphite and glassy carbon is an indication that the sites on the less ordered carbon surface are actually chemically very close to those on the edge graphite surface. Although physically these surfaces are very different, microscopically their behavior is much the same.

Differences exist between O_2 and CO_2 uptake at 300°C. Under our conditions the absolute oxygen coverage reached nearly a monolayer using O_2 at 300°C. Exposure to CO_2 under the same conditions resulted in oxygen uptake only to one half monolayer coverage. Herein lies a significant difference between O_2 and CO_2 reactive chemisorption at 300°C. After saturation of the small number of very active sites, the adsorption efficiency of CO_2 and O_2 is approximately 10^{-10}. O_2 is able to sustain this efficiency to high coverages. The efficiency drops to 10^{-14} for CO_2 before a half monolayer oxygen coverage can be achieved. The adsorption efficiency must drop many more orders of magnitude for CO_2 at higher oxygen coverage.

The thermal stability studies in UHV for the resultant 300°C oxidized surfaces yielded estimates for the energetics of product formation. The energetics are related to the absolute oxygen surface coverage. The energies are similar at constant absolute oxygen coverage for oxygen generated from either O_2 or CO_2. The energies increase with decreasing oxygen coverage going from 75 kcal/mole at θ_o = 0.4 to 95 kcal/mole at θ_o = 0.05 coverage. Under our conditions, O_2 is capable of generating higher oxygen coverages, and the CO formation energy decreases to 70 kcal/mole at the highest coverage.

The adsorbed oxygen species are strongly bound. The observation of large heats of adsorption and low adsorption efficiencies (10^{-10} -10^{-14}) imply a substantial energy barrier for adsorption. We can estimate the barriers for adsorption for CO_2 and O_2 at several oxygen coverages by assuming a Boltzman energy distribution and the temperature of the gas equal to the surface temperature. At θ_o = 0.1 this yields a barrier height of 13 and 15 kcal/mole for O_2 and CO_2 respectively. At θ_o = 0.4 we find that the barrier increases to 25 kcal/mole for O_2 and 35 kcal/mole for CO_2. At θ_o = 0.9 the value increases to 33 kcal/mole for O_2. The value for CO_2 must be substantially greater at this high oxygen coverage. Estimates based on adsorption efficiencies at higher surface temperatures of CO_2 exposure as well as extrapolation of the efficiencies at 300°C to θ_o = 0.9 yield barriers in the range of 50 - 60 kcal/mole. Marsh has used an energy-reaction coordinate diagram to help illustrate the kinetics of adsorption and CO formation (2). We have been able to quantify parts of this diagram which we just described and are also illustrated in Figure 5 for the reaction of glassy carbon with CO_2 and O_2 to form CO.

Higher oxygen concentrations can be developed (13) by oxidation of carbon with O_2 above 400°C but this leads to in situ gasification and complicates the reaction-energy coordinate diagram. We have observed CO and CO_2 as gaseous products during thermal desorption of glassy carbon oxidized above 400°C in O_2. There are several possible origins for CO_2 production. Some carboxylic groups may be produced by O_2 at very high oxygen coverages. Studies (17) of nitric acid oxidized glassy carbon indicate that CO_2 can be produced from decomposition of carboxylic oxygen functionalities. The decomposition of surface carboxylic groups to form CO_2 will complicate the O_2 reaction with carbon. Another possible route at high oxygen coverages is the formation of CO with consecutive oxidation by surface oxygen to CO_2. Indications are that formation energy for CO declines further below 70 kcal/mole at very high oxygen coverages (7) but CO_2 eventually becomes a competitive reaction route. We have minimized the complications of CO_2 formation from O_2 oxidation in our studies by limiting the concentration of surface oxygen.

Activation energy for the O_2 adsorption step has been estimated at higher temperatures and presumably higher coverages and tends to higher values. Lussow et al. (13) report an activation energy of 29 kcal/mole for O_2 adsorption between 450°C and 675°C. In carbon gasification studies a value near 38 kcal/mole has been reported for the O_2 adsorption step.[18,19] Our

results at lower coverages show that the barrier for adsorption is greater for CO_2 than for O_2 at a given oxygen surface coverage and that the barrier increases for both gases as the oxygen coverage increases. The values reported for O_2 at high temperatures are of the same order that we find at high oxygen coverages in our studies.

The differences in adsorption behavior of CO_2 and O_2 at high oxygen coverages must be related to the much greater gasification activity for O_2. Our data suggest that CO_2 and O_2 produce similar kinds of adsorbed oxygen species at low and medium coverages. This is most likely carbonyl type oxygen functionality, carbon which is coordinated to one oxygen. The stability of this kind of oxygen is dependent on the amount already present. This can be interpreted as oxygen bound to one carbon having the ability to modify the energetics of the interaction of neighboring free carbon sites with oxygen and CO_2. At higher coverages, there are pronounced differences between CO_2 and O_2. The adsorption barrier for CO_2 relative to O_2 increases with increasing oxygen coverage, while the stability of the adsorbate decreases and gasification to CO becomes more facile. The observations suggest that the energy barrier for oxygen adsorption from O_2 is much lower than for CO_2 for sites which have lower subsequent CO formation energetics. At high oxygen coverages, the magnitude of the adsorption barrier increases while the energetics of gaseous product formation declines. For both CO_2 and O_2 at a given reaction temperature a steady state situation will develop. At higher temperatures the reaction coordinate energy diagram is thought to be one with a greater barrier for gas dissociation but a lower barrier for gaseous formation. The kinetics of CO_2 gasification of glassy carbon has been measured near atmospheric pressure above 650°C. The activation energy for CO_2 gasification was 67 kcal/mole (20). There is a correspondence between this value and the CO formation energetics that we observe at high oxygen coverages. In addition the oxygen coverages determined by AES following CO_2 gasification are also comparable. These results imply that the steady state surface situation during CO_2 gasification is close to that found for the highest oxygen coverages in this study. On the other hand greater oxygen concentration are developed with O_2. The energetics of CO_2 and O_2 dissociation under gasification conditions will be different and from our estimates it will be substantially lower for O_2. The increased gasification activity for O_2 is associated with a more facile gaseous dissociation step at high oxygen coverages which generates lower CO formation energy sites.

V. REFERENCES

1. P. L. Walker, Jr., F. Rusnko, L. G. Austin, Adv. Catalysis 11 (1959) 133.
2. H. Marsh, Spec. Publ.-Chem. Soc. 1977 32 (Oxygen Met. Gaseous Fuel Ind.) 133.
3. N. M. Laurendeau, Prog. Energy Combust. Sci. 4 (1978) 221 and references therein.
4. J. B. Donnet, Carbon 20 (1982) 267.
5. S. R. Kelemen and C. A. Mims, Surface Science 133(1983) 71.
6. S. R. Kelemen, H. Freund and C. A. Mims, J. of Vac. Sci. and Technol. A 2(2) (1984) 987.
7. S. R. Kelemen and H. Freund, submitted to Carbon.
8. P. L. Walker, Jr., F. J. Vastola and P. J. Hart, Fundamentals of Gas-Surface Interactions p. 307 (Academic Press, New York, 1967).
9. D. T. Clark in: Handbook of X-ray and Ultraviolet Photoelectron Spectroscopy (Heyden, London, 1978).
10. R. Schlogl and H. P. Boehm, Carbon 21 (1983), 345.
11. A. Ashitani, Carbon 19 (1981) 269.
12. T. Takalagi and A. Ashitani, Carbon 22 (1984) 43.
13. R. O. Lussow, F. J. Vastola dn P. L. Walker, Jr. Carbon 5 (1967) 591.
14. S. R. Kelemen and C. A. Mims, Surface Science, 136 (1984) L35.
15. P. J. Hart, F. J. Vastola and P. L. Walker Jr., J. Colloid Interface Sci. 32 (1970) 187.
16. M. Barber, E. L. Evans and J. M. Thomas, Chem. Phys. Letl. 18 (1973) 423.
17. S. R. Kelemen and H. Freund, unpublished results
18. P. L. Walker Jr., Carbon 18 (1980) 447.
19. P. F. Lewis and G. A. Simons, Combustion Sci. Tech. 20 (1979) 117.
20. H. Freund, submitted to Fuel.

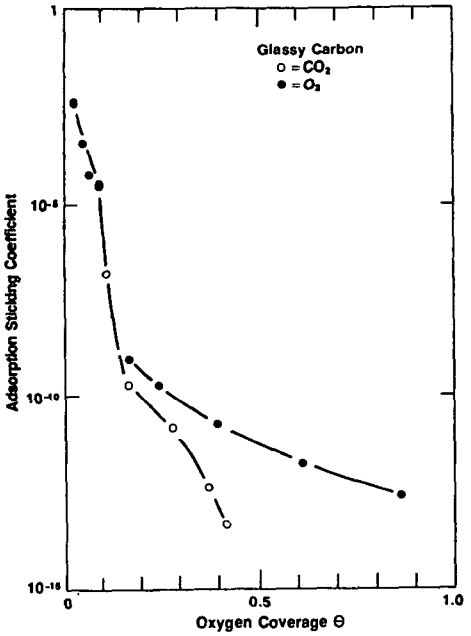

Figure 1: Reactive adsorption efficiency for O_2 and CO_2 as a function of the amount of oxygen already present on the glassy carbon surface held at 300°C.

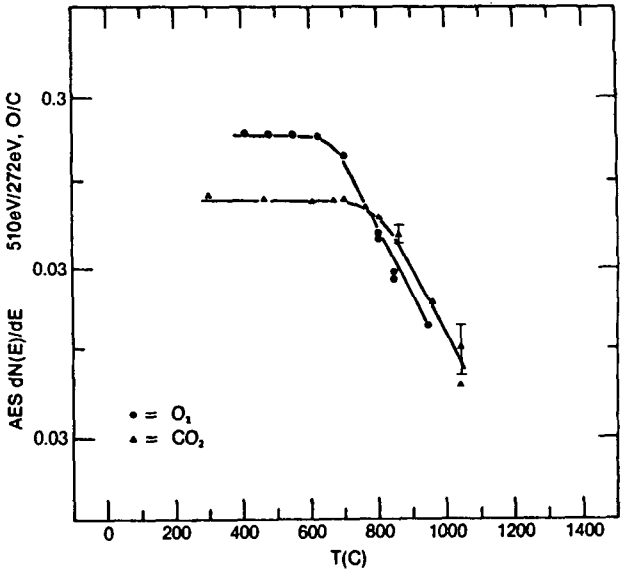

Figure 2: Oxygen AES signal after O_2 and CO_2 oxidation at 300°C and following heating in UHV for 300 sec at each data point.

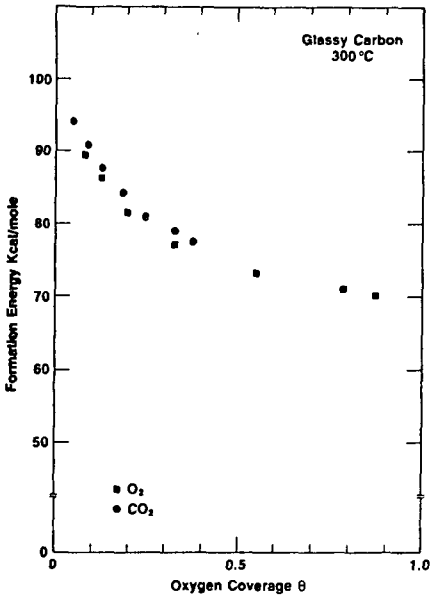

Figure 3: Formation energy of gaseous CO product as a function of oxygen coverage after O_2 and CO_2 oxidation at 300°C.

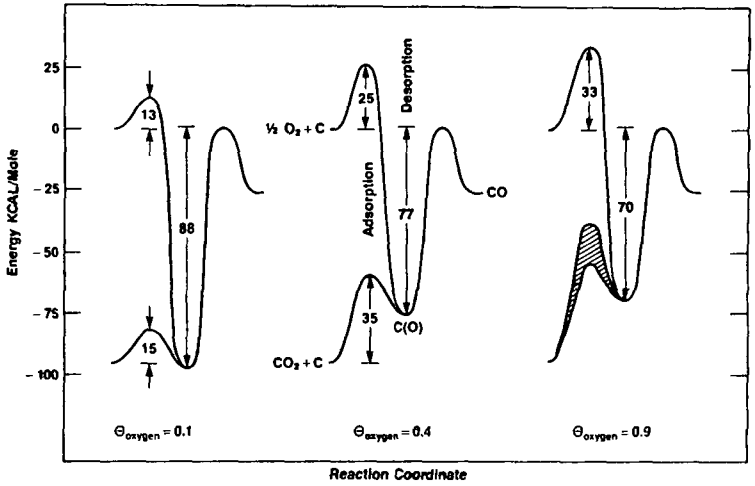

Figure 4: Energy - reaction coordinate diagram at different oxygen surface coverages in the reaction of CO_2 and O_2 with glassy carbon to form CO.

TRANSIENT KINETIC STUDIES OF CHAR REACTIONS: GASIFICATION IN STEAM-ARGON MIXTURES

J.M. Calo, R. Ganapathi, and S.E. Ellison

Division of Engineering
Brown University
Providence, RI 02912

I. INTRODUCTION.

In our laboratory we have been engaged in the study of the gasification behavior of chars using a transient kinetic approach. Previous work [1,2] concentrated on the development of the experimental techniques and carbon dioxide gasification. In the current communication we present some of our most recent data on the kinetic behavior of char gasification in steam-argon mixtures, and in so doing attempt to point out some of the significant advantages of transient techniques in studying the reactive behavior of chars, and in obtaining fundamental data.

The basis for this approach lies in the observation that the transient response of a reaction system to a perturbation in one or more of its state variables exhibits certain characteristics which are reflective of the "true" nature of the reaction mechanism under the appropriate experimental conditions. In comparison, steady-state rate measurements reveal relatively little concerning the detailed sequence of elementary steps that constitutes the "intrinsic" reaction mechanism. Thus, transient response data can be used in a qualitative sense to discriminate among competitive kinetic models. In addition, once an appropriate kinetic model has been identified, quantitative analysis of the transient data, using multiparameter estimation techniques, yields the model parameters. Moreover, the steady-state data, obtained at the end of each transient experiment, are available as well. The overall result of this approach is a more robust model of the reaction system under investigation.

II. EXPERIMENTAL.

A simplified schematic of the transient kinetic apparatus that was developed for the current experimental applications is presented in Figure 1. This system consists primarily of: (1) a continuous gas flow, fixed solids, Berty-type gradientless, isothermal reactor for carrying out the reaction under well-mixed conditions; (2) a solenoid/ control valve network for generating step function changes in feed composition; (3) a modulated, supersonic molecular beam mass spectrometer for monitoring the transient response of the composition of the gas phase at the reactor effluent; and (4) automated data logging and mass programming of the mass spectrometer utilizing a PDP 11/34-IBM 7406 device coupler combination. Additional system details and data on system performance establishing the "gradientless" nature of the reactor with respect to gas phase mixing and interphase heat and mass transport have been fully documented and are available elsewhere [3,4].

For the steam-argon gasification studies reported on here, an important modification to the original apparatus involved the addition of a steam generation system and a condenser/gas-liquid separator. The steam generator, which appears in schematic in Figure 1, consisted of a stainless steel cylindrical reservoir for feed water and a high temperature evaporator. From the reservoir, the liquid water was metered into an argon carrier stream. The water flow rate was measured with a digital flowmeter (American Flow Systems AQ 300; up to 20 cm^3/min). The combined water/argon flow was fed to an electric resistance-heated evaporator which produced superheated steam at the local thermodynamic conditions. All the upstream lines were heated and insulated to prevent steam condensation.

Various experimental considerations dictated that it was not desirable to attempt to maintain steam in the vapor phase downstream of the reactor up to the mass spectrometer sampling point. This would have involved heating and insulating the downstream lines, the adoption of another

method of flow rate measurement than the rotameters used in our previous studies, and would have created sampling problems due to the high fraction of water vapor expanding through the sampling orifice and condensing due to adiabatic cooling. Instead, therefore, it was decided to remove the bulk of the water immediately downstream of the reactor. This was accomplished using a specially-developed condenser. Insofar as the transient nature of the experiments is concerned, the introduction of any volume in the flow circuit of a magnitude comparable to that of the reactor would introduce an undesirable lag time in the system response, which if too large would tend to obfuscate the intrinsic transient response of the reactor. In addition, from an operational viewpoint it was essential to have whatever time lag that was ultimately introduced be invariant with the amount of collected liquid water in the condensate receiver. Of course, this could be accomplished by continuous removal of condensate; but this approach quickly leads to a complex control problem. Therefore, a simpler alternative approach was adopted. A baffle plate was installed at the bottom of the inlet dip tube to the condenser with circumferential slots for gas and condensate flow. In this manner, condensate could accumulate in the lower volume of the condenser, but the noncondensable fraction of the gas flow effectively "short-circuits" the condenser, immediately flowing to the outlet located in proximity, and thereby minimizing the imposed lag time. The effect of the condenser on the system transient response was measured by monitoring the exponential rise of an argon signal in the reactor effluent upon instantaneously switching this gas to the reactor feed line. Without the condenser in the flow circuit it was found, as previously [2], that the intrinsic time delay of the system was about 2 s. The effect of the condenser was the introduction of an additional additive lag time of 4 s, thereby making the new total system lag time about 6 s, which was found to be invariant with the liquid water level in the condensate receiver. This lag time proved to be of no practical consequence in the analysis of the data.

III. EXPERIMENTAL PROCEDURES.

The two gas phase product species that were monitored with the molecular beam mass spectrometer during the course of the transient experiments were CO (m/e=28) and H_2 (m/e=2). Automatic mass programming allowed alternate monitoring of these two species at a sampling frequency of about 1 Hz (0.5 Hz each), which was sufficient for the experiments conducted. (It is noted that the limiting factor in the current configuartion is not the mass programming, but rather the characteristic time of the lock-in amplifier which was used to extract the modulated portion of the signals.) Water, although also present in the sampled product gas, was not monitored, since the m/e=18 signal simply corresponded to the saturation vapor pressure of water at room temperature, the bulk of the water having been removed upstream in the condenser.

Since all the species of interest here are also normally present in the background of the oil diffusion-pumped mass spectrometer vacuum envelope, to a greater or lesser degree, it was important to insure that the mass spectrometer signals corresponded to the instantaneous composition of the gas phase at the sampling orifice, and were not being influenced primarily by the background. A modulated beam technique was employed for this purpose. The gas at the sampling point was expanded through a 25 μm diameter orifice into the first stage of a two-stage, differentially pumped vacuum system. In this stage (maintained ca. 1×10^{-4} torr) the expansion was cored by a 200 μm diameter, 60^0 conical skimmer, and admitted into the second, mass spectrometer stage (maintained ca. 5×10^{-7} torr). In this stage the beam was mechanically modulated with a 200Hz tuning fork chopper, and then passed through the ion source of the quadrupole mass spectrometer. The signal for each mass peak was then processed through a lock-in amplifier which extracted the rms value of the 200 Hz modulated signal only, thereby discriminating against the background contribution to the total signal. Mass discrimination in the sampled flow due to the jet expansion was found to be small [3], most probably due to sampling into the second stage while the beam was still relatively under-expanded.

In order to insure that the CO and H_2 signals observed with the mass spectrometer could be entirely attributed to the steam-carbon reaction occurring within the reactor, a series of "blank" transient experiments was performed using steam-argon mixtures with non-porous glass beads in the solids basket in lieu of char. Two different reactor space times, 12 s and 18 s, were used. For each space time, experiments were performed at total pressures of 1.0, 1.3, and 2.0 MPa, and steam contents by volume of the steam-argon feed mixture of 50 and 70%. The char bed temperature in all cases was about 740 °C. No significant trace of either species was observed under these conditions. Thus, it was concluded that the CO and H_2 observed during the course of the transient gasification experiments originated from the steam-carbon reaction.

Another experimental concern related to the gas phase composition involved the water-gas shift reaction. This reaction is exothermic and thermodynamically favored under conditions of high steam partial pressure in the presence of CO to produce CO_2 and H_2. It has been reported that this reaction is approximately at equilibrium at temperatures of 800°C and above in coal gasification systems [5]. However, it can be kinetically limited and, therefore, rather slow, unless it is appreciably catalyzed by impurities in the char. Insofar as the current experiments are concerned, its relative importance can be readily assessed by monitoring CO_2. Although we examined the m/e=44 signal during the course of our scoping studies, no appreciable modulated signal was observed. Thus, under the current experimental conditions, the practical effects of this reaction seem to be minimal.

Transient experiments were conducted by first establishing the reactor temperature and pressure under a continuous pure argon purge. The flowrates of the pure argon purge and steam-argon reactive mixture were matched using the upstream and downstream control valve system (cf. Figure 1) such that the space time of the reactor remained constant at reactor conditions upon switching the two flows. (In order to accomplish this, the measured liquid water flowrate was converted to equivalent steam flowrate at reactor conditions.) All these operations were accomplished without exposing the char to the steam-argon mixture by alternate switching between the purge and bypass lines. (The pressure drop across the reactor is negligible in comparison to that imposed by the solenoid/control valve system, and thus the open bypass line adequately models the reactor flow resistance.) Once the pressure, temperature, and flowrates were set in the preceding manner, the transient experiment was initiated by activating the solenoid valve system to switch between the two flows. Pre-set mass programming and automated data logging were initiated simultaneously with the inception of the experiment.

IV. KINETIC MODELING

Various models have been proposed for the steam-carbon gasification system (e.g., see [6-10]). In the current studies, however, the complexity of the kinetic model required to explain the steam-char reaction was limited by the experimental conditions selected; i.e., only pure steam-argon feeds were used. Furthermore, for reactor space times of 12 to 18 s, the steam conversion never exceeded 10%. In addition, no significant amounts of methane or CO_2 were detected for the pressure and temperature ranges used. Under these conditions, the following mechanism was found to incorporate the basic features common to most of the models in the literature, and was found to suitably explain all the current data:

$$C_f + H_2O \underset{k_{-1}}{\overset{k_1}{<==>}} C(H_2O) \qquad [R.1]$$

$$C(H_2O) + C_f \xrightarrow{k_2} C(O) + C(H_2) \qquad [R.2]$$

$$C(O) \xrightarrow{k_3} CO + C_f \qquad [R.3]$$

$$C(H_2) \xrightarrow{k_4} H_2 + C_f \qquad [R.4]$$

This mechanism is basically that of Curran et al. [10], except that reactions [R.2]-[R.4] are treated as irreversible; the latter two by virtue of the relatively low amounts of CO and H_2 produced in the reactor. Although this assumption seems to be quite good a priori for CO, it has been noted that under steady-state conditions, H_2 significantly inhibits the steam-char reaction, with a resultant multiplicative factor in the denominator of the Langmuir-Hinshelwood steady-state specific gasification rate expression of almost an order of magnitude greater than that for steam (e.g., see [6,8]). However, under the current transient experimental conditions with initially no H_2 in the reactor, and eventually very low amounts even at pseudo-steady-state, the sensitivity of the transient data to the rate of the reverse of reaction [R.4] seemed to be relatively low. Therefore, it was omitted from the current analysis on these grounds. It is noted, however, that it is certainly possible to determine this rate constant with the current techniques using either pure or high partial pressure H_2 feeds.

All the basic mechanisms represented in the literature employ a step like reaction [R.1] (i.e., steam adsorption); however, there is a range of treatment on subsequent details and rate-limiting steps. For example, Gadsby et al. [6] assumed essentially instantaneous decomposition of the carbon-steam surface complex to gaseous CO and H_2. Ergun [11] and Strickland-Constable [12] suggested this mechanism for H_2, but postulated a surface carbon-oxygen complex with an appreciable lifetime that eventually decomposes to yield gaseous CO. Long and Sykes [7] and Blackwood and McGrory [8] proposed decomposition to dual-site hydroxyl and hydrogen atom surface complexes simultaneously with steam adsorption (i.e., fast equilibration), followed by irreversible rearrangement to carbon-oxygen and carbon-hydrogen surface complexes. These differences are relatively indistinguishable from each other in the current data. Therefore, the combination of reactions [R.1] and [R.2] were selected as being most generally representative.

Once the model has been defined, the approach becomes quite similar to other general treatments of "lumped" transient kinetic models that have been presented in the literature (e.g., see [13,14]), and to our previous CO_2 gasification work [1,2]. The use of a "gradientless" reactor guarantees that the resultant mass balances are always ordinary differential equations (i.e., "lumped" parameter systems), although, as in the current case, they may be nonlinear. Basically, the transient continuity expressions for the various species involved in the reaction system, incorporating the rate expressions derived from the kinetic mechanism, comprise the set of ordinary differential equations which defines the model of the system.

Formulated in this fashion, the model employed to analyze our steam gasification data consisted of seven first order differential equations with a total of six parameters: C_{so} (the "effective" concentration of active sites; g mol/g mol carbon), k_1, k_{-1}, k_2, k_3, and k_4. The resultant system of equations is omitted from the current communication for the sake of brevity. Its derivation is relatively straightforward and is presented in reference [4].

V. PARAMETER ESTIMATION.

The multiparameter estimation algorithm employed in the analysis of the current data was patterned after a scheme outlined by Luus and Jaakola [15]. The Luus-Jaakola (LJ) scheme is a direct random search method combined with search space reduction. Basically, the procedure is as follows. An initial range is selected for each parameter, and a number of different parameter sets are then selected on a random basis. For each parameter set the model is solved numerically and an unweighted least squares objective function value, $\emptyset$, is determined using all the CO and H_2 partial pressure data over the entire course of the transient experiment; i.e.,

$$\phi = \sum_{i=1}^{2} \{\sum_{j} (P_{i,j} - P^*_{i,j})^2\}, \qquad (1)$$

where the $P_{i,j}$ and the $P^*_{i,j}$ are the measured and predicted partial pressures, respectively. After an arbitrarily large number of parameter sets have been evaluated, a fraction of the "best" resultant cases (i.e., those with the lowest ϕ values) are then selected and the parameter ranges of these sets are scanned to define new reduced parameter ranges to be used for the next round of iteration. The entire procedure is then repeated until a pre-specified tolerance on the differential change in the objective function is met. The associated parameter set for the "best" value of ϕ after the last iteration is taken as the final optimum parameter set for the data.

The LJ method was applied to the steam gasification data on an experimental basis, with reasonable results, as part of an ongoing investigation on multiparameter regression schemes for transient kinetic data analysis [16]. Previously [1,2] we had used a Marquardt-type search scheme employing a Green's function method [17] for determining the first order gradients required for the technique. As for all such schemes, we found both advantages and disadvantages in using the LJ scheme. Perhaps its most obvious disadvantage lies in its inherent inability to converge to the optimum parameter set if it is inadvertently not included in the initial ranges of all the parameters. If the initial range is too large, the rate of region reduction can be drastically slower than if the range is capable of being more narrowly specified. Also, since a finite, albeit large, number of parameter sets are examined, there is always the possibility of missing the "true best" parameter set. Counterbalancing these debits is a potentially significant savings in computation time due to the absence of the requirement for evaluating first order gradients and, possibly, higher derivatives. Also, in reducing the parameter search space, the LJ method increases the probability of encountering a near-optimum parameter set, in comparison to totally random search methods. However, these arguments notwithstanding, our experience with the data considered here, suggests that a more effective method might involve a hybrid scheme wherein an LJ-type algorithm is used as the "front end" of an optimization procedure for reducing the parameter search space, with a more powerful local gradient technique, such as a Marquardt scheme, used to actually focus in on the optimum parameter set. Such a scheme is currently under consideration.

Typically, in the current application of the LJ method, the parameter ranges obtained after 11 iterations, using a 5% case reduction rate, were used as the initial ranges for the subsequent set of iterations. When the "best" value of ϕ did not change by more than 5%, the parameter set associated with this minimum value of the objective function was taken to be the optimum set. As an approximate average, about 25 overall iterations were sufficient to fit the experimental data with a good degree of accuracy.

VI. RESULTS AND DISCUSSION.

Two types of chars were studied in the current work: Fisher activated coconut char, and a char prepared from Darco lignite (PSOC 623) (800°C for 2 hr. in an inert atmosphere). Typical transient experiment results are presented in Figures 2 and 3. The six model parameters were determined for each transient experiment using the LJ algorithm as described above. The apparent activation energies for each parameter were then determined from Arrhenius plots of the parameter values. The resultant parameter expressions are summarized in Table I.

From the results in Table I it can be seen that the apparent activation energies are, on the whole, higher for the lignite than for the coconut char. However, the activation energies for k_1 are very nearly identical for the two chars, thereby implying that the mechanism for steam adsorption on the two chars is very similar. As in our previous CO_2 gasification studies, we found that the apparent activation energies of the effective active site concentrations were negative. This result, as previously, is attributed to the diminution of active sites via thermal annealing of the char upon heating [1,2,9,18,19,20]. Moreover, the C_{so} parameter expression determined in the current steam gasification studies for the coconut char is very similar to that

determined for the same char from previous CO_2 gasification studies: viz., $C_{so}=1.7\times10^{-9}$ exp(+27000/RT) [1,2,3]. This result implies that virtually the same active carbon sites participate in steam and CO_2 gasification under the current experimental conditions. This is also direct evidence that the transient technique can yield good estimates of the effective active site concentrations of chars under actual gasification conditions.

It is interesting to note that C_{so} for the lignite char is comparable to that of the coconut char, even though their total surface areas are quite different (1038 m^2/g for the coconut char; and 24.7 m^2/g for the lignite char). However, C_{so} decreases more rapidly with temperature for the coconut char than for the lignite char, as evident from the relative magnitudes of their negative apparent activation energies. This result probably reflects the fact that the coconut char is "older" than the lignite char, and , thus, more graphitic in nature and more susceptible to thermal annealing, and, therefore, exhibits a stronger temperature behavior. Also, the fact that that disordered regions in char have been reported to react more rapidly than ordered regions [21], is consistent with the comparable C_{so} values of the two chars in spite of the significant difference in total surface areas.

Although values for all the rate constants determined in the current work are not available in the literature, comparisons can be made with steady-state Langmuir-Hinshelwood expression parameter values. Setting all the time derivatives equal to zero in the transient model and solving for the pseudo-steady-state specific gasification rate, W_{ss}, yields the following expression:

$$W_{ss} = K_1 P_w/[1 + K_2 P_w], \text{ min}^{-1}, \qquad (2)$$

where the correspondence between the new parameters and the rate constants is given by:

$$K_1=k_1k_2C_{so}'/[k_{-1}+k_2]; K_2=k_1[1 + k_2(1/k_3 + 1/k_4)]/[k_{-1}+k_2] \qquad (3)$$

A comparison of the parameter values calculated from these expressions with corresponding values given in the literature are presented in Table II. As can be seen, the comparison is fairly good. The primary source of the variability observed is most probably due to differences in the chars. For example, the total surface area of the coconut char used by Blackwood and McGrory [8] was reported as 46.5 m^2/g, in comparison to the 1038 m^2/g for the activated coconut char used in the current work.

Pseudo-steady-state operation is attained at the end of each transient experiment corresponding the "leveling off" of the signal traces (e.g., after ca. 1.2 min). These data can also be analyzed in the usual steady-state fashion to show that they are consistent with traditional Langmuir-Hinshelwood kinetics. The steady-state expression given by Eq. (2) can be recast into the following form:

$$P_{w,ss}/W_{ss} = P_{w,ss}C_oRT/qP_{c,ss} = 1/K_1 + (K_2/K_1)P_{w,ss}, \qquad (4)$$

where the subscript "ss" denotes steady-state values, $P_{c,ss}$ is the steady-state CO partial pressure determined from the data, q is the volumetric flowrate at the reactor exit, R is the universal gas constant, and T is the effluent gas temperature. Therefore, a plot of the lefthand side of Eq. (4) against $P_{w,ss}$ should be a straight line. One such plot for the coconut char data is presented in Figure 3; the linear behavior is quite evident.

VII. CONCLUDING REMARKS.

It has been shown that char gasification in steam-argon mixtures, under the current experimental conditions, is reasonably well represented by the transient kinetic model presented in this communication. Multiparameter analysis of the resultant transient kinetic data yielded separate Arrhenius temperature-dependent expressions for each of the model rate constants, as well as the effective active site concentrations for the two chars examined. Although corresponding rate constant expressions are not available for direct comparison, related kinetic parameters found in the literature agreed with the appropriate combinations of the current rate constant values.

The transient kinetic technique has been shown to be a valuable tool for examining char reaction mechanisms, and for determining rate parameters for direct use in modeling, design, and analysis of new or existing gasification and related systems. With automated data handling, the technique is capable of quickly and efficiently yielding a large amount of information concerning the reactivity and behavior of chars in various gaseous environments directly in a single type of experiment. The advantages of this technique over other more commonly accepted steady-state methods are significant.

ACKNOWLEDGEMENT

The authors gratefully acknowledge the support of the U.S. Department of Energy under Grant Nos. DE-FG22-81PC40786 and DE-FG22-83PC60800. However, any opinions, findings, conclusions, or recommendations expressed herein are those of the authors and do not necessarily reflect the views of DOE.

REFERENCES

1. Sy, O. and J.M. Calo, ACS Div. Fuel Chem. Prepr. 28, 6 (1983).
2. Sy and Calo, Proc. 1983 Int. Conf. on Coal Science, Pittsburgh PA, p. 445.
3. Sy, O., "Transient Kinetic Studies of Char-Gas Reactions in a Gradientless Reactor: CO_2 Gasification," Master's Dissertation, Princeton University, Princeton, N.J., 1982.
4. Ganapathi, R., "Transient Kinetic Studies of Char Gasification in Steam-Argon Mixtures," Master's Dissertation, Brown University, Providence, RI, 1984.
5. Squires, A.M., Trans. Inst. Chem. Eng. (London) 39, 3 (1961).
6. Gadsby, J., C.N. Hinshelwood, and K.W. Sykes, Proc. Roy. Soc. (London) A187, 129 (1946).
7. Long, F.J., and K.W. Sykes, Proc. Roy. Soc. (London) A193, 377 (1948).
8. Blackwood, J.D., and F. McGrory, Aust. J. Chem. 12, 533 (1959).
9. Johnson, J.L., Kinetics of Coal Gasification, John Wiley & Sons, New York, 1979.
10. Curran, G.P., C.E. Fink, and E. Gorin, ACS Div. Fuel Chem. Prepr. 12, 62 (1968).
11. Ergun, S., U.S. Bur. Mines Bull. (598), 1962.
12. Strickland-Constable, R.F., J. Chim. Phys. 47, 356 (1950).
13. Bennett, C.O., AIChE J. 13, 890 (1967).
14. Cutlip, M.B., C.C. Yang, and C.O. Bennett, AIChE J. 18, 1073 (1972).
15. Luus, R., and T.H.I. Jaakola, AIChE J. 19, 760 (1973).
16. Ellison, S.E., "Nonlinear Parameter Estimation in Ordinary Differential Equation Systems: Newton-Raphson and Gauss Techniques," Sc.B. Thesis, Division of Applied Mathematics, Brown University, 1984.
17. Kramer, M.A., J.M. Calo, and H. Rabitz, Appl. Math. Model. 5, 432 (1981).
18. Duval, X., J. Chim. Phys. 47, 339 (1950).
19. Boulangier, F., X. Duval, and M. Letort, Proc. Third Int. Conf. Carbon, p. 257, Pergamon Press. N.Y. (1959).
20. Blackwood, J.D., D.J. McCarthy, and B.D. Cullis, Aust. J. Chem. 20, 1561, 2525 (1967).
21. Chang, H.W., and S.K. Rhee, Carbon, 16, 17 (1978).

Table I.

Model parameter values* obtained with the Luus-Jaakola search scheme for steam gasification of lignite and coconut char.

Values for Darco lignite char (PSOC 623):

$C_{so} = 1.6 \times 10^{-6} \exp(+13646/RT)$, g mol/g mol C

$k_1 = 4.86 \times 10^{9} \exp(-42286/RT)$, $min^{-1}\ atm^{-1}$

$k_{-1} = 2.65 \times 10^{10} \exp(-51341/RT)$, min^{-1}

$k_2 = 9.32 \times 10^{7} \exp(-33840/RT)$, min^{-1}

$k_3 = 4.21 \times 10^{9} \exp(-42075/RT)$, min^{-1}

$k_4 = 5.07 \times 10^{10} \exp(-47262/RT)$, min^{-1}

Values for Fisher activated coconut char:

$C_{so} = 2.21 \times 10^{-8} \exp(+23592/RT)$, g mol/g mol C

$k_1 = 1.41 \times 10^{10} \exp(-45183/RT)$, $min^{-1}\ atm^{-1}$

$k_{-1} = 1.04 \times 10^{7} \exp(-35233/RT)$, min^{-1}

$k_2 = 9.67 \times 10^{4} \exp(-19448/RT)$, min^{-1}

$k_3 = 1.20 \times 10^{6} \exp(-25995/RT)$, min^{-1}

$k_4 = 2.04 \times 10^{6} \exp(-25867/RT)$, min^{-1}

*All activation energies are given in cal/g mol.

Table II.

Comparison of kinetic parameters from different studies with coconut char.

Temperature (K)	973.2	1023.2	1063.2
1. Current Work			
$K_1 C_{so} \times 10^4$, [$min^{-1}\ atm^{-1}$ g mol/g C]	3.6	6.1	8.9
K_2, [atm^{-1}]	1.1	1.8	2.7
2. Gadsby et al. [6]			
$K_1 C_{so} \times 10^4$, [$min^{-1}\ atm^{-1}$ g mol/g C]	3.6	-	-
[$min^{-1}\ atm^{-1}$ g mol/g C]			
K_2, [atm^{-1}]	1.0	-	-
3. Long and Sykes [7]			
$K_1 C_{so} \times 10^4$, [$min^{-1}\ atm^{-1}$ g mol/g C]	1.6	7.8	25.0
[$min^{-1}\ atm^{-1}$ g mol/g C]			
K_2, [atm^{-1}]	0.97	1.61	2.33
4. Blackwood and McGrory [8]			
$K_1 C_{so} \times 10^4$, [$min^{-1}\ atm^{-1}$ g mol/g C]	-	0.36	1.25
K_2, [atm^{-1}]	-	0.06	0.09

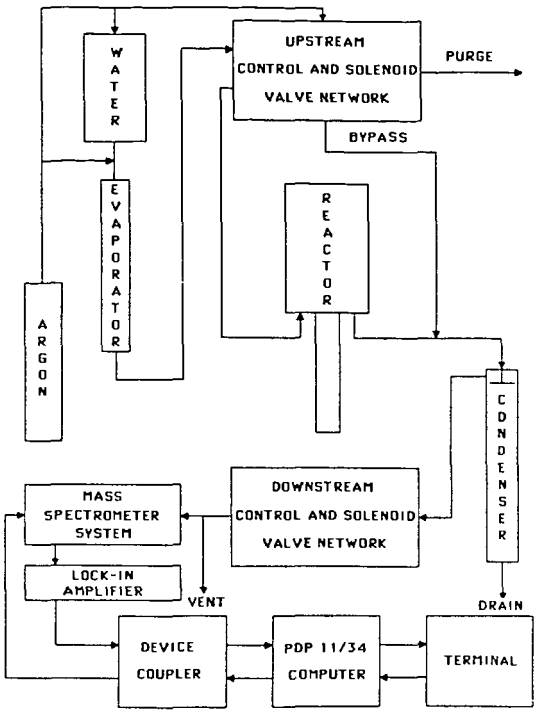

Figure 1. Schematic of experimental system.

EXPERIMENTAL RESPONSE OF [CO] AND [H2] VERSUS MODEL PREDICTION

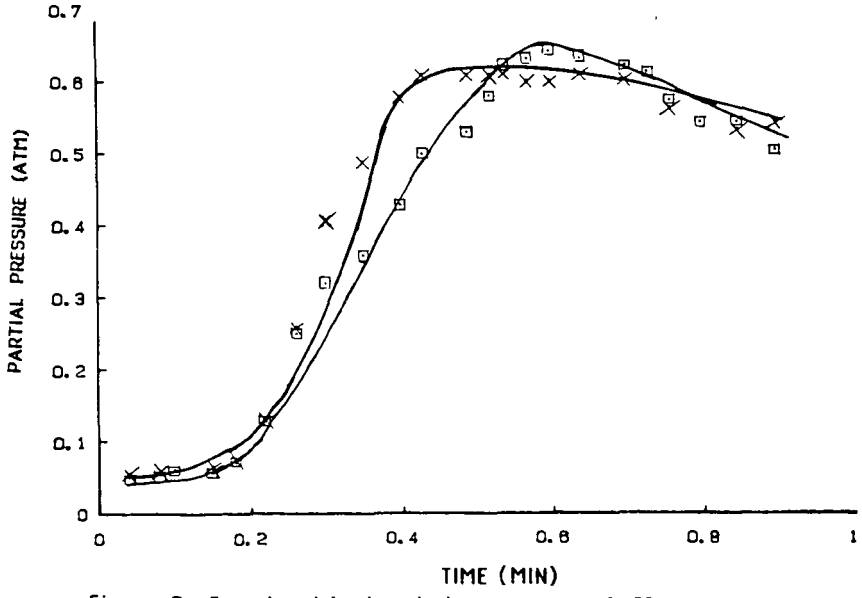

Figure 2. Experimental transient responses of CO and H_2 versus model predictions for steam gasification of Fisher activated coconut char (2.135 g mol of char; T_{bed}=757 °C, P_{total}=13.6 atm; P_{steam}=7.5 atm).

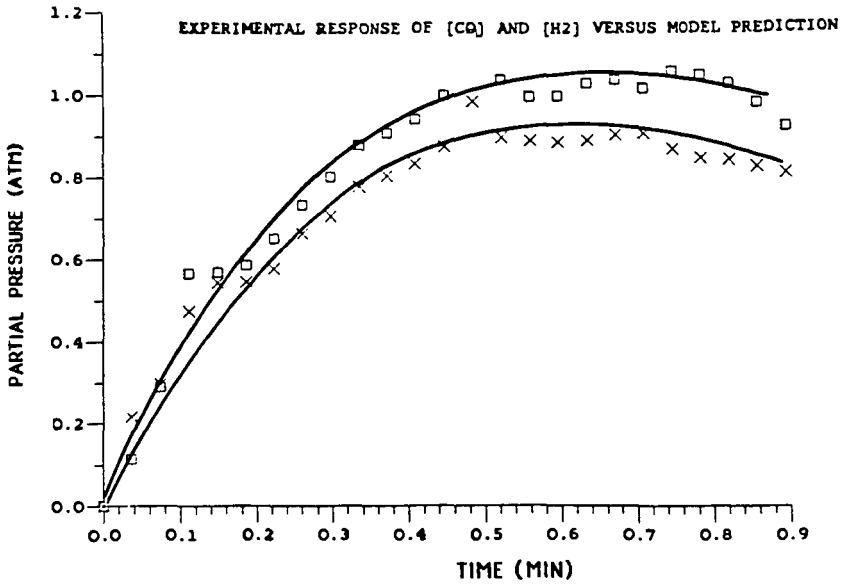

Figure 3. Experimental transient responses of CO and H_2 versus model predictions for steam gasification of Darco lignite (PSOC 623) char (2.903 g mol of char; T_{bed}=765 ^{0}C, P_{total}=23.4 atm; P_{steam}=14 atm).

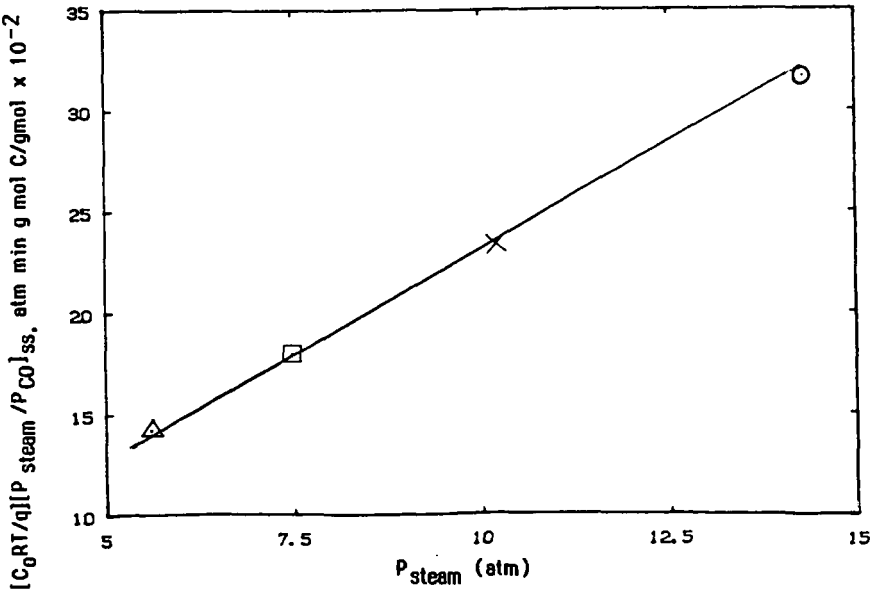

Figure 4. Pseudo-steady-state steam gasification rate data for Fisher activated coconut char (T_{gas}=1058 K, 2.135 g mol of char).

POPULATION AND TURNOVER NUMBER OF ACTIVE POTASSIUM SITES ON BITUMINOUS COALS DURING GASIFICATION

C. T. Ratcliffe*

Corporate Research-Science Laboratory
Exxon Research and Engineering Company
Route 22 East, Annandale, N.J. 08801

S. N. Vaughn

Exxon Research and Engineering Company
P. O. Box 4255
Baytown, Texas 77520

Introduction

The activity of alkali metal salts as catalysts for steam gasification on carbon surfaces has been well documented.[1-2] The kinetics of catalyzed gasification with potassium salts on carbon and the data obtained from characterizing alkali metal treated carbon is consistent with potassium in a highly dispersed and ionic state.[3-5]

The rate of potassium catalyzed gasification on bituminous coals, when plotted as a function of carbon conversion, tends to decrease at higher carbon conversions and can be highly variable depending on the source of coal and method of catalyst treatment. The mechanism(s) of catalyst deactivation are not well understood; loss of potassium sites due to reaction with mineral matter, limited mobility after initial reaction, detachment from the coal surface and collapse of pore structure have all been suggested as reasons.[6-8] A key factor in developing a fundamental understanding of the change in rate behavior will be the ability to accurately count the population of active alkali sites during gasification as a function of carbon conversion.

We have recently found that carbon dioxide chemisorbs in an irreversible manner on the surface of potassium treated Spherocarb, a high surface area carbon.[9] The molar quantity of CO_2 adsorbed on this surface at 300°C, after initial thermal treatment at 850°C, correlated with the level of potassium loading and suggested a facile method of measuring alkali dispersion. The value of 0.5 to 0.6 adsorption sites per K_2O impregnated on the surface also agreed with the initial number of active sites measured by the derivitization technique.[10]

The purpose of this investigation has been to establish CO_2 chemisorption as a tool to selectively measure the population of active alkali sites on gasified coal chars and to determine the specific activity or turnover number of the active sites under gasification conditions.

* Current address: Union Oil Company of California, Union Science and Technology Division, P. O. Box 76, Brea, California, 92621.

Experimental

Samples of bituminous coals were obtained in 5 gallon containers from the mines under a nitrogen atmosphere. The coals are identified by mine and state as: Monterey No. 1, Illinois #6, Hawk's Nest, Colorado; Valley Camp, Utah; Walden, Colorado. The samples were sealed in an inert atmosphere for shipment and opened in a controlled atmosphere dry box. Impregnation of the coals with aqueous solutions of potassium carbonate or potassium hydroxide were performed in a controlled atmosphere environment by the method of incipient wetness. Alkali salts were obtained commercially (reagent grade K_2CO_3, ultra pure KOH,) with aqueous solutions prepared immediately before impregnation. After impregnation, the samples were dried under inert atmosphere and stored in sealed glass vessels. While an apparent dispersion was observed with all KOH treated coals, the K_2CO_3 treated coals required rewetting the samples, followed by stirring and drying to obtain an even dispersion of K_2CO_3. The loading of potassium was in the range of 7-10%.

Adsorption and gasification studies were performed with a Mettler 2000C TGA/DSC thermal analysis unit equipped with a corrosive gas head [9] and a DuPont 951 TGA unit with a pressurized housing for operation up to 500 psig (Figure #1).

Technique for Adsorption, Gasification

The adsorption properties of bituminous coal and catalyzed coal samples were measured by means of the following procedure. A sample of approximately 80 milligrams was loaded into a ceramic crucible with an equivalent amount of SP-1 graphite prepared in a crucible of identical color and approximately the same mass. The preweighed crucibles were loaded onto the TGA/DSC platform and outgassed at ambient temperature by mild evacuation (10^{-3}mm) for one half hour. The sample and reference material were subsequently temperature programmed at 29.9°/min. to 850°C in flowing helium. After heat treatment, samples were cooled to the desired temperature of 300°C for adsorption studies. While the sample was maintained at the selected isothermal temperature, a measured flow of CO_2 was introduced into the helium carrier. The reactive gas flow, as measured by the Tylan flow meter, was maintained at 2cc per minute with the carrier flow of 20cc per minute helium; thus a partial pressure ratio of 1:10 of CO_2 to inert carrier was utilized during the adsorption study.

Adsorption of CO_2 was monitored by weight gain recorded on a strip chart. Adsorption was normally rapid with a plateau in total weight reestablished in 15-30 minutes. The mixed gas stream was replaced with a pure helium stream with a second period of 10-15 minutes allowed for any subsequent change in weight. The total adsorbed gas could thus be divided into physical and chemical adsorbed fractions as the former was desorbed when the reactive gas was replaced by helium and the latter was retained as a net weight gain.

A measured flow of CO_2 or H_2O vapor was mixed with the He carrier gas flows and the temperature of the sample was raised to an isothermal value of 700-800°C to perform partial gasification of the char. After a steady state period was established, the rate of weight loss per unit time was obtained. The reactive gas flow was subsequently terminated and the above described procedure was repeated for CO_2 measurement of the active site density.

High pressure measurements were performed on a modified DuPont 951 TGA which had been enclosed in a pressurized housing (Figure 1). A similar procedure was used to obtain the rate of gasification; the reactive gas composition was 30% H_2O, 7% CO, 13% CO_2, 15% CH_4 and 35% H_2. Operating conditions were 500 psig and 705°C. Adsorption measurements with CO_2 were obtained at 300°C, one atmosphere pressure, by the procedure described above with a flow of N_2 as the inert carrier gas.

Results and Discussion:

Adsorption of CO_2 was examined on each of the neat coals after thermal treatment to 850°C. While physisorption was observed at lower temperatures (100°C) in all cases, only Walden and Valley Camp chars revealed any measureable chemisorption at 300°C. The thermal desorption profile of Walden or Valley Camp chars after CO_2 adsorption identified $CaCO_3$ formation from CO_2 interaction with CaO as the source of the chemisorption. The quantity of CO_2 was always an order of magnitude lower than adsorption on alkali treated chars. A display of the quantity of CO_2 adsorbed on K_2CO_3 and KOH treated coals is shown in Figures 2 and 3. The molar quantity of CO_2 adsorbed (measured by TGA) has been normalized with the molar quantity of impregnated potassium salt to represent relative dispersion values on the ordinate axes. As the chemisorption measurement with CO_2 is performed after each thermal heat cycle to 850°C in inert atmosphere, only active potassium sites which are bonded to the carbon will chemisorb CO_2. Any free potasium oxide, hydroxide, or basic salt will irreversibly adsorb CO_2 on the first cycle and remain as thermally stable K_2CO_3. Thus, the efficacy of the technique is its ability to selectively measure only the active potassium complexes bonded to the carbon surface, as they regenerate on each thermal heating cycle to 850°C in He.

The similarity of the four bituminous coals in their number of available active sites is in contrast to the higher and more constant value of K_2CO_3 impregnated Spherocarb ($800m^2/g$, mineral free amorphous carbon) as shown in the dotted line of Figure #2. The low population of active sites on the KOH and K_2CO_3 treated coal chars may represent a limited surface area, as recently reported by Shadman.[11] The lower initial values on KOH - coals do not correspond to lower surface areas with our BET measurements, but do correlate in a positive manner with lower volatile matter release on initial thermal tereatment. Deposition of carbon or non-volatile carbonaceous residue on the active base sites may limit the availability of alkali after initial thermal treatment. Franklin, Peters and Howard have detailed the effect of mineral matter and especially in exchanged alkali on reducing the volatile matter and tar upon pyrolysis of bituminous and sub-bituminous coals.[12-14] The greater reduction in volatile matter with KOH vs. K_2CO_3 treated coals, due to the stronger base, most probably results in a higher localized coating of condensed tar on the active alkali sites. The temporary "poisoning" of the sites to CO_2 adsorption in KOH or K_2CO_3 treated chars is removed after the initial 5-10% gasification.

The maximum population of sites in the 20-50% char conversion range, representing about 30% dispersion of K_2O, is only one-half the value obtained with potassium impregnated Spherocarb. Interaction of the basic potassium salts with the mineral matter may well have consumed a portion of the impregnated salt (7) in addition to a possible lower dispersion of the salts on the lower surface area chars. The decline in the site population at 60-90% carbon conversion indicates the continued neutralization of the alkali with mineral matter in addition to the detachment of alkali from the carbon.

When the rate of gasification with CO_2 is corrected for the population of active sites at each level of char conversion, a specific activity or turnover number can be obtained. The turnover number for Valley Camp and Hawk's Nest coal (both impregnated with KOH) as a function of char conversion are shown in Figure #4 for CO_2 gasification. The constant value of the turnover number for the entire range of char conversion now establishes the density of active potassium sites as the rate controlling parameter in CO_2 gasification of these coals. While the results in Figure #4 clearly remove the quantity of carbon in the char as a rate controlling parameter, the change in the concentration or composition of the vapor phase reactant atmosphere is also known to affect catalyzed gasification. Samples of the same impregnated Valley Camp and Hawk's Nest coals have been studied under high pressure conditions with a reactive atmosphere typical of a fluid bed steam/coal gasification environment. The plot of turnover number vs char conversion under this set of reaction conditions is shown in Figure #5. The difference in the average turnover number shown for the two sets of gasification conditions can be attributed to differences in reactivity of the two gas atmospheres. It is again obvious that the constant turnover number for potassium over the range of char conversion confirms the rate controlling nature of the potassium site density for coal gasification.

Summary:

Chemisorption of CO_2 at 300°C provides a selective and rapid technique to measure the active site density of alkali catalysts on coal at intermittent periods of coal gasification. With a thermal balance/reactor, the specific activity per catalyst site (turnover number) has been measured for catalyzed gasification of CO_2 or steam/product gases with bituminous coals. The site density of potassium on carbon as the rate controlling parameter in gasification of coal as shown by a constant value for the turnover number over the full range of char conversion.

REFERENCES

1. International Symposium, Fundamentals of Catalytic Coal and Carbon Gasification, Special Issue, Fuel, 62, 1-261 (1983)
2. For Review, D. W. McKee, Chem. Phys. of Carbon, 16, 1-118 (1981)
3. C. A. Mims, J. J. Chludzinski, J. A. Pabst, R. T. K. Baker, J. Catalysis, 88, 97 (1984)
4. F. J. Long, K. W. Sykes, J. Chim. Phy., 47, 361 (1950)
5. C. L. Spiro, D. W. McKee, P. G. Kosky, E. J. Lamby, Fuel 63, 686, (1984)
6. F. Kapteijn, J. A. Moulijn, Fuel 62, 205, (1963)
7. L. Kuhn, H. Plogmann, Fuel, 62, 205 (1983)
8. D. Douchanov, G. Angelova, Fuel 62, 231 (1983)
9. C. T. Ratclffe, Proceedings of the 13th North American Thermal Analysis Society, p.90, September 23-26, 1984, Philadelphia, PA
10. C. A. Mims, K. D. Rose, M. T. Melchior, J. A. Pabst, J. Am. Chem. Soc., 104, 886 (1982)
11. F. Shadman, D. A. Sams, Div. of Fuel Preprints, 29(2), 160 (1984)
12. H. D. Franklin, W. A. Peters, J. B. Howard, Fuel, 61, 155, (1982)
13. Ibid, 1214
14. H. D. Franklin, R. G. Cosway, W. A. Peters, I&EC Process Des. Dev., 22, 42 (1983)

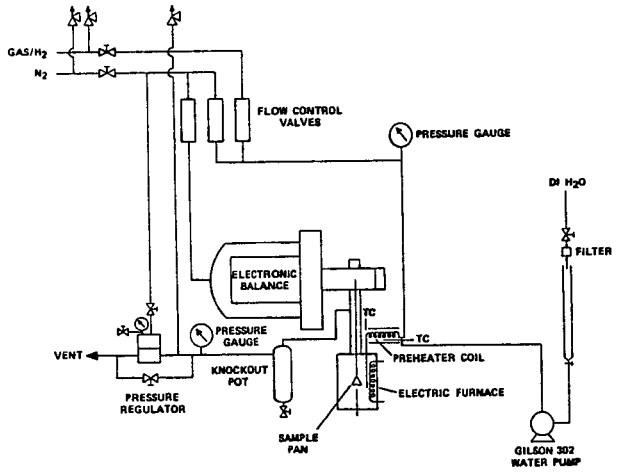

Figure 1. High Pressure TGA Reactor System for Char Gasification

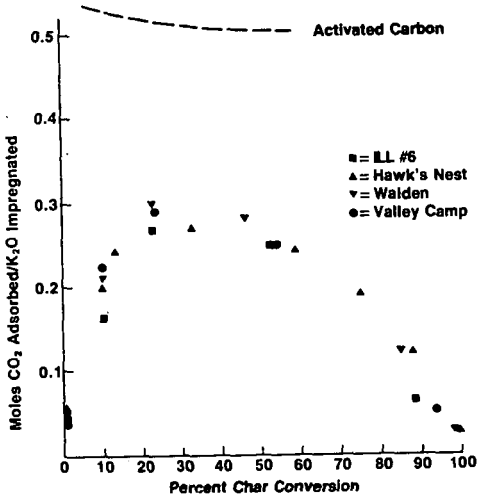

Figure 2, Dispersion of KOH treated coal chars vs carbon conversion as measured by CO_2 chemisorption at 300°C.

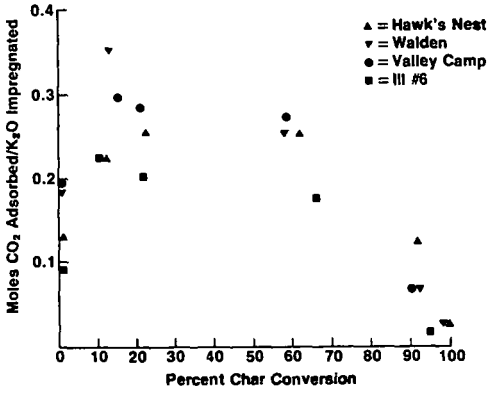

Figure 3. Dispersion of K_2CO_3 Treated coal chars vs carbon conversion as measured by CO_2 chemisorption at 300°C.

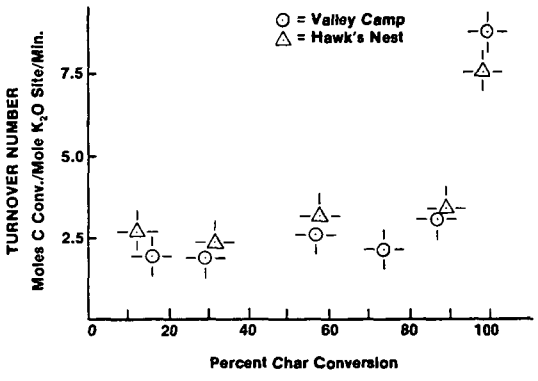

Figure 4. Specific activity per site of KOH treated coals v carbon conversion; CO_2 gasification, ⊙ Valley Camp, △ Hawk's Nest.

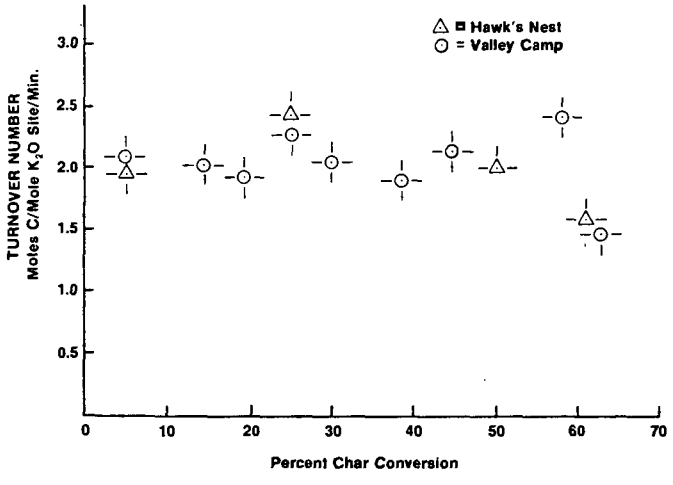

Figure 5. Specific activity per site of KOH treated coals vs carbon conversion; H_2O/CO_2/recycle atmosphere gasification, 500 psig, vs carbon conversion; ⊙ Valley Camp, △ Hawk's Nest.

THE KINETICS OF CARBON GASIFICATION BY CO_2

H. Freund

Exxon Research and Engineering Company
Corporate Research - Science Labs
Clinton Township, Route 22 East
Annandale, NJ 08801

INTRODUCTION

Considerable work has been done in the area of catalytic carbon gasification(1-3) and recently an entire issue of Fuel was devoted to this area.(4) And yet there is still considerable uncertainty about the basic fundamentals. Different kinetic measurements have been reported for similar systems and different theories and mechanisms appear for catalytic gasification.

The mechanism for the gasification of uncatalyzed carbon has been postulated to be a simple two step oxygen exchange mechanism (5):

$$C_f + CO_2 \underset{k_{-1}}{\overset{k_1}{\rightleftharpoons}} C(O) + CO \qquad (1)$$

$$C(O) \xrightarrow{k_2} CO + C_f \qquad (2)$$

where C_f is an available active site, and C(O) is one which is occupied has been applied to uncatalyzed gasification. In this paper, it will be applied to Ca- and K-catalyzed as well. From a kinetic analysis the rate constant k_2' can be determined. k_2' is the product of the active site density and the intrinsic decomposition rate constant, k_2. It still remains to uncouple the active site density from k_2' to determine k_2.

Such an uncoupling can be accomplished by a transient kinetics experiment. Other workers have examined the transient kinetics during the establishment of steady state gasification conditions and have reported k_1 and k_2. The activation energy for k_2 of 44.8 kcal/mole seems low.(6) In this present paper, the transient kinetics are studied as a steady state gasifying system relaxes when the oxidant is suddenly removed from the system.

Under steady state conditions, in an atmosphere of CO_2, reaction (1) is driven to the right, populating all available sites and producing one CO molecule for each active site reacted. A second molecule of CO is formed when this complex decomposes. If the oxidant were to be rapidly removed from the system, reaction (1) would be shut down but the surface complex would decay with a characteristic time constant k_2, if $k_{-1}[CO]$ were negligible compared to k_2. One can estimate the magnitude of k_2 and k_{-1} using the results of Sy and Calo.(6) k_{-1} can be determined from Sy and Calo's k_1 and Ergun's (5) equilibrium constant. At 1000 K and [CO] = 100 ppm, $k_{-1}[CO] = 9.1 \times 10^{-4}$ min^{-1} and $k_2 = 1.6$ min^{-1}. Indeed $k_2 >> k_{-1}[CO]$. At sufficiently low temperatures the decay time constant in the transient experiment will be long enough to be measurable. If one were

monitoring CO, one would expect to see ideally an instantaneous decline of the CO to one half of its steady state level followed by an exponential decay of CO.

EXPERIMENTAL

TGA experiments were done with a Dupont model 951 thermogravimetric analyzer. CO_2, CO, and Ar were prepurified grade and were used without further purification. The carbon samples used were Analab's Spherocarb (-60+80 mesh), Supelco's Carbosieve S (-120+140 mesh), glassy carbon obtained from Atomergic Chemetals Corp., and a 1000°C char made from Illinois #6 coal. Research grade anhydrous K_2CO_3 was used as the source of potassium and was co-crushed with the spherocarb to make various mixtures of K_2CO_3 on spherocarb. The Carbosieve was oxidized overnight in HNO_3 to prepare carboxylic acid sites on the carbon. To prepare Ca-treated carbon this material was then ion-exchanged in an ammoniated Ca $(NO_3)_2$ solution.

For a run, approximately 50 mg of sample were loaded into the TGA. All samples were first heated under argon up to a pre-designated temperature (50°/min up to 900°C, for non-potassium samples, 20°/min up to 800°C for potassium samples). Gasification was then generally done at or below these preheat temperatures. This was done to minimize any pyrolysis effects which might occur during gasification. Mixtures of CO and CO_2 (10% CO in CO_2 was the most common) were prepared using Matheson mass flow controllers and passed into the TGA at around 300 cc/min at a pressure of 10 kPag.

The TGA data were obtained measuring sample weight as a function of time. Steady state slopes were usually measured. For the Ca samples, generally the initial rate was taken as there was rather rapid catalyst deactivation. The rate of carbon gasified, R, is defined as 1/w dw/dt where w is the weight where the slope (tangent) was drawn and dw/dt is the slope or rate of weight loss. The units of this are g/g/min or grams of C gasified per gram of material per unit time. Figure 1 is an Arrhenius plot for one sample (20% K_2CO_3 on Spherocarb) showing the effect of the CO/CO_2 ratio.

The flow reactor experiments were done in a 1 cm ID quartz flow reactor within an open ended vertical furnace. The carbon samples sat on a quartz frit, ~20μ pore size. Gas flow was about 1000 cc/min (Ar + CO_2) and was passed down over the sample. The sample thermocouple passed through a 0.64 cm OD quartz tube through the length of the reactor and was positioned just above the frit.

In order to minimize O_2 contamination, both CO_2 and Ar were passed through an O_2 scrubber. This was a packed bed (45 cm x 1.1 cm ID) of copper chromite catalyst (Harshaw Chem) operated at 150-160°C. The catalyst was activated by H_2 reduction. The bed should reduce O_2 below 1 ppm. CO was monitored using a Thermo Electron Corporation Model 48 CO analyzer. CO_2 was monitored with a Beckman Model 865 infrared analyzer.

The procedure was to charge the reactor with sample and heat to 800-850°C under flowing Ar. This established a common reference condition

for all samples. The temperature was then dropped into the range 570-670°C and 10% CO_2 was added to the gas flow. When steady state was reached, CO_2 was turned off and the decay in CO monitored as a function of time. The observed time constant for CO_2 to be swept out of the system was about 5 sec (10%-90%). The CO analyzer instrumental time constant was 30 sec (0-95%).

ANALYSIS

In order to properly reduce the TGA data, the effect of the CO/CO_2 ratio had to be taken into account. Using Langmuir-Hinshelwood kinetics and applying the steady state assumption to C(O) in reactions (1) and (2) and assuming that the number of free sites remain constant with burn off, the global surface rate for CO_2 gasification can be shown to be

$$R \equiv \frac{1}{w}\frac{dw}{dt} = \frac{k_1(CO_2)[C_T]}{1 + k_1/k_2(CO) + k_1/k_2(CO_2)} \qquad (3)$$

where R is the measured rate of carbon weight loss, (CO_2) and (CO) are the gas concentrations of CO_2 and CO and $[C_T]$ is the active site density, g active carbon per g of total carbon. An active site is either free or occupied and hence $C_T = C_f + C(O)$. Ergun(5) has shown that Eqn. (3) reduces to

$$R = \frac{k_2[C_T]}{1+(CO/CO_2K_{eq})} \qquad (4)$$

under mild gasification conditions (low T, low pressure). In Equation (4), K_{eq} is the equilibrum constant for reaction (1) which is equilibrated at these conditions. Eqn. (4) can be rearranged so that

$$(\frac{CO}{CO_2}) = K_{eq}\ k_2[C_T]\ (\frac{1}{R}) - K_{eq} \qquad (5)$$

Hence a plot of CO/CO_2 vs 1/R should yield a straight line with y-axis (CO/CO_2) intercept of $-K_{eq}$ and an x-axis $(\frac{1}{R})$ intercept of $1/k_2[C_T]$.

The author has applied this mechanism to his data from experiments on catalytic gasification by CO_2 using K and Ca as catalysts as well as experiments with no catalyst present. The CO_2 data for K_{eq} is plotted in Figure 2. The curve in Figure 2 is the published Ergun(5) value for K_{eq} multiplied by 2. In his paper he mentioned that K_{eq} can differ by a factor of 2 depending on which of two algebraic expressions he used to obtain K_{eq}. Using K_{eq}, a value of $k_2[C_T]$ $(\equiv k_2')$ can then be obtained from eqn (4). These have been plotted as Arrhenius plots in Figure 3.

For the flow experiments, two typical CO traces are shown in Figures 4 and 5 for the carbon sample and for the Ca impregnated sample. Note that in Figure 4 there is a substantial dip which occurs when the CO_2 is first turned off. This phenomenon will be discussed later. Two pieces of information were taken from each plot: the steady state value for CO_2 gasification and the rate of CO decay.

The steady state value of CO produced can be converted into the rate constant, k_2' knowing the total molar gas flow and the carbon loading in the bed. From the overall gasification stoichiometry and the molar gas flow, the observed CO concentration can be related to the moles of carbon being gasified per unit time. Knowing the initial bed weight, k_2' ($\equiv$ 1/w dw/dt) can then be determined.

If the rate of CO decay is exponential, the decay constant is the intrinsic rate constant for the decomposition of the surface complex. In most cases, at a given temperature, a small non-zero CO value was obtained in the absence of CO_2. This value was subtracted out; it was generally less than 10% of the steady state value.

The values of k_2' derived from the steady state data are shown as an Arrhenius plot in Figure 6. The data scatter about the lines obtained from the TGA work on similar samples. Also included in Figure 6 are the decay constants from the transient experiment, i.e. the intrinsic rate constant, k_2. Least square analysis yields an average value of:

$$k_2 = 10^{11.6\pm2.3} \exp \frac{-53700\pm9400}{RT} \text{ min}^{-1}.$$

(uncertainties determined for a 95% confidence limit).

DISCUSSION

The experimental values for K_{eq} (Eqn. 1) determined in this work fall quite close to the line determined by Ergun (see Figure 2). This is strongly suggestive that the equilibrium in equation (1) is <u>not</u> affected by the presence of a catalyst. This is further corroborated by the fact that after correcting for the CO/CO_2 ratio in the manner described, the four lines in Figure 1 collapse to one line in Figure 3. Ergun determined the activation energy for uncatalyzed CO_2-carbon gasification to be 59 kcal/mole. Except for glassy carbon, in the present experiments, least squares analyses on those systems with at least seven points show activation energies within 3.2 kcal of Ergun's value. Because the lines in Figure 3 are parallel to one another, the activation energy for reaction (2), the desorption of CO, is independent of catalyst. This means that the reactive surface intermediate in the catalytic cases must decompose as if the catalyst were not present i.e., it must decompose like reactive adsorbates in uncatalyzed gasification. This author interprets the parallel Arrhenius plots shown in Figure 3 for different carbon-catalyst combinations to mean that the catalyst is effectively acting solely to increase the active site density.

The observation of a decrease in CO in the transient flow experiments of about one half followed by an exponential decay strongly suggests that the two step gasification mechanism is indeed controlling. One can now determine the fraction of total carbons which are "active" ---- dividing k_2' by k_2 yields the active site density. For the uncatalyzed carbon, one obtains a value, 4.7×10^{-5} active carbon/total C. This exceedingly small value is quite unexpected. In terms of "active surface area", this corresponds to about .019% of the total BET surface area (this was obtained using 1000 m^2/g as the BET surface area of the carbon and

8×10^{-16} cm^2 as the area for an active site(7)). This is a factor less than 1/10 that of active surface measured via O_2 chemisorption of Graphon(4). For high surface area chars, Radovic et al(8) found active surface area/total surface area ~10%. These chemisorption techniques measure active carbons with respect to O_2 adsorption. In carbon gasification by CO_2 it is not the case that all the sites available to O_2 are assessible by CO_2(9). Furthermore not all of the active sites by chemisorption are active in gasification since some represent very active sites which are probably unavailable for reaction because of a stable carbon-oxygen complex while others of low reactivity will form the carbon-oxygen reaction intermediate only very slowly.

The fact that a catalytic system yielded the same k_2 strongly supports the contention that Ca (and presumably other alkaline earth as well as alkalies) catalyze the system by increasing the number of sites. It does not affect k_2, the rate constant controlling the removal of carbon atoms as CO from the lattice.

The implication of these experiments is that a simple two step oxygen exchange mechanism, although an oversimplification, can still be used to explain CO_2 gasification. The data herein are self-consistent. The steady state values for k_2' scatter about extrapolated TGA data obtained earlier for the same samples. Activation energies for k_2' are ~ 58-60 kcal/mole. Two different carbon systems which yield k_2' (c.f. Figure 6) differing by a factor of 100 yield the same k_2 (within the scatter) with an activation energy roughly the same as k_2'.

The value of k_2 can be compared to the value obtained by Sy and Calo. At 1000 K they obtain $k_2 = 1.6$ min^{-1}. In this work, at 1000 K, $k_2 = .71$ min^{-1}, fairly good agreement for a high temperature rate constant. Although the uncertainty in the activation energy is fairly large (53.7 ± 9.4) and encompasses the value determined by Sy and Calo (44.8), this author feels that a ΔE closer to that obtained from gasification kinetics[5,10], i.e., ΔE ~ 59 kcal/mole would be most consistent with the available data and the 2-step oxygen exchange mechanism.

There still remain questions regarding the interpretation of the data presented here. One problem can be seen in the Ca plot in Figure 5. After about 60% of the surface complex has decomposed, the rate of CO decrease slows down, i.e. more CO is liberated than expected for an exponential decay. Apparently another mechanism for CO release becomes appreciable; perhaps as just mentioned, complexes of lower reactivity begin to decompose.

In Figure 4, after CO_2 is turned off, the CO signal dips well below the 50% value before beginning an exponential decay. If one extrapolates back to t=0, however, it appears to intersect a CO value about half of the initial (because of the dilution effect of the Ar, the value should be 10% larger than 1/2). What appears to be happening is the following: In the case of uncatalyzed carbon, CO initially produced is scavenged by some surface species and can not escape as CO. This scavenging species becomes depleted and CO is able to escape from the bed, thus "resuming" the exponential decay. For Ca-catalyzed carbon either the species does not exist or the effect is swamped by the higher level of CO produced. The

observation of such a large dip suggests more complicated chemistry than a simple two-step oxygen exchange mechanism.

Other carbon systems also suggest more complicated chemistry. A different Ca-catalyzed carbon (Ca-impregnated spherocarb) gave entirely different results: on CO_2 removal (in the same temperature regime), the CO signal dropped to ~90-95% of the steady state value, and no decay constant could be measured. This kind of behavior was observed with K_2CO_3/spherocarb samples. The CO concentration dropped to about 90% and declined further slowly with time. In work done subsequent to that reported herein, spherocarb gave a similar rate constant as determined here but the CO fell more than half of the steady state value. The results seem to depend on the particular carbon system not on the experimental arrangement. It is not surprising that the structure of the carbon, the micro-pore distribution, the nature of the catalyst or its dispersion may have an effect on the result in these kinds of experiments.

Acknowledgements

The technical help of James Pizzulli is gratefully acknowledged.

References

1. Walker, P. L., Shelef, M. and Anderson, R. A., Chemistry & Physics of Carbon 4, 287-383 (1968).

2. Wen, W. Y., Catal. Rev. - Sci. Eng., 22, 1-28 (1980).

3. Laurendeau, N., Prog. Energy Combust. Sci. 4 221-270 (1978).

4. Fuel 62 (1983) contains the papers presented at the International Symposium, "Fundamentals of Catalytic Coal and Carbon Gasification," held in Amsterdam the Netherlands, September 27-29, 1982.

5. Ergun, S., J. Phys. Chem. 60, 480-485 (1956).

6. Sy, O. and Calo, J. M., AIChE Annual Meeting, preprint #56b, November 14-18, 1982.

7. Laine, N. R., Vastola, F. J. and Walker, P. L., Jr., J. Phys. Chem. 67, 2030 (1963).

8. Radovic, L. R., Walker, P. L., Jr., Jenkins, R. G., Fuel 62, 849 (1983).

9. Freund, H. and Kelemen, S. R., in preparation.

10. Sundareson, S. and Amundsen, N. R., Ind. Eng. Chem. Fundam. 19, 351 (1980).

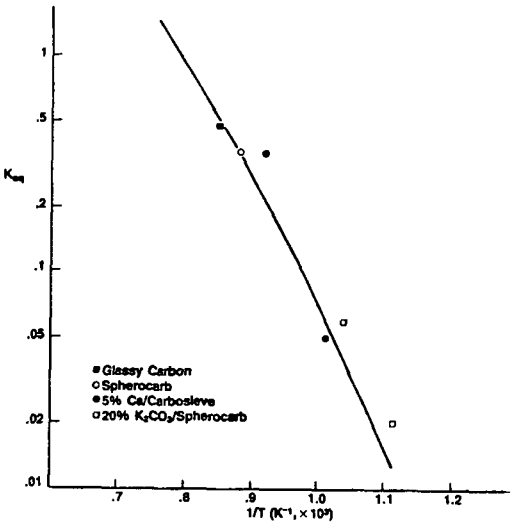

Figure 1: Oxygen Exchange Equilibrium Constant, K_{eq} as a Function of Temperature. Line is from Ergun (5), Data are from Present Experiments.

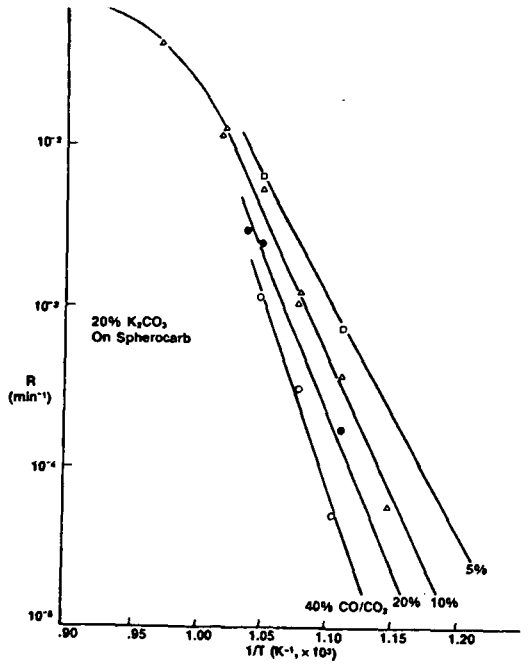

Figure 2: Effect of CO/CO_2 Ratio on Gasification Rate

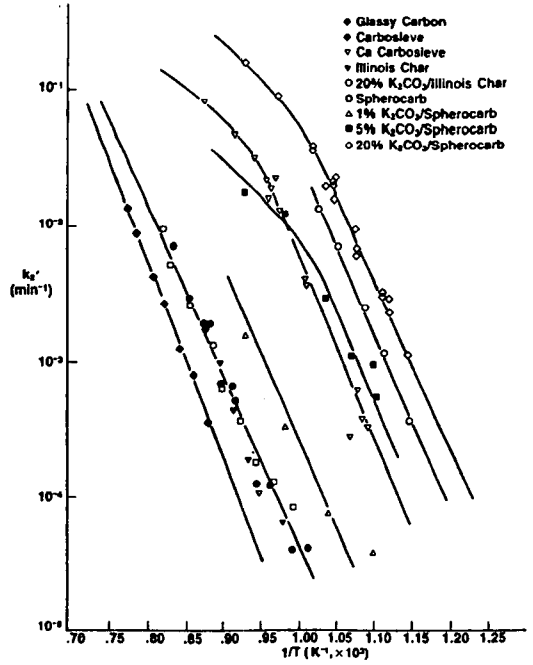

Figure 3 Arrhenius Plots of k_2 for Different Catalytic and Noncatalytic Systems.

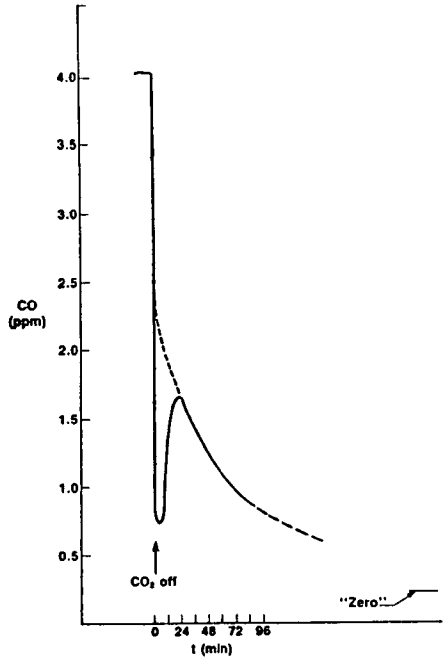

Figure 4: Experimental CO Trace for Uncatalyzed Carbon T=607°C.

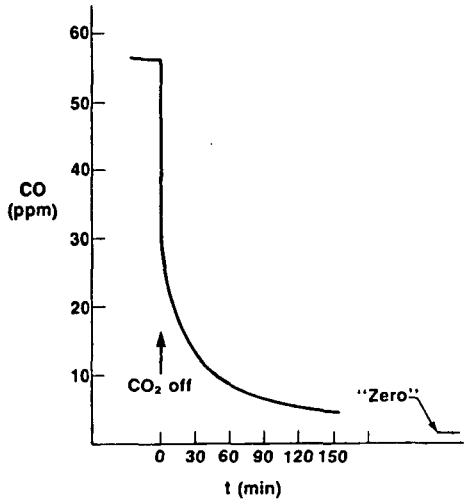

Figure 5: Experiment CO trace for Ca-catalyzed carbon, T = 629°C

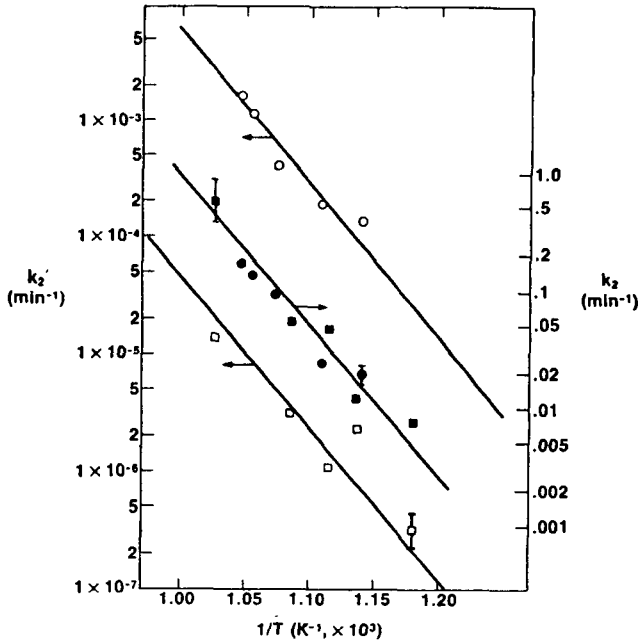

Figure 6: Arrhenius Plot of Rate Constants k_2 and k_2'; o and ○- Ca- Catalyzed Carbon; and - Uncatalyzed Carbon. The lines of k_2 are from the TGA data.

CHAR GASIFICATION BY CARBON DIOXIDE: FURTHER EVIDENCE FOR THE TWO-SITE MODEL

P.C. Koenig, R.G. Squires, N.M. Laurendeau

Coal Research Center, Purdue University, West Lafayette, IN 47907

1. INTRODUCTION

Several experimental studies of the C-CO_2 gasification reaction have been made. Many investigators have noted that the kinetic data substantiate a rate equation of Langmuir-Hinshelwood form [1,2,3,4]:

$$R = \frac{b_1[CO_2]}{1 + b_2[CO] + b_3[CO_2]} \tag{1}$$

where R is the intrinsic reactivity ($g/m^2 s$), and the b's represent rate coefficient ratios. Laurendeau [4] summarizes the evidence supporting the following oxygen exchange mechanism which is in agreement with Eqn. (1):

$$C_f + CO_2 \underset{k'_{-1}}{\overset{k'_1}{=}} C(O) + CO \tag{2}$$

$$C(O) \overset{k'_2}{\rightarrow} CO \tag{3}$$

where C_f represents a free carbon site and C(O) a chemisorbed oxygen atom. Applying the steady state approximation to C(O) and a balance on active sites,

$$[C_t] = [C_f] + [C(O)], \tag{4}$$

yields the following values for b_1, b_2, and b_3:

$$b_1 = m_c k'_1 [C_t], \quad b_2 = \frac{k'_{-1}}{k'_2}, \quad b_3 = \frac{k'_1}{k'_2}, \tag{5}$$

where m_c is the mass of a carbon atom.

Inverting Eqn. (1) gives

$$\frac{1}{R} = \frac{b_3}{b_1} + \frac{b_2}{b_1}\frac{[CO]}{[CO_2]} + \frac{1}{b_1}\frac{1}{[CO_2]}. \tag{6}$$

Thus, the following relationships should exist at constant temperature, if the above model holds:

1. 1/R vs. $1/[CO_2]$ should be linear for constant [CO];

2. 1/R vs. $1/[CO_2]$ should be linear for constant [CO]/[CO2];

3. 1/R vs. [CO] should be linear for constant $[CO_2]$;

4. 1/R vs. $1/[CO_2]$ should be linear for near-zero [CO].

The purpose of this paper is to examine these relationships for data obtained from our laboratory and the literature. In the course of this analysis, we will show that sufficient experimental evidence exists to question the validity of Eqn. (6) and hence the single-site oxygen exchange mechanism. A two-site model is proposed to explain the available experimental data.

2. EXPERIMENTAL PROCEDURE

A differential packed-bed reactor made from 15 mm ID quartz was employed to study the gasification kinetics of Saran char at temperatures between 858 and 956°C, and a total pressure near 1 atm (101.3 kPa). The Saran char was made by heat-treating Dow Chemical Saran polymer in nitrogen at 1300 K for three hours. The reactor was typically loaded with between 0.15 and 3.75 gm of ~250 μm char particles yielding a bed height between 0.5 and 10.0 cm. Carbon dioxide, carbon monoxide and argon at 99.99% purity were flowed through the char bed at a total flow rate of between 200 and 1000 cc/min (STP). Carbon dioxide was used as the reactant gas, carbon monoxide was added to study its inhibitive effect on gasification, and argon was employed to vary the inlet CO_2 and CO concentrations. The reaction rates were determined from the amount of CO produced by gasification as measured by an Infrared Industries dual beam nondispersive infrared analyzer (IR-703D). In order to compare the rate data at a commmon extent of reaction, the rate dependence on CO_2 and CO was determined using a method similar to Tyler and Smith [5]. The percent conversion was maintained below 4.0% to ensure differential conditions. Experimental tests and theoretical criteria indicated the absence of transport limitations. The intrinsic reactivities presented in this study are based on the specific surface area at ~10% burn-off (1285 m^2/g; Dubinin-Radushkevich isotherm with CO_2 at 298 K).

3. RESULTS

Data for 1/R vs. $1/[CO_2]$ for [CO] ~ 15 kPa and for [CO]/[CO2] ~ 0.25 were fit using a linear regression analysis and appear in Figs. 1 and 2. The plots are linear with positive intercepts for all temperatures. Strange and Walker [6] noted similar results for SP-1 graphite when $[CO_2]$ is varied for a fixed [CO], and when [CO2] is varied for a fixed [CO]/[CO2] ratio. Thus, Eqn. (6) adequately fits gasification data in the presence of carbon monoxide.

Plots of 1/R vs. [CO] for $[CO_2]$ ~ 60 kPa appear in Figure 3. The plots are linear as anticipated with positive intercepts. Gadsby et al. [2] and Wigmans et al. [7] also obtained this result for coconut charcoal and activated peat char, respectively. Consequently, this test also supports Eqn. (6).

Data for 1/R vs. $1/[CO_2]$ for no CO in the inlet were also fit using a linear regression analysis and appear in Fig. 4. The data exhibit a concave downward curvature about the best-fit lines. From replicate data, the ratio of the mean square "linear-model" error to the mean square experimental error was calculated. A statistical F test indicates that the curvature is not due to random experimental error. Concave downward curves for plots of 1/R vs. $1/[CO_2]$ with no CO in the inlet can also be discerned [9] in the data of Tyler and Smith [5], Gadsby et al. [2], and in data from our laboratory for coconut char [10]. Turkdogan and Vinters [8] found their gasification rates for no CO in the inlet to be proportional to $[CO_2]^{0.5}$ over a 100 fold change in $[CO_2]$. Although Eqn. (1) allows a fractional order dependence on $[CO_2]$, it is not consistent with a constant fractional dependence over a wide $[CO_2]$ range. These and other results [6,10] suggest that the current single-site model must be modified.

4. DISCUSSION

A suitable modification involves the two-site adsorption of CO_2 shown below [10]:

$$CO_2 + 2\,C_f \underset{k_{-1}}{\overset{k_1}{=}} C^* \tag{7}$$

$$C^* \underset{k_{-2}}{\overset{k_2}{=}} C(O) + C(CO) \tag{8}$$

$$C(CO) \underset{k_{-3}}{\overset{k_3}{=}} C_f + CO \tag{9}$$

$$C(O) \overset{k_4}{\rightarrow} CO, \tag{10}$$

where C^* is the two-site surface complex. Temperature programmed desorption and isotopic tracer experiments [3,11,12] indicate that $[C^*]$ and [C(CO)] are probably small in comparison to [C(O)] and $[C_f]$ during gasification. Thus, using the same site balance as in Eqn. (4) and applying the steady state approximation to each surface species will yield the following equation after rearrangement [10]:

$$[C(O)]^2 \left\{ \frac{k_2 k_{-2}(k_4 - k_{-3}[CO])}{(k_2 + k_{-1})k_3} + \frac{k_1 k_2 [CO_2]}{(k_2 + k_{-1})} - \frac{k_{-2}(k_4 - k_{-3}[CO])}{k_3} \right\}$$
$$+ [C(O)][C_t] \left\{ \frac{k_2 k_{-2} k_{-3}[CO]}{(k_2 + k_{-1})k_3} - \frac{2k_1 k_2 [CO_2]}{(k_2 + k_{-1})} - \frac{k_{-2} k_{-3}[CO]}{k_3} - k_4 \right\}$$

$$+ [C_t]^2 \frac{k_1 k_2 [CO_2]}{(k_2 + k_{-1})} = 0. \qquad (11)$$

The preceding general equation can branch in two directions depending on the amount of CO.

4.1 Case I: Significant [CO]

Since Rxn. (10) is irreversible, increasing [CO] is expected to decrease [C(O)] via the reverse of Rxns. (8) and (9). If [C(O)] becomes sufficiently small, then

$$[C_t] \gg [C(O)]. \qquad (12)$$

Analysis of the first and second sets of bracketed terms in Eqn. (11) suggests that the sets are similar in magnitude. Eqn. (12) implies that multiplying the first set of bracketed terms by $[C(O)]^2$ and the second set by $[C(O)][C_t]$ will make the first term in Eqn. (11) negligible in comparison to the second term. Since

$$R = m_c k_4 [C(O)],$$

Eqn. (11) yields

$$R = \frac{m_c \frac{k_1 k_2}{k_{-1}} [C_t][CO_2]}{1 + \frac{k_{-2} k_{-3}}{k_3 k_4}[CO] + \frac{2k_1 k_2}{k_{-1} k_4}[CO_2]}, \qquad (13)$$

where k_{-1} has been assumed to be much larger than k_2 (i.e., CO_2 desorption rate is much faster than CO_2 decomposition rate).

Eqn. (13) is of same form as Eqn. (1) with the following values for b_1, b_2, and b_3:

$$b_1 = m_c \frac{k_1 k_2}{k_{-1}} [C_t], \quad b_2 = \frac{k_{-2} k_{-3}}{k_3 k_4}, \quad b_3 = \frac{2k_1 k_2}{k_{-1} k_4}. \qquad (14)$$

Hence, for significant [CO], 1/R vs. $1/[CO_2]$ should be linear for constant [CO] and constant $[CO]/[CO_2]$, and 1/R vs. [CO] should be linear for constant $[CO_2]$ as demonstrated previously. When sufficient [CO] is available, the previous single-site model and the proposed two-site model are indistinguishable with respect to the final rate expression. Moreover, both explain the available rate data.

The slopes and intercepts from Figs. 1-3 can be used to calculate values for $m_c k_4 [C_t]$, $m_c k_1 k_2 [C_t]/k_{-1}$, and $m_c k_{-2} k_{-3} [C_t]/k_3$ (Table 1). The intercepts of the 1/R vs. $1/[CO_2]$ plots at constant [CO] directly yielded $m_c k_4 [C_t]$ values. These values also had the least error (95%

confidence limits). Similarly, the slopes of the 1/R vs. $1/[CO_2]$ plots at constant [CO]/[CO2] gave the best $m_c k_1 k_2 [C_t]/k_{-1}$ values. Values for $k_{-2}k_{-3}m_c[C_t]/k_3$ were calculated from the slopes of the 1/R vs. [CO] plots at constant $[CO_2]$ and using the above values for $k_4 m_c [C_t]$ and $k_1 k_2 m_c [C_t]/k_{-1}$.

4.2 Case II: Insignificant [CO]

If the same assumption regarding the rate coefficients is made as for the first case (i.e., $k_{-1} >> k_2$), and any term containing [CO] is set to zero, Eqn. (11) yields after applying the quadratic equation [10]:

$$R = (m_c k_4) \frac{k_4 + \frac{2k_1k_2}{k_{-1}}[CO_2] - \sqrt{\frac{4k_1k_2k_4}{k_{-1}k_3}(k_{-2} + k_3)[CO_2] + k_4^2}}{\frac{2k_1k_2}{k_{-1}[C_t]}[CO_2] - \frac{2k_{-2}k_4}{k_3[C_t]}}. \quad (15)$$

If we further assume that k_{-2} is much larger than k_3 (i.e., C(CO) reacts with C(O) faster than it desorbs from the surface), then it is reasonable to presume that

$$\sqrt{\frac{k_1k_2k_4k_{-2}}{k_{-1}k_3}[CO_2]} >> \frac{k_1k_2}{k_{-1}}[CO_2],$$

and (16)

$$\frac{k_{-2}k_4}{k_3} >> \frac{k_1k_2}{k_{-1}}[CO_2].$$

Applying Eqn (16) and also assuming that k_4^2 is small compared to the CO_2 term under the square root sign in Eqn. (15), we find that the reaction rate has a square root dependence on $[CO_2]$:

$$R = m_c \left\{\frac{k_1k_2k_3k_4}{k_{-1}k_{-2}}\right\}^{0.5} [C_t][CO_2]^{0.5} - m_c \frac{k_3k_4}{2k_{-2}}[C_t] \quad (17)$$

This predicted square root dependency is consistent with the results of Turkdogan and Vinters [8] with no CO in the inlet. Moreover, the Saran char data demonstrates good linear R vs. $[CO_2]^{0.5}$ plots with the anticipated negative intercept when no CO is present in the inlet gases (Fig. 5). However, a slight concave upward curvature can be discerned in all the plots. To test the ability of Eqn. (15) to account for this departure from linearity, we fit the data with the following equation:

$$R = \frac{d_1 + d_2[CO_2] - \sqrt{d_3[CO_2] + d_4}}{d_5[CO_2] - d_6} \quad (18)$$

Parameters d_2 and d_5 were fixed with values from Table 1. Parameters d_1, d_3, d_4, and d_6 were determined by a non-linear regression analysis using Marquardt's method. Values for $k_4 m_c [C_t]$ can be calculated from d_1 and d_4 and compared to the values in Table 1. Table 2 demonstrates the agreement. Parameters d_1 and d_4 were not constrained in any way, but still yielded almost identical values for $k_4 m_c [C_t]$. This agreement supports the proposed two-site model.

5. CONCLUSIONS

Proposed models for gasification by CO_2 should account for the following experimental observations obtained in this investigation and the literature:

1. 1/R vs. [CO] is linear for constant $[CO_2]$.
2. R vs $[CO_2]^{0.5}$ is near-linear for no CO in the inlet and differential reaction conditions ([CO] ~ 1 kPa).
3. 1/R vs. $1/[CO_2]$ is linear for higher concentrations of CO in the inlet ([CO] ~10 kPa).

The model proposed here to account for these observations involves a two-site adsorption and dissociation of CO_2 on the surface.

ACKNOWLEDGEMENTS

This study was supported by a grant from Conoco, Inc. through the Coal Research Center at Purdue University. We appreciate the helpful comments of Prof. R.P. Andres, Prof. W.N. Delgass, Prof. C.G. Takoudis, and other members of the catalysis group in the Chemical Engineering Department of Purdue University. In addition, we are thankful to P.R. Abel and B.J. Waters for their assistance with this work.

REFERENCES

1. P.L. Walker, Jr., F. Rusinko, Jr., and L.G. Austin, Advances in Catalysis, Vol. 11, p 133. Academic Press, New York (1959).
2. J. Gadsby, F.J. Long, P. Sleightholm, and K.W. Sykes, Proc. R. Soc., London A103, 357 (1948).
3. M. Mentser and S. Ergun, "A Study of the Carbon Dioxide-Carbon Reaction by Oxygen Exchange," U.S. Bureau of Mines Bulletin 664 (1973).
4. N.M. Laurendeau, Prog. Energy Combust. Sci. 4, 221 (1978).
5. R.J. Tyler and J.W. Smith, Fuel 54, 100 (1975).
6. J.F. Strange and P.L. Walker, Jr., Carbon 14, 345 (1976).

7. T. Wigmans, A. Hoogland, P. Tromp, and J.A. Moulijn, Carbon 21, 13 (1983).

8. E.T. Turkdogan and J.V. Vinters, Carbon 7, 101 (1969).

9. P.C. Koenig, M.S. Thesis, Purdue University (1983).

10. P.C. Koenig, R.G. Squires, and N.M. Laurendeau, Carbon in press.

11. F. Kapteijn, G. Abbel, and J.A. Moulijn, Fuel 63, 1036 (1984).

12. S.S. Barton and B.H. Harrison, Carbon 13, 283 (1975).

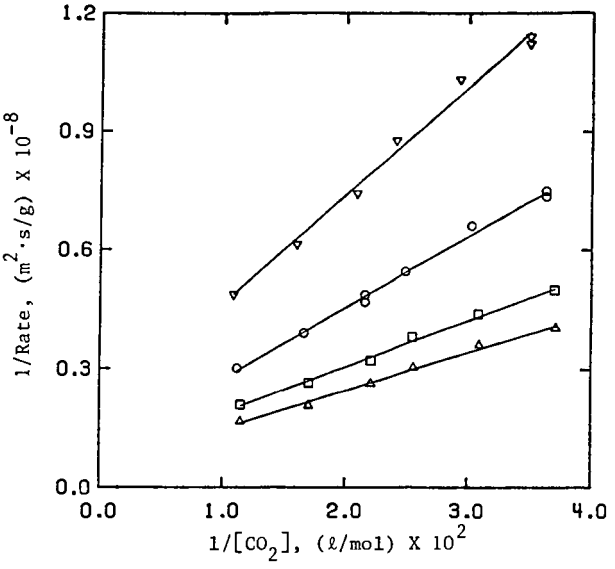

Figure 1. Test of Eqn. (6) for Saran Char with [CO] ∿ 15 kPa (1.5×10^{-3} mol/ℓ). ∇ - 1189 K, 0 - 1206 K, □ - 1217 K, Δ - 1229 K.

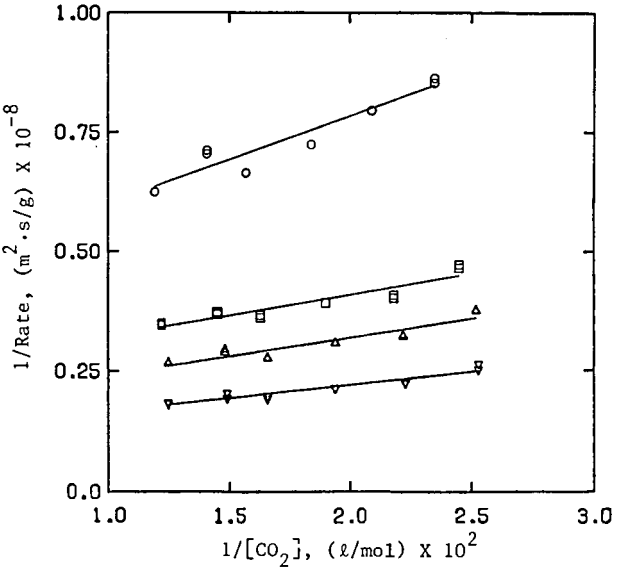

Figure 2. Test of Eqn. (6) for Saran Char with [CO]/[CO_2] ∿ 0.25. 0 - 1189 K, □ - 1206 K, Δ - 1217 K, ∇ - 1229 K.

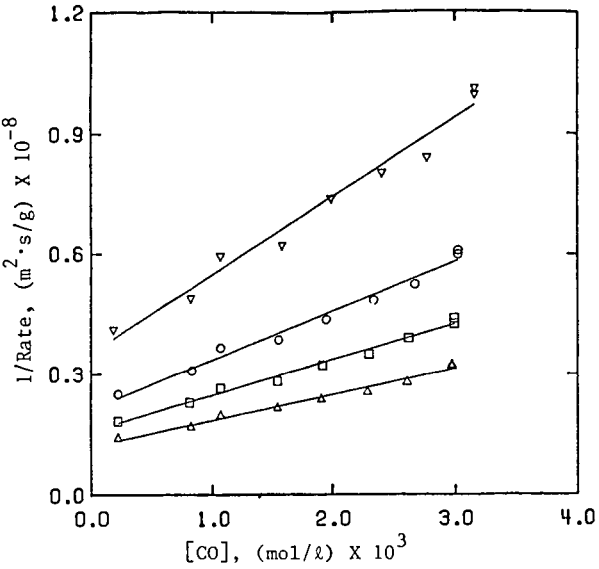

Figure 3. Test of Eqn. (6) for Saran Char with $[CO_2] \sim 60$ kPa (6×10^{-3} mol/ℓ). ▽ - 1189 K, 0 - 1206 K, □ -1217 K, Δ - 1229 K.

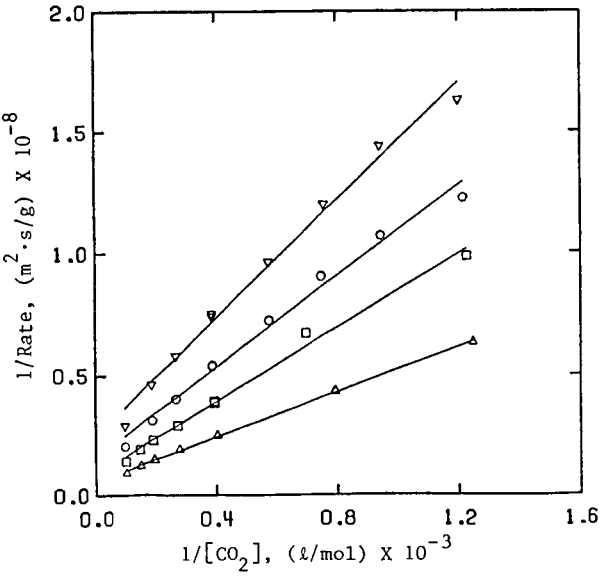

Figure 4. Test of Eqn. (6) for Saran Char with $[CO] \sim 1$ kPa (1×10^{-4} mol/ℓ). ▽ - 1189 K, 0 - 1206 K, □ - 1217 K, Δ - 1229 K.

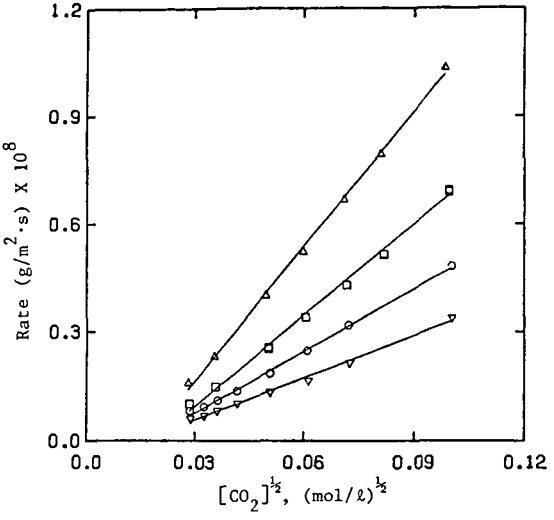

Figure 5. Test of Eqn. (17) for Saran Char with [CO] ∿ 1 kPa (1 X 10^{-4} mol/ℓ). ∇ - 1189 K, O - 1206 K, □ - 1217 K, Δ - 1229 K.

Table 1. Experimental Values for Rate Coefficient Ratios.

Temp., K	$m_c k_4 [C_t]$ ($\frac{g}{m^2 s}$ X 10^7)	$m_c \frac{k_1 k_2}{k_{-1}} [C_t]$ ($\frac{g}{m^2 s} \cdot \frac{\ell}{mol}$ X 10^5)	$m_c \frac{k_{-2} k_{-3}}{k_3} [C_t]$ ($\frac{g}{m^2 s} \cdot \frac{\ell}{mol}$ X 10^4)
1189	1.07 ± 0.46	0.55 ± 0.18	0.71 ± 0.64
1206	2.09 ± 0.72	1.15 ± 0.32	1.77 ± 1.32
1217	2.75 ± 0.86	1.27 ± 0.34	1.82 ± 1.24
1229	3.78 ± 1.52	1.85 ± 0.43	2.64 ± 2.00

Table 2. Comparison of $m_c k_4 [C_t]$ ($\frac{g}{m^2 s}$ X 10^7) Values.

Temp., K	$m_c k_4 [C_t]$ from Table 1	$m_c k_4 [C_t]$ from d1	$m_c k_4 [C_t]$ from d4
1189	1.07 ± 0.46	1.06 (0.77-1.29)	1.08 (0-1.28)
1206	2.09 ± 0.72	2.44 (1.82-2.94)	2.45 (1.70-2.82)
1217	2.75 ± 0.86	2.80 (2.72-2.87)	2.80 (2.72-2.88)
1229	3.78 ± 1.52	3.52 (3.10-3.89)	3.52 (3.00-3.87)

KINETIC AND MECHANISTIC ASPECTS OF CO_2 GASIFICATION ON ALKALI TREATED CARBON

C. T. Ratcliffe*

Corporate Research - Science Laboratory
Exxon Research and Engineering
Route 22 East, Annandale, N. J. 08801

Introduction

While catalysis of CO_2 gasification of carbon or coal chars by alkali metals has been the subject of many investigations (1), the state of the catalyst site during gasification and the mechanism involved in the rate limiting step have yet to be resolved. An inherent problem in catalyzed gas-solid reactions at the required high temperatures is the inability to separate the reaction into discrete steps which can be monitored under isothermal reaction conditions. The approach taken in this study has been to decouple the reaction into three steps: catalyst activation, CO_2 chemisorption and reaction/desorption, with only the adsorption step examined under isothermal conditions. The strong chemisorption of CO_2 on thermally activated potassium sites, which showed similarities via our MAS-NMR analysis to the electrostatically held CO_2 on alkali treated Al_2O_3 or SiO_2-Al_2O_3 catalysts as reported by Krupay et al. (2), Sefcik et al. (3,4) and Barrer et al. (5) has allowed the population of active sites to be measured by the quantity of CO_2 that irreversibly chemisorbed at 300°C on the active surface (6). The state of this intermediate is similar to the type suggested much earlier by Long and Sykes (7) and more recently by Mims and Pabst (8), but in disagreement with a mechanism involving K_2CO_3 formation and subsequent reduction to the metal as proposed by McKee (9) and Vera and Bell (10).

The objective of this study has been to examine the thermochemical reaction(s) of each adsorbed CO_2 complex with an atom of carbon on the surface to eventually yield two molecules of CO. Isotope labelled $^{13}CO_2$ has been adsorbed on the active sites so that the reaction chemistry of CO_2 with the carbon lattice could be monitored by Temperature Programmed Desorption (TPD) with the carbon label differentiated by mass spectral examination of the products. While the TPD analysis technique has been primarily employed for examining desorption of single crystal catalyst surfaces (11), the technique can be applied to porous catalyst materials with proper precautions (12). If discrete desorption states can be identified, details of the kinetics of desorption process can be obtained (13). Feats and Keep have examined graphite (thermal or reactor irradiated) after CO_2 or O_2 adsorption by TPD and found discrete states for desorption of CO and CO_2 (14). Linear TPD analysis and a step-TPD technique were studied by Tremblay et al. to determine the energetics of oxygen removel as CO from non-catalyzed carbons. These authors summarized their results with two major points; more than one functional group is present on carbon and the activation energies for these complexes must be a distributed function (15). Frericks has reported TPD spectra for CO_2 and H_2O on potassium doped carbon samples but the spectra were not analyzed for kinetic information (16).

* Present Address: Union Oil Company of California, Science and Technology Division, P. O. Box 76, Brea, California 92621

Discrete desorption states for 13-labelled CO and lattice carbon derived CO have been obtained in this study by TPD at one atmosphere in a flowing inert gas stream. Analysis of the TPD spectra by the methods outlined by Redhead, Cvetanovic and Amenomiya and Taylor and Weinberg are presented (11,13,17).

EXPERIMENTAL

Samples and Reagents

Spherocarb, a low ash form of activated carbon with a surface area of 800 m^2/g, was purchased from Analabs Inc., New Haven, Connecticut. Isotope labelled $^{13}CO_2$ (98% ^{13}C) was purchased from Isotec, Inc., Centerville, Ohio, with the percentage isotope label verified by M.S. analysis. A high purity source of He (99.9999%) was used as a carrier gas in all experiments. The He stream was passed through a heated trap containing Cu turnings for O_2 removal followed by molecular sieve traps to insure H_2O removal. The purity of He was found to be critical in adsorption/desorption runs on carbon and was checked periodically by verifying a constant weight of carbon in the TGA/DSC at elevated temperatures (800°C) while flowing a He stream for 2-3 hour period.

Potassium carbonate was purchased from B&A Chemicals (reagent grade). Aqueous solution of K_2CO_3 were used to impregnate Spherocarb samples with the volume of the aqueous solution equated to the quantity of moisture required to fully wet the surface but not allow excess solution (method of incipient wetness). After impregnation, samples were dried to 60-70°C in a vacuum oven and sealed in glass containers under inert atmosphere.

Isothermal adsorption and temperature programmed desorption runs were performed in a Mettler 2000C TGA/DSC Analyzer. The balance platform, sample crucibles and chamber were constructed of α-alumina with no artifacts in adsorption of desorption noted in blank runs. Analysis of the exit gas was performed with a UTI model 100 mass spectrometer that was interfaced with a Spectra Link unit to a M1NC 1123 laboratory computer. Multiple ions could be monitored on a continuous basis during TPD runs. In a typical run, eight amu valves were monitored in a cyclic manner in which data for each mass unit was collected for one second with a total cycle comprising about ten seconds. In this manner, a sufficient number of counts could be obtained for each ion to provide an accurate ratio of partial pressures while the frequency of cycling was fast enough to gain peak temperatures (T_p) for CO and CO_2 fragments at programming rates up to 0.5 K/sec. A small portion (5-10%) of the exit flow from the reaction chamber was differentially pumped through a capillary tube to minimize lag time to the M.S. chamber. The flow pattern, as outlined on Figure #1, was designed to minimize readsorption during TPD experiments (12).

Adsorption of CO_2 was always performed with 90% He dilution. Samples of K_2CO_3-Spherocarb were preconditioned by heating to 850°C in an inert gas flow prior to the adsorption/TPD study. After an isothermal temperature was established, the adsorption was carried out at 60°C followed by a period of approximately one hour to purge the chamber of residual CO_2.

RESULTS AND DISCUSSION

Product Formation and Isotope Distribution

The profile of desorbed products, as shown in Figures 2 and 3, identifies three regions of desorption for CO. Desorption of CO_2 can also be detected in much

lower concentrations with a low temperature peak centered at 170°C and a broad desorption peak at 500°C. The C-13 label on adsorbed CO_2 readily differentiates the source of carbon for both CO and CO_2. Desorption of CO with mass 29 is clearly present in peaks at 200°, 490°, and 685°, while mass 28 (CO from lattice carbon) is only observed in the 750°C peak. Only labelled CO_2 (mass 45) can be seen in the desorption spectra. The lack of coincidence in desorption states for ^{13}CO or ^{12}CO should be noted as it indicates distinct desorption processes. Adsorption of CO_2 at isothermal temperatures from 25-100°C had no effect on the relative ratio of products or the peak maxima. Higher temperature adsorption of CO_2 decreased the contribution of the lower temperature states in the TPD spectrum. Continued evolution of CO above 800°C is also evident in all the spectra. Removal of tightly bound oxygen in chars is known to require very high temperatures (1000°C in vacuum) (18,19) in addition to eventually volatilizing the alkali metal (20). The chemistry in this temperature region was not examined as it is not relevant to the catalytic reaction.

Continued cycling of CO_2 adsorption at 25°C or 100°C followed by TPD programming to 800-850°C demonstrated the reproducible stoichiometry of the Boudouard reaction as monitored during each cycle with the TGA unit:

$$CO_2(44\ \text{amu}) + C(12\ \text{amu}) \rightarrow 2CO\ (56\ \text{amu}).$$

Thus, separation of the adsorption process and the subsequent thermal desorption into separate steps allowed gasification to be performed on a "one turnover" per cycle basis. That is, for each active site that chemisorbed one molecule of CO_2, one atom of lattice carbon was reacted during the TPD process to yield two molecules of CO. The quantity of adsorbed CO_2 could readily be controlled by introducing a limited amount of CO_2 into the gas stream and observing the weight gain with the TGA. Thus the effect of desorption at different loading levels could be quantified with the measured weight of adsorbed CO_2 and desorbed CO as known gravimetric values and the isotope contribution determined from the area under the mass spectral profiles. The TPD profiles in Figures 2-4 correspond to desorption of a full saturation of chemisorbed sites (0.6 sites/mole of K_2CO_3 impregnated). A decline in the total mass of desorbed ^{13}CO as compared to ^{12}CO with lower loadings was observed upon integrating the area under the respective M.S. profiles shown in Figures 2 and 4. A similar decrease in the ratio of $^{13}CO/^{12}CO$ was noted with equal coverages of CO_2 but decreasing ramping rates. Readsorption of ^{13}CO after its release from lower energy binding states appears probable from these results with a visual illustration of the decline in ^{13}CO with lower loading shown in Figure 4.

Adsorption of CO_2 at elevated isothermal temperatures was examined up to 500°C. TPD analysis of the surface after adsorption at elevated temperatures showed a dominance of CO desorption in the anticipated 700°C region, with little contribution from the lower states.

Determination of Rate Parameters via TPD Analysis

Interpretation of TPD spectra allows the activation energy, frequency factor and order of a process to be determined as the shape of the peaks and the position of the peaks maxima bear a fundamental relationship to the desorption process (11-13).

Data obtained from TPD spectra with variable surface coverage was analyzed from the basic equation,

$$\frac{E_d}{RT_p^2} = \frac{V^n}{\beta} \quad C^{n-1} \exp \frac{-E_d}{RT_p} \qquad (1)$$

n = reaction order
C = surface conc.
V = frequency factor
E_d = activation energy
T_p = peak desorp. temp.
β = ramping rate

Rearrangement of this equation reveals the dependence of surface concentration on temperature as a function of reaction order.

$$C^{n-1} = \exp. \frac{E_d}{RT_p} \cdot \frac{E_d \beta}{RT_p^2 V^n} \qquad (2)$$

If little change in the energy or frequency factor is assumed as a function of loading level, the relative shift of T_p as a function of C will allow a determination of the reaction order. The temperature of the desorption peak for lattice derived carbon (^{12}C) remained constant in the region of surface coverages used in this study (40-100%) and thus represented the profile of a first order desorption process. The three desorption peaks for ^{13}CO (derived from $^{13}CO_2$) also showed constant T_p values at surface coverages in the range mentioned above as shown in Figure #3 which is consistent with first order desorption processes.

TPD experiments were also performed at constant surface coverage values of CO_2, as measured with the thermal balance, and at variable heating rates of 0.5 K/sec. to 0.033 K/sec. Surface coverages above 80% were used in all cases. Analysis of the activation energies and preexponential factors could be determined from the log form of equation (1) as mass transfer problems were not anticipated based on the design parameters of Gorte (12) and the effect of readsorption on the preexponential term was small compared to the error in the intercept under the conditions of this study (21). Adsorption of CO on this surface had also been shown by independent studies to be a non-activated process, thus $\Delta H = E_d$.

$$2 \ln T_p - \ln \beta = \frac{E_d}{RT_p} - \ln \frac{V^n R}{E_d} \qquad (3)$$

The values of T_p were obtained from both the mass spectral plot and the DTGA peak from the weight loss profile. Desorption of ^{13}CO in the higher temperature region required dependence on only the M.S. values as the derivative weight loss peak (DTGA) usually appeared as a shoulder on the larger ^{12}CO peak. The series of M.S. spectra generated from the desorption of m/e = 28 at different β values is shown in Figure 5. The values of T_p, which required a temperature correction for heat transport effects, were utilized to calculate parameters for activation energies and factors. The desorption energy for the lower temperature release of ^{13}CO, as shown in Figure 6, gave a value of 45 ± 3 Kcal/mole with a frequency factor of 4×10^{12}. Desorption of ^{12}CO and ^{13}CO at the higher temperature region revealed higher energy values of 73 ± 3 Kcal/mole and 72 ± 5 Kcal/mole, respectively with frequency factors of 10^{15}-10^{16} range for both processes (see Figures 7,8). The temperature dependence

plot for ^{12}CO in Figure 7 displays the experimental values for DTGA and M.S. derived values of T_p while Figure 6 and 8 were taken from mass spectral profiles.

Energetics and Mechanism of CO Formation and Desorption

Exothermic adsorption of CO_2 on discrete alkali containing sites results in the formation of a CO_2 containing complex that appears stable up to 400°C. The chemical shift of 13 labelled carbon (from adsorbed CO_2) by MAS-NMR clearly showed that K_2CO_3 and $KHCO_3$ have not formed, but the surface intermediate appears to be "carbonate" in nature. Temperature programmed desorption up to 400°C in this study revealed no enthalpy changes as noted with the DSC probe, precluding any chemical change involving gain or loss of energy although CO and CO_2 evolution from weakly held sites occurred at 200°C. Thus, the breaking of the CO_2 complex on a potassium salt treated carbon surface to transfer oxygen and the desorption of CO appear to occur as a single endothermic process at 400°C. This transfer of oxygen and desorption of CO most probably is catalyzed by the potassium site. Bonner and Turkevich (22), Lang and Magnier (23) and Tonge (24) have independently studied the transfer of oxygen from CO_2 to different forms of non-catalyzed graphite of carbon. Desorption of CO was found to occur at temperatures as low as 450°C (Tonge) although the rate of exchange of oxygen from CO_2 to carbon was very low (1700 hrs for completion at 500°C) and the surface coverage was minimal (7×10^{-6} C atom sites/C atom). The inability to desorb all the labelled ^{13}CO in this study at the 400°C endothermic transition, either due to readsorption of CO or the presence of more than one type of site, precludes any statement from this study claiming a single event for the first step in the classic mechanism of CO_2 gasification as outlined by Long and Sykes (25), where (0) refers to an adsorbed oxygen on the carbon surface.

$$CO_2 + (0) \rightarrow CO \qquad (a)$$
$$C + (0) \rightarrow CO \qquad (b)$$

The demonstrated ability of K-Spherocarb to chemisorb CO, with eventual desorption of the majority of the oxygen from a higher dissociated state, places more emphasis on the third step in above mechanism of gasification as shown below:

$$CO \underset{j}{\overset{i}{\rightleftharpoons}} (CO). \qquad (c)$$

While readsorption of CO was not found to be significant in the kinetic study with carbon (8,25) it may be important with potassium treated carbon. The desorption energy for the removal of CO at 490°C from K-Spherocarb via TPD analysis in this study (45 $\pm$ 3 Kcal/mole) with a frequency factor of 10^{12} represent a considerably more facile process than the initial transfer process of Long and Sykes (a) for extracted charcoal (E_{act} = 68, V = 3×10^9) or for the original charcoal (E_{act} = 58.8 Kcal, V = 6×10^8) (8). Our studies of CO adsorption on K-Spherocarb showed a non-activated process (thus $\Delta H_{desorp.} = E_{act}$); the lower activation energy and higher pre-exponential factor therefore represent the catalytic activity of potassium in this first step (a). The low temperature transition for release of oxygen on alkali treated carbon surfaces is consistent with earlier oxygen exchange studies (19-22) in addition to the aforementioned work by Long and Sykes (8,25).

The energetics and isotope distribution of CO adsorption states allows additional insight on the nature of the surface complexes. The release of CO above 600°C involves separate and discrete sites for lattice derived carbon and CO_2

derived carbon as distinguished by the carbon isotope label. The relative increase in the quantity of ^{13}CO desorbed in the 600-700°C region with a decrease in coverage of adsorbed $^{13}CO_2$ is consistent with preferential bonding to this site (either directly or by readsorption) vs the weaker sites desorbing at 490 and 200°C. As the total quantity of desorbed ^{13}CO is similar to desorbed ^{12}CO, and much greater than the predicted quantity of lattice carbon exposed on the higher surface area Spherocarb, the labelled carbon must be either bonded to or in close proximity to an oxygen atom. The similarity of the desorption enthalpy for ^{13}CO and ^{12}CO above 600°C also implies a similar form of bound intermediate, although the desorption profile always revealed ^{13}CO evolution at a lower temperature than ^{12}CO. The high activation energy for the above processes is equal or greater than values reported for CO release by others from non-catalyzed carbon system. The value of 59 Kcal reported by Ergun (26,27) on three different carbons (Ceylon Graphite, activated graphite and activated carbon) and the value of 67 Kcal for graphite reported by Tyso (28) et al. were obtained under controlled differential flow conditions. A recent steady state kinetic investigation by Freund (29) has shown an activation energy of 58 ± 3 Kcal for CO_2 gasification of catalyzed and non-catalyzed carbon samples.

The higher energy values obtained in this TPD investigation as compared to steady state kinetic results is probably not due to CO inhibition problems as they have been accounted for in the above quote studies. The inability to measure accurate reaction bed temperatures during the endothermic gasification presents a more plausible explanation. The temperature values obtained in our TPD study, despite the small sample size and low concentration of adsorbed CO_2, required a correction at higher temperatures due to the endotherm of CO desorption. The actual temperature of our desorption peaks were corrected with factors determined from DSC measurement of the melting of metals (also an endothermic process) at the desorption temperature. Localized cooling of the bed during any steady state kinetic run would also result in artificially high temperatures from a thermocouple value which would lower the value of the calculated activation energy from a reaction rate vs. reciprocal temperature plot.

CONCLUSIONS

Isotope labelled TPD under one atmosphere inert gas flow has provided a method of decoupling alkali catalyzed gasification into steps. Distinct desorption states for CO have been identified which help explain the mechanism of CO_2 interaction with the alkali catalyzed carbon surface. The rate limiting step has been shown to involve removal of lattice carbon as CO. As the activation energy for this step does not appear to be lowered by potassium, alkali serves as a catalyst by increasing the number of active sites in CO_2 gasification of carbon and exchanging oxygen from CO_2 to the carbon surface.

Acknowledgments

The author wishes to thank R. A. Salher for technical assistance in the experimental program.

REFERENCES

1. W-Y. Wen Catal. Rev. Sci. Eng 22 (1) 1-28, (1980); D. W. McKee, Chemistry and Physics of Carbon, 16, Marcel Dekker, New York, 1981; International Symposium on the Fundamentals of Catalyzed Coal Gasification, Fuel, 62 (1983).
2. B. Krupay, Y. Amenomiya, J. Catalysis 67, 362 (1981).
3. M. D. Sefcik, J. Schaefer, E. O. Stejskal, ACS Symposium Series #40, Molecular Science II, Ed. J. R. Katzer (1977).
4. M. D. Sefcik, H. V. Yuen, Thermochemica Acta 26, 297 (1978).
5. R. M. Barrer, R. M. Gibbons, Trans. Faraday Society, #509 61 (5), 948 (1965).
6. C. T. Ratcliffe, S. N. Vaughn, Div. of Fuel Preprints, Vol. 30, This Symposium.
7. F. J. Long and K. W. Sykes, J. Chem, Phy. 47, 361 (1950).
8. C. A. Mims, J.K. Pabst, Fuel 62(2), 176 (1983).
9. D. W. McKee, Fuel 62(2) 170 (1983).
10. M. J. Vera, A. T. Bell, Fuel, 57, 194 (1978).
11. P. A. Redhead, Vacuum 12, 203 (1962).
12. R. J. Gorte, J. Catalysis, 75 164 (1982).
13. R. J. Cvetanovic and Y. Amenomiya, Adv. in Catalysis, 17, 103 (1967), Catal. Rev. 6 (1), 21-48 (1972).
14. F. S. Feates and C. W. Keep, Trans. Faraday Soc. 66, 3156 (1970).
15. G. Tremblay, F. J. Vastola and P.L. Walker, Jr., Carbon 16, 35 (1978).
16. I. L. C. Freriks, J. M. H. van Wechem, J. C. M. Stuiver, R. Bouwman, Fuel, 60 1463 (1981).
17. J. L. Taylor, W. H. Weinberg, Surf. Sci., 78, 259 (1978).
18. H. Marsh, D. W. Taylor, Fuel, 54, 218 (1975).
19. N. R. Laine, F. J. Vastola, P. L. Walker, Jr., J. Phys. Chem.,67, 2030 (1963).
20. B. J. Wood, R. D. Brittain, K. H. Lau, Division of Fuel Preprints, 28, (1), 55 (1983).
21. J. S. Rieck, A. T. Bell, J. Catalysis 85, 143 (1984).
22. F. Bonner, J. Turkevich, J. Am. Chem. Soc. 73, 561 (1951).
23. F. M. Lang, P. Magnier, Chemistry and Physics of Carbon, Vol. 3, Ed. P. L. Walker, Jr., Marcel Dekker, N. Y., 1968.
24. B. L. Tonge, Proceedings of the Fourth Carbon Conference, 8uffalo, pp. 87-93 (1960).
25. F. J. Long, K. W. Sykes, Proc. Roy. Soc. (London) A215, 100, (1952); J. Gadsby, F. J. Long, P. Sleightholm and K. W. Sykes, Proc. Roy. Soc. (London) A193, 357 (1948).
26. S. Ergun, J. Phys. Chem. 60 480 (1956).
27. S. Ergun, M. Mentser, Chemistry and Physics of Carbon, pp.203, Vol. 1, Ed. P. J. Walker, Jr., Marcel Dekker Inc. 1965.
28. W. T. Tyso, J. Carrazza and G. A. Somorjai, Div. of Fuel Preprints, 29 2, 190 (1984).
29. H. Freund, Fuel, (to be published).

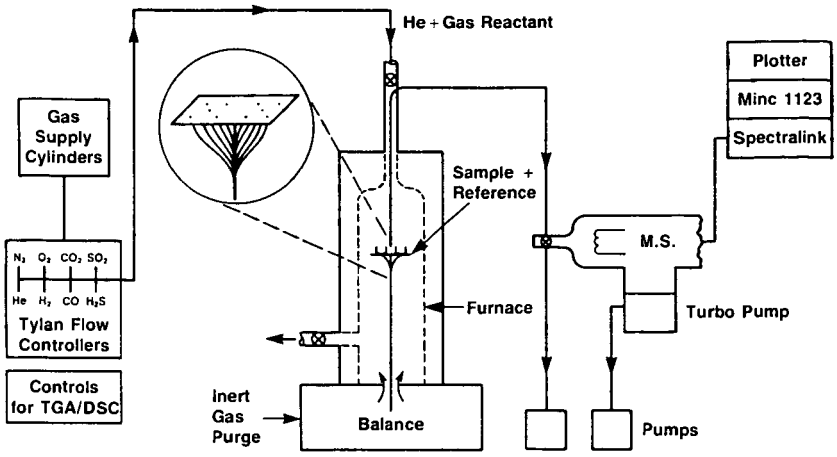

Figure #1. Mettler 2000C Thermal Analysis unit equipped with gas flow control system and on-line M.S. analysis system.

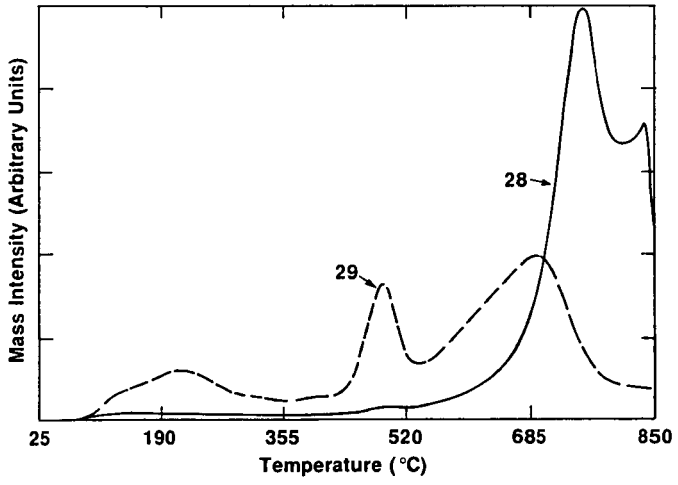

Figure #2. Profile of mass intensity for evolved ^{13}CO (mp=29) and ^{12}CO(m/e=28), temperature programming rate of 0.5 K/s, K-treated Spherocarb powder with $^{13}CO_2$ adsorbed ($\theta \cong 100\%$) at 60°C.

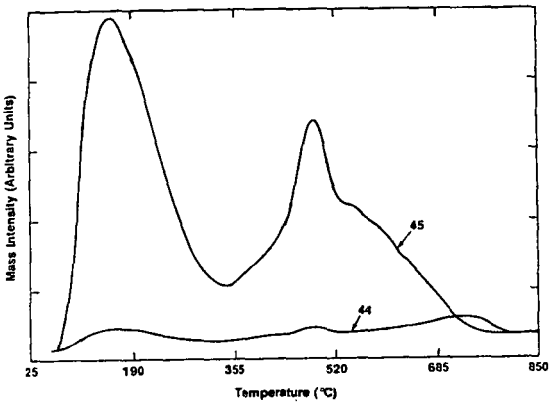

Figure #3. Profile of mass intensities for evolved $^{13}CO_2$(m/e = 45) and $^{12}CO_2$(m/e = 44), intensity scale magnified 7.5x, same run as Figure #2.

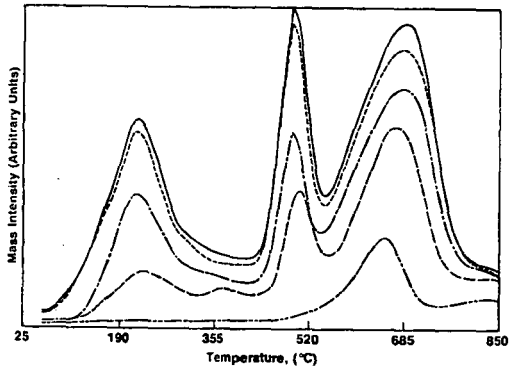

Figure #4. Profile of mass intensity for evolved ^{13}CO (m/e = 29) at different loading levels (θ in %) of $^{13}CO_2$. 1, 6%. 2, 16%. 3, 52%. 4, 76%. 5, 100%.

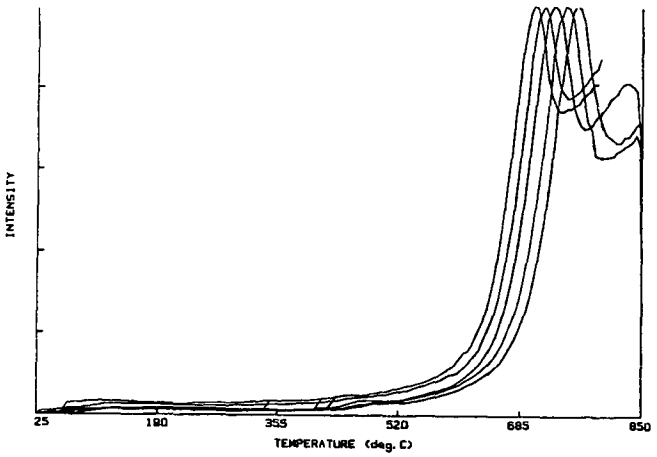

Figure #5. Profile of mass intensities for ^{12}CO desorption (m/e = 28) at different ramping rates (8) 1, 0.083K/sec. 2, 0.125K/sec. 3, 0.167K/sec. 4, 0.0333K/sec. 5, 0.5 K/sec.

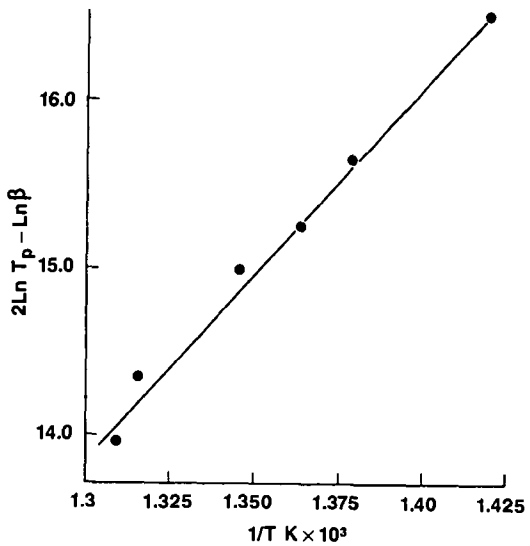

Figure #6. Plot of ^{13}CO desorption values from 420-500°C peak, ΔH from slope 45±3 Kcal/mole, V_1 = $4x10^{12}$.

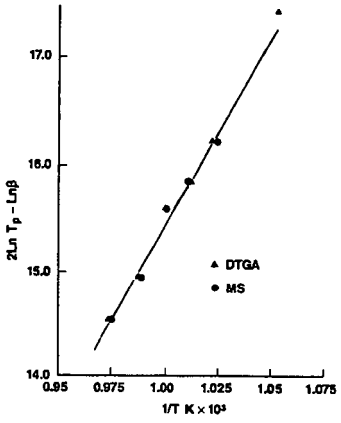

Figure #7. Plot of ^{12}CO desorption values from. 690°C-750°C peak, ΔH from slope 73±3 Kcal/mole, $V_1 = 2x10^{15}$.

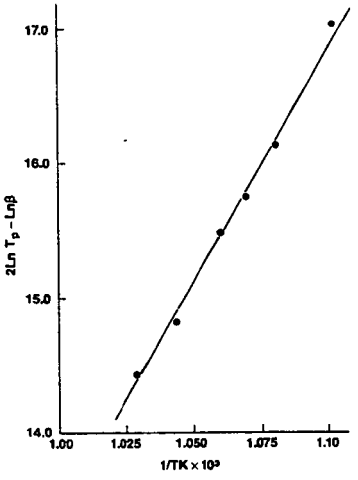

Figure #8. Plot of ^{13}CO desorption values from 650°-690°C peak, ΔH from slope = 72_5 Kcal/mole, $V_1 = 2x10^{16}$.

TEMPERATURE PROGRAMMED REACTION STUDIES OF POTASSIUM/CARBON INTERACTIONS AND CATALYST LOSS

D.A. Sams, T. Talverdian and F. Shadman

Department of Chemical Engineering
University of Arizona
Tucson AZ 85721

INTRODUCTION

The catalytic effect of alkali metals on the gasification rate of carbonaceous materials has been the subject of a number of studies in recent years (1-16). Despite these efforts, the active form of the catalyst during gasification and the effects of catalyst loss remain unclear. The understanding of the reduction of alkali metal catalysts from its initial oxidized form and the identification of the reduced form are necessary requisites for determining the reaction mechanism. Experimental observations from this laboratory clearly indicate that catalyst loss occurs simultaneously with the reduction (12). In addition, the rate of catalyst loss from the surface is directly influenced by the reduced form it takes. The present study provides insight into this subject by examining the reduction of potassium carbonate on the surface of a pure carbon substrate and the accompanying phenomenon of catalyst loss.

EXPERIMENTAL

An uncoated graphitized carbon from Supelco, 60/80 Carbopack B (180-250 μm), with a surface area of approximately 100 m^2/g was used as the substrate in this study. The samples were impregnated with potassium by an incipient wetting technique, then dried at room temperature and stored under vacuum.

The data in this study was generated in a thermogravimetric reactor system utilizing an electronic microbalance and a quartz downtube reactor which enclosed the platinum sample tray as shown in Figure 1. The other major components were a movable electric furnace, a temperature controller and an auxiliary type K thermocouple. The system also included a gas preparation section for mixing and metering the feed gas at the desired compositions and flow rates. The reactant gas was a mixture of 15% CO_2 and 85% N_2. Ultra high purity (UHP) N_2 was used as the purge gas. The product gases were analyzed by an on-line gas chromatograph and nondispersive infrared CO and CO_2 analyzers.

To prepare a run, 20-30 mg of sample were loaded onto the microbalance tray and the reactor was placed in position. The system was purged with UHP N_2 to remove the oxygen and the furnace was raised to enclose the reactor. Two heat-up procedures were used: a linear 5°C/min rate and a rapid one step process where the furnace was preheated to 800°C and then raised to enclose to reactor.

RESULTS AND DISCUSSION

To examine the interaction of the potassium catalyst with the carbon surface, a series of temperature programmed reaction experiments were conducted where the sample mass and the reaction products were continually monitored. Figure 2 shows typical temporal profiles for the CO and CO_2 peaks when the sample is heated to 800°C in a reducing atmosphere at a moderate rate (5°C/min). For clarity in describing the various processes which occur during the transient heat-up period, the results are divided into five separate stages.

Stage I occurs below 250°C and represents the physical desorption of gases such as CO_2 and H_2O from the surface. Stage II (250-700°C) corresponds to the evolution of very small amounts of CO_2 due to the partial decomposition of the catalyst and possibly reactions with chemisorbed oxygen. This is followed by Stage III (700-800°C) where the catalyst is reduced through interaction with the carbon surface and large amounts of CO are generated. Stage IV represents an isothermal heat treatment period where the sample is exposed to UHP N_2 at 800°C. Although no measurable amounts of CO or CO_2 are observed during this stage, a steady weight loss occurs. Finally, Stage V represents the gasification of the carbon sample at 800°C.

When a freshly impregnated sample is heated to 250°C (Stage I), both CO_2 and H_2O are desorbed. The amount of CO_2 generated, normalized with respect to the initial amount of carbon present, is given in Figure 3 as a function of the initial potassium level, $(K/C)_o$. A linear response is observed where one mole of CO_2 is desorbed for every two moles of potassium present. This linearity clearly indicates that the potassium strongly influences the amount of CO_2 adsorbed and the stoichiometry suggests that each mole of potassium carbonate interacts with one mole of CO_2. The amount of CO_2 desorbed was independent of the rate at which the sample was heated to 250°C. The scatter in the data implies that other factors may influence the amount of CO_2 adsorbed.

As the sample temperature approaches 700°C, CO begins to evolve as the catalyst is reduced on the carbon surface (Stage III). The total amount of CO generation is shown in Figure 4 where the CO/C ratio is given as a function of the initial K/C ratio. For each sample, three moles of CO were generated for each mole of potassium carbonate originally present indicating complete reduction of the carbonate:

$$K_2CO_3 + 2\ C = 2\ 'KC' + 3CO \qquad 1)$$

where 'KC' represents the reduced form. The nature of this reduced form is not clearly known but one possibility is a complex involving K, C and possibly O. This unknown complex readily decomposes in the 700-800°C temperature range under reducing conditions and releases alkali metal vapor to the gas phase. The total amount of CO generated during this stage was the same whether the sample was heated at a moderate rate or in one rapid step directly from room temperature to 800°C. For the samples with an initial catalyst concentration high enough to saturate the surface, the rate of CO generation reached a maximum independent of the initial loading and remained constant until the

reduction was nearly complete at which time a normal first order decay profile was observed. In other words, by doubling the initial catalyst concentration, the time for complete catalyst reduction would also be doubled. This phenomenon suggests that the rate is limited by the available surface area.

To analyze the kinetics of catalyst loss by vaporization, the change in the potassium content of several samples undergoing heat treatment was determined both by direct analysis of the samples after quenching and by indirect determination by weight loss measurements. A typical overall temporal profile of catalyst loss when a sample impregnated with potassium carbonate is gradually heated to 800°C in a reducing atmosphere is shown in Figure 5. For comparison, a sample impregnated with potassium hydroxide is also given. The results indicate that a large fraction of the catalyst is lost in a narrow temperature range around 800°C, denoted by Stage III in Figure 2.

Many investigators have suggested that alkali metal catalyzed gasification involves a process where the catalyst continually undergoes an oxidation/reduction cycle (7,13). The catalyst, after first being reduced during the transient start-up period, is oxidized upon the introduction of CO_2 and produces a CO profile characterized by an overshoot. The oxidized form then interacts with the carbon surface to liberate another CO thus returning to the reduced form completing the cycle. Moulijn et al. (1,5) have described this process with a simple two step reaction sequence:

$$'KC' + CO_2 = 'KCO' + CO \qquad 2)$$
$$'KCO' + C = 'KC' + CO \qquad 3)$$

where 'KC' represents the reduced form and 'KCO' the oxidized form. A supporting observation for this type of mechanism is a slight weight gain which accompanies the CO overshoot at the onset of gasification due to the oxidation of the reduced form of the catalyst.

Regardless of the exact chemical form of the catalyst following Stage III, it seems that the formation of the reduced catalyst is a prerequisite for the observed rapid weight loss of catalyst around 800°C. In fact, the rapid weight loss does not seem to be directly related to the melting point of K_2CO_3 (891°C). Rather, it is due to the fact that at this temperature the catalyst is rapidly converted to its reduced form which is readily vaporized. This speculation is supported by the results obtained from samples impregnated with KOH. As shown in Figure 5, the KOH sample shows the same rapid loss of catalyst around 800°C even though KOH has a melting point of only 380°C.

In conclusion, the process of catalyst reduction appears to be an activated one which requires intimate contact with active sites so that for samples which are initially saturated with catalyst, the rate of reduction is limited by the available surface area. The amount of CO generated during this process indicates that the catalyst is completely reduced. Furthermore, catalyst loss kinetics suggest that the formation of a reduced form of the catalyst is a prerequisite for rapid vaporization and escape to the gas phase.

ACKNOWLEDGMENTS

This work was partially supported by the U.S. Department of Energy under grant DE-FG22-82PC50794. David A. Sams appreciates support from a Mining and Mineral Resources Research Institute Fellowship and a Sulzer Scholarship.

REFERENCES

1. Cerfontain, M.B. and Moulijn, J.A., 16th Biennial Mtg. of ACS, San Diego, CA. July, 1983.

2. Hamilton, R.T., Sams, D.A. and Shadman, F., Fuel, 63, (7) (1984).

3. Huhn, F., Klein, J. and Juntgen, H., Fuel, 62 (2) (1983).

4. Kapteijn, F., Jurriaans, J. and Moulijn, J.A., Fuel, 62, (2) (1983).

5. Kapteijn, F. and Moulijn, J.A., Fuel, 62 (2) (1983)

6. Kuhn, L. and Plogmann, H., Fuel, 62 (2) (1983).

7. McKee, D.W. and Chatterji, D., Carbon, 16, 53 (1978).

8. KcKee, D.W. and Chatterji, D., Carbon, 13, 381 (1975)

9. Mims, C.A. and Pabst, J.K., Am. Chem. Soc., Div. Fuel Chem., Preprints, 25 (3) 258 (1980).

10. Mims, C.A. and Pabst, J.K., Am. Chem. Soc., Div. Fuel Chem., Preprints, 25 (3) 263 (1980).

11. Sams, D.A. and Shadman, F., Fuel, 62 (8) (1983).

12. Talverdian, T., M.S. Thesis, University of Arizone, Dec. 1984.

13. Veraa, M.J. and Bell, A.T., Fuel, 57 (4) (1978).

14. Wigmans, T., Elfring, R. and Moulijn, J.A., Carbon, 21 (1) (1983).

15. Wigmans, T., Groebel, J.C. and Moulijn, J.A., Carbon, 21 (3) (1983).

16. Wigmans, T., Haringa, H. and Moulijn, J.A., Fuel, 63 (6) (1984).

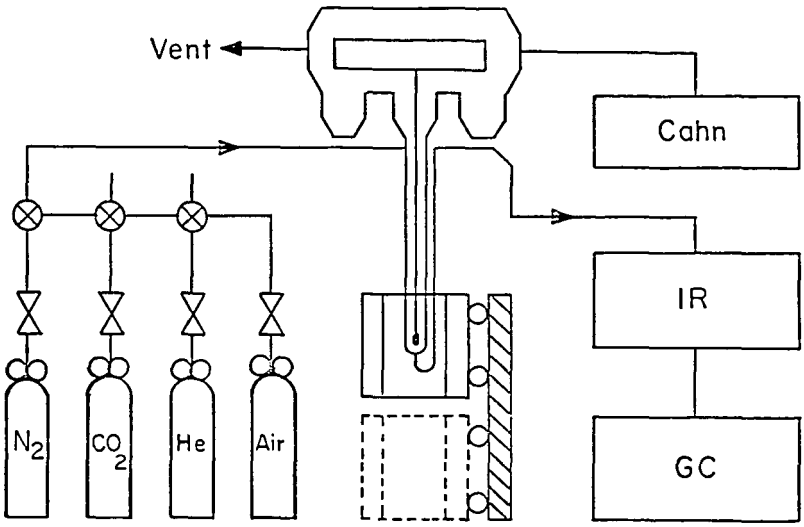

Figure 1. Schematic diagram of the Cahn microbalance system.

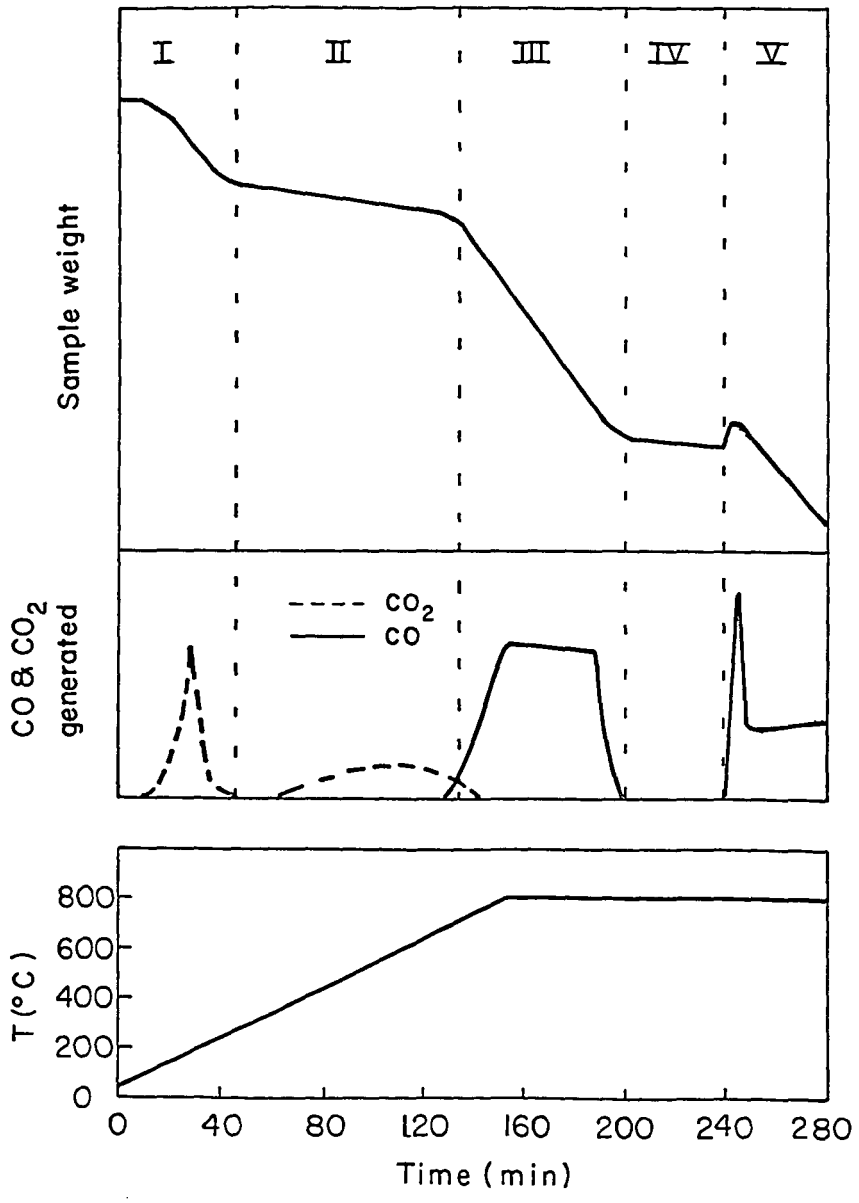

Figure 2. Characteristic stages during a typical TPR experiment.

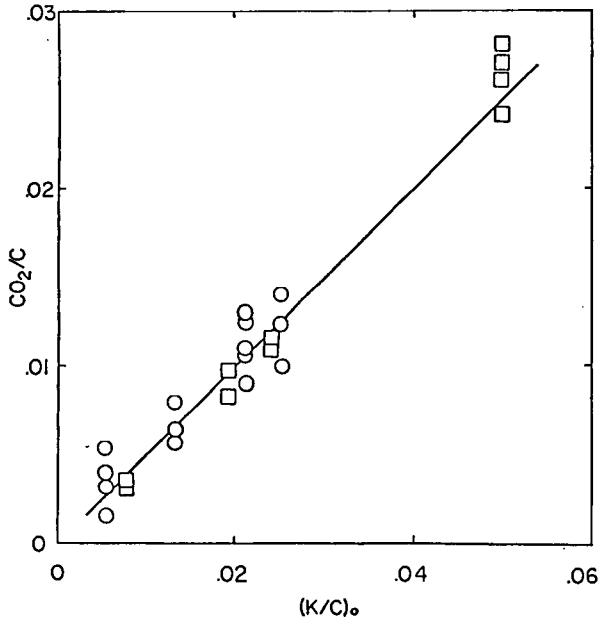

Figure 3. Dependence of low temperature CO_2 desorption on the initial catalyst loading; (○) K_2CO_3, (□) KOH.

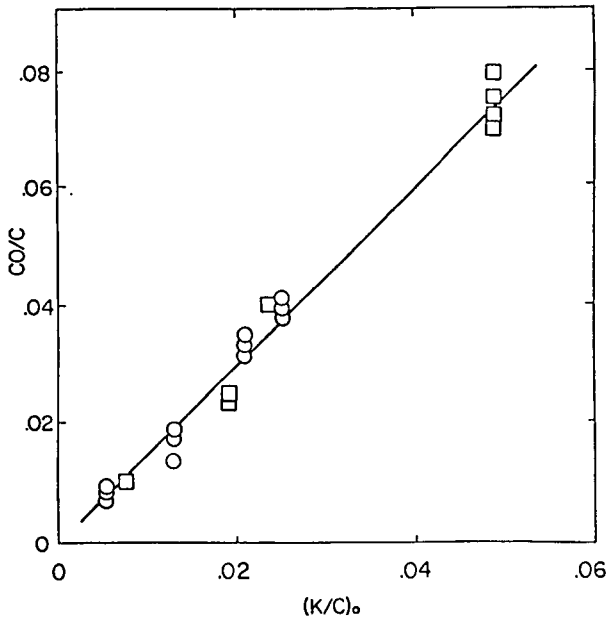

Figure 4. Dependence of high temperature CO generation on the initial catalyst loading; (○) K_2CO_3, (□) KOH.

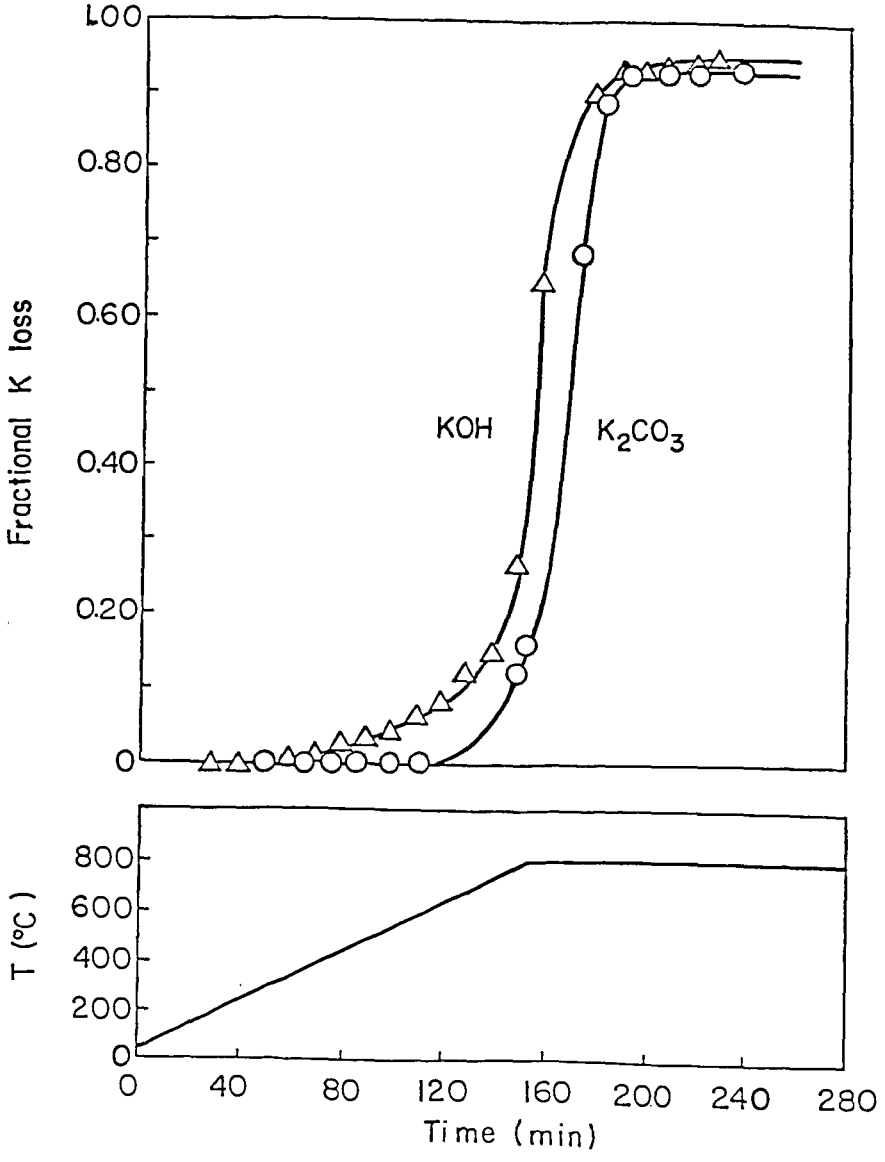

Figure 5. Catalyst loss profiles during a typical TPR experiment.

CHARACTERIZATION OF POTASSIUM CATALYSTS ADDED AS KOH TO CARBON SURFACES

Simon R. Kelemen
Howard Freund
Charles Mims

Exxon Research and Engineering Company
Corporate Research Science Laboratories
Clinton Township, Route 22 East
Annandale, New Jersey 08801

ABSTRACT

Potassium catalysts active toward gasification of carbon by H_2O and CO_2 can be generated by addition of KOH to carbon. We have characterized the controlled addition of KOH to the edge surface of graphite and the surface of a glassy carbon using AES, XPS and UPS. Submonolayer concentrations of potassium-oxygen surface species are formed from KOH on pre-oxidized edge graphite and glassy carbon surfaces which are stabilized to 800°C in vacuum. These surfaces have two O(1S) peak envelopes centered near 531 eV and 533 eV. The higher binding energy peak is characteristic of oxygen strongly bound to carbon. Heating to 950° C results in the loss of potassium and the lower binding energy oxygen peak associated with the potassium catalyst. In contrast the interaction of KOH with the atomically clean edge graphite surface does not produce the active potassium form. The initial oxygen content of the carbon surface is important in catalyst preparation from KOH.

INTRODUCTION

Additions of alkali metal salts to carbon are known to produce catalytic effects toward gasification by CO_2 or H_2O (1-7). KOH and K_2CO_3 are especially active precursors to catalytically active states on the carbon surface (8). The catalytic form can be prepared by heating a mixture of the sample and the salt in the reactive gaseous environment. In kinetic studies this is usually a temperature greater than the maximum in the range used for the kinetics. The potassium catalyst when in an active form is believed to be mobile on the carbon surface yet stable to vaporization under gasification conditions. The catalyst's stability is demonstrated by the retention of potassium following prolonged heating in an inert environment at the reaction temperature of 700°C subsequent to gasification (9). The active potassium form is found to be associated with surface bound oxygen based on akylation studies (9,10). A better understanding of potassium catalyzed carbon gasification will come from more knowledge of the details of the potassium complex and the carbon surface composition. For this reason the initial interaction of alkali salts such as KOH with well defined carbon substrates are of fundamental interest.

The importance of the oxygen content in relation to the catalytic gasification activity of KOH and K_2CO_3 toward various carbons has been recently emphasized (11,12). The clean oxygen free edge surface of graphite was studied under ultra high vacuum conditions in order to isolate the pure interaction of KOH with active carbon surface sites. The interaction of KOH films contaminated by exposure to H_2O or O_2 was studied on the "passive" basal

surface of graphite to determine the influence of direct KOH oxidant interaction in the absence of "active" carbon sites. In this way the chemistry of KOH with pre-oxidized carbon surfaces could be differentiated.

EXPERIMENTAL

Experiments were performed in a standard ultra-high vacuum spectroscopy chamber. A double-pass cylindrical mirror analyzer (Physical Electronics) was used for AES, XPS and UPS measurements. The details of the sample preparation and characterization of the oxygen-free edge surface of graphite and glassy carbon can be found in previous communications (13,14). Two different sample holders were used in the study. One was a standard UHV manipulator which could access a KOH evaporation source. The details of the KOH evaporation source used in the UHV studies appear elsewhere (15). The other holder was a Leybold Heraeus design which allowed rapid introduction of samples from atmospheric pressure to the UHV environment. The carbon samples were oxidized in O_2 at 300°C in an isolated high pressure preparation section. The oxidation kinetics by O_2 of the edge graphite surface and glassy carbon have been examined and conditions chosen which produced substantial amount of surface oxidation.

Nitric acid oxidation of the glassy carbon samples was accomplished by boiling the samples for 4 hours in HNO_3 under reflux conditions. KOH was added to carbon surfaces in laboratory air by physically contacting the carbon surface in air with a moist KOH pellet. This formed a liquid coating across the entire carbon surface. The procedure was accomplished within one minute and the sample was returned to the UHV environment by use of the rapid introduction sample holder.

RESULTS

I. KOH on Basal Graphite With H_2O and O_2

When KOH is used as the precursor in gasification catalysis it is usually added from solution or directly added in atmospheric conditions. Furthermore, the carbon surfaces with the salt precursor are exposed to the oxidizing reactant gaseous environment prior to reaction. These are potential sources for chemical modification of parent KOH. In order to examine the effect of direct KOH gas interactions we have performed model experiments on the basal plane of graphite. The basal surface of pyrolytic graphite contains a preponderance of "inactive" carbon sites and provides a suitable surface to examine direct KOH gas interactions. We have found that the surfaces of pure KOH films evaporated in-situ in the UHV chamber will rapidly take up oxygen from exposure to H_2O and O_2 at room temperature.

The KOH films exposed to H_2O and O_2 on the basal graphite surface had only slightly greater thermal stabilities toward desorption in UHV than those found for pure KOH films. The vapor pressure of pure KOH is substantial above 300°C. This is also true for surfaces with KOH added in atmosphere. Following KOH addition in air H_2O was the major gaseous species produced along with KOH upon heating in UHV. Clean basal graphite surfaces were recovered upon heating to 500°C in vacuum.

Addition of KOH to carbon in air will therefore always introduce oxygen containing gases into the system. Basal graphite surfaces which have been contacted by KOH in air have similar thermal stabilities to the H_2O and O_2 exposed pure KOH films. Although prolonged atmospheric exposure of KOH leads to the uptake of CO_2 and formation of potassium carbonate, our exposures to air were short. Potassium carbonate formation should show itself by increased thermal stabiliity of the potassium species since bulk potassium carbonate decomposes at much higher temperature. We could not find any evidence for appreciable carbonate formation.

II. KOH On Clean Edge Graphite

We have studied the interaction of KOH on the clean edge graphite surface to determine if stable potassium states are formed on an "active" carbon surface in the absence of oxygen. The potassium, oxygen and carbon AES signals were monitored as a function of coverage following KOH deposition on the oxygen free edge surface of graphite held at room temperature and following heating in vacuum. We wll report our AES results in the dN(E)/dE mode normalized to the carbon substrate signal which circumvents problems associated with absolute intensity calibrations. These results are shown in Figure 1 and are compared to the results obtained on the basal surface in a previous investigation (15).

The studies on the basal graphite surface established that a 1:1 O:K stoichiometry was maintained during room temperature deposition and subsequent heating in vacuum. On the basal suface of graphite an AES K/C ratio ~0.4 corresponded to a surface with a coverage of one KOH per eight carbon atoms. On this basis the present AES results for KOH on the edge surface indicate that a 1:1 O:K stoichiometry exists at multilayer as well as submonolayer coverages during the deposition near room temperature and after heating in ultra high vacuum to temperatures where the loss of potassium and oxygen occurs.

The coverage of KOH was monitored by AES following heating to a given temperature for 300 sec in UHV. The initial coverage corresponded to a K/C ratio near 2.0 and represents an amount in excess of a monolayer. The KOH coverage remains almost constant as the surface temperature neared 200°C. The potassium signal decreased between 200-500°C. Above 300°C the vapor pressure of KOH is substantial and this is one likely mode of multilayer loss at these temperatures. Submonolayer coverages of KOH persist in the range of 400°C. The presence of submonolayer concentrations of adsorbate at these higher temperatures is attributed to a stabilizing interaction with the carbon substrate. The same type of behavior was observed for pure KOH on the basal surface of grapite. KOH interacts with the oxygen free edge graphite surface in a manner which does not produce strongly bound potassium-oxygen surface complexes.

III. KOH on Oxidized Edge Graphite

We have determined the surface elemental composition and the thermal stability of the potassium containing species on the oxidized edge surface of graphite prepared by adding KOH external to the vacuum system in air. The edge surface of graphite was first oxidized in pure O_2 at 300°C near atmospheric pressure and then the KOH was added. This method of preparation of the

KOH overlayer has a dramatic effect on the thermal stability of the potassium complex. The single layer coverage range, AES K/C ~0.4, persists between 700-800°C. The potassium is ultimately lost at temperatures above 800°C. The stability of potassium is very different on the oxidized edge graphite surface. There are also major compositional changes in the KOH overlayer as well as in the carbon surface. Figure 1 shows the oxygen and potassium AES signals relative to the carbon substrate signal for the oxidized sample contacted with KOH. The solid lines in Figure 1 represent integral oxygen to potassium stoichiometric values as defined from the previous results. In the high coverage multilayer regime the KOH overlayer has between 2 and 3 times the oxyen content as the stoichiometric KOH compound. This is evidence that the KOH layers have taken up and retained substantial quantities of oxygen species from atmospheric gases, predominantly H_2O. Upon heating the sample in UHV the overlayer coverage decreases and the potassium content decreases. Figure 1 shows that as the potassium coverages decrease into a submonolayer regime, AES K/C ~0.4, there is a substantial amount of oxygen present as measured by AES several times the 1:1 stoichiometry. A good portion of this oxygen is associated with the carbon substrate. The carbon surface is heavily oxidized. This has a profound effect on the vacuum stability of the potassium species in the submonolayer coverage range. Oxygen appears to be associated with the species since there is a corresponding loss of a portion of the oxygen.

IV. KOH On Oxidized Glassy Carbon

The method of KOH addition to oxidized glassy carbon surface was the same as on the oxidized edge surface. This method of preparation was also used to add KOH to glassy carbon samples which were found to be catalytically active toward CO_2 carbon gasification (16).

We will compare the results for glassy carbon samples which were oxidized differently. One method was oxidation in O_2 at 300°C which was the same method previously used, the other was oxidation by HNO_3 and produced a surface which was oxidized to a greater extent. Figure 2 contains the results of the thermal stability experiments following heating for 300 sec in UHV at each temperature. In both cases a coverage greater than a monolayer was deposited and subsequently heated in UHV. The multilayer coverages were lost in the 500-600°C range on the O_2 oxidized substrate. This is similar to the results on the HNO_3 oxidized sample which are not shown. In both cases the potassium Auger signal persists to much higher temperatures. The potassium levels are approximately three times greater for the HNO_3 oxidized sample for the O_2 case at any given temperature. There are differences in the surface elemental composition of these samples. Figure 3 shows the oxygen and potassium AES signals relative to the carbon substrate signal for the two samples. The solid lines in Figure 3 represent integral oxygen to potassium stoichiometric values as defined from the previous results contained in Figure 1 based on 1:1 oxygen to potassium KOH stoichiometry. In the high coverage multilayer regime the KOH overlayer has between 2 and 3 times the oxygen content as the stoichiometric KOH compound independent of the method of glassy carbon preoxidation. This is again evidence that the KOH layers have taken up substantial quantities of oxygen containing gases from the air. Upon heating the sample in UHV the overlayer coverage decreases and the potassium content decreases. Figure 3 shows that as the potassium coverages decrease into a submonolayer regime, AES K/C ~0.4, there is a substantial amount of oxygen present which is greater than a 1:1 stoichiometry as measured by AES. We see

that as the amount of potassium decreases in the low coverage regime there is a corresponding loss of a fraction of the oxygen present. As in the case with the edge graphite substrate oxygen appears to be associated with the potassium species. In both glassy carbon samples the carbon surface remains heavily oxidized following the loss of potassium. The oxygen Auger signal for the HNO_3 oxidized sample is slightly more than double that of the sample oxidized in O_2. This reflects the different extents of initial oxidation. The vacuum stability of the potassium species is enhanced on the more oxidized surface. The degree of carbon surface oxidation is related to the stability of the potassium species generated from KOH.

We have used XPS in order to characterize the electronic structure of the oxidized glassy carbon surfaces after KOH addition and thermal treatment in vacuum. KOH was added to an HNO_3 oxidized glassy carbon sample. The O(1S) XPS spectra was recorded following 5 min heating to the temperature shown in Figure 4. As previously determined by AES the 500°C spectrum corresponds to multilayers of the potassium containing overlayer. The 500°C spectrum has a FWHM of 2.4 eV and a B.E. of 531.7 eV with respect to the Fermi level. This is close to the value reported for KOH (17). We know that the KOH overlayer contains more than the stoichiometric amount of oxygen yet we are unable to resolve different oxygen(1S) peaks. Upon heating to 800°C the overlayer concentration was decreased into the monolayer regime. The 800°C XPS spectrum shows a broad O(1S) signal, FWHM - 4.5 eV. There appears to be two O(1S) peak envelopes, one centered near 531 eV, the other at 533 eV. Heating to 950°C results in the loss of potassium. A O(1S) peak centered near 533 eV remains and this value is associated with oxygen strongly bound to glassy carbon. The 531 eV O(1S) peak occurs in the presence submonolayer concentrations of potassium. The work function of the different glassy carbon surfaces were determined from photoelectron spectroscopy. The clean glassy carbon surface had a work function of 4.2 eV. Oxidation by O_2 increases the work function to 4.4 eV and increases further on a heavily oxidized HNO_3 sample to a value of 4.5 eV. The oxidized glassy carbon surface with the potassium complex corresponding to the 800°C XPS spectrum showed a work function decrease to 3.6 eV. If these values are used to estimate binding energies of the oxygen (1S) peaks with respect to the vacuum level we find almost a three eV binding energy difference between the oxygen associated with the potassium species and oxygen bound to carbon. Lower binding energies of a given element are generally identified with more electropositive electronic environments. The carbon surface with the potassium complex therefore shows oxygen in two generally different electronic environments: one associated with potassium and in an electropositive environment; the other in a more electronegative environment which is typically observed on the potassium-free surface.

DISCUSSION

We have studied the interaction of KOH on clean graphite surfaces in order to isolate the pure interaction of KOH and carbon. AES results show that a constant 1:1 oxygen to potassium stoichiometry is maintained throughout deposition with the edge graphite surface held at 30°C independent of coverage as well as after heating in vacuum to produce submonolayer coverages. On the basal surface of graphite submonolayer coverages of KOH were thermally stable above the melting point of solid KOH where the KOH vapor pressure is substantial. Likewise the results on the edge surface show an increased stability

for the adsorbate a low concentation. Submonolayer concentrations of potassium species persist up to 500°C. Our results are consistent with the picture that KOH interacts reversibly with the edge surface of graphite. The adsorbate is stabilized with respect to solid KOH by the interaction with the carbon substrate. Pure KOH overlayers on the edge graphite surface do not form stable adsorption states above 500°C.

The interaction of H_2O and O_2 with a pure KOH overlayer on the basal surface of graphite emphasize direct salt gas interactions. The KOH surface was very active toward H_2O and O_2 at 30°C. Their presence does not directly lead to a significantly different interaction with the carbon surface. Essentially clean basal graphite surfaces are recovered upon heating in UHV to 500°C. The interaction of KOH with H_2O or O_2 on a passive basal graphite surface is not sufficient to produce potassium species which are stabilized with respect to vacuum at high temperatures.

The interaction of H_2O and KOH with the "passive" basal graphite surface or KOH alone on an "active" edge graphite surface does not generate potassium species which are stable above 500°C. Oxygen already bound to carbon is an important element in determining the formation of stable potassium species. Catalytic precursor alkali salts are generally added to carbons under oxidizing conditions of the gaseous environment or the carbon surface. The edge graphite and glassy carbon surfaces were preoxidized to introduced oxygen strongly bound to carbon. The interaction of KOH with these surface produces potassium containing overlayers with enhanced thermal stability. Only submonolayer concentration of a potassium complex remained above 700°C. The concentration of these species was increased with the extent of carbon preoxidation. The potassium form exists on a carbon surface that is heavily oxidized. The carbon surface with the potassium complex shows oxygen in two different electronic environments. One is associated with potassium is in an electropositive environment. The other is in a more electronegative environment which is typically observed on the potassium-free surface. We cannot distinguish from these results if potassium is bound to oxygen which is on the carbon surface from potassium which interacts with carbon and promotes the formation of oxygen in a more electropositive configuration bound to carbon. In the latter case this form of oxygen might exist on the carbon surface alone or promoted by materials other than potassium. Species where potassium binds to the surface through oxygen, C-O-K have been postulated to exist on catalyzed carbon surfaces (10,12,18). In the other interpretation potassium would be considered an adsorbate which interacts with an oxidized carbon site. In either case it is the initial oxidation of carbon which leads to their formation from KOH.

It is generally agreed that no single mechanism can be used to interpret all of the many different manifestations of catalytic carbon gasification. The oxygen transference mechanism has been widely used to explain alkali catalyzed carbon gasification (1,19). The action of the catalyst is to form intermediates in the oxidizing gaseous environment which decompose to oxidize carbon in the proximity. In doing this the catalyst returns to its original state and the action continues (20). Within the class of alkali gasification catalysts for the reaction of carbon with either H_2O or CO_2 and even for the single element potassium there are a variety of different intermediates postulated for the mechanism (21). Microscopic studies suggest that gasification activity may not be restricted to a single physical form as

catalytic gasification is observed for systems in the presence (22) and absence of discrete particles (23). The mechanisms and intermediates involved in alkali catalyzed carbon gasification by H_2O and CO_2 are still open issues.

We have found in the study of CO_2 and O_2 interaction with the edge surface of graphite and glassy carbon samples that the surface can possess considerable amounts of oxygen which is strongly bound and much less active for CO formation. The CO formation energy decreases as the total oxygen surface concentration increases (24). The efficiency for producing the needed high oxygen coverages from either CO_2 or H_2O is extremely low, $<10^{-14}$ (24). The surface potassium complex is thought to be the active center for gas dissociation whereby CO or H_2 is formed and oxygen transferred to the carbon surface. This increases the carbon surface oxygen concentration in the vicinity of the complex and thus we would expect this to lower the CO formation energy. The action of the catalyst would be to increase the local oxygen coverage in a carbon domain and thereby increase the number of domains having lower CO formation energetics. For glassy carbon these are in the 60-70 kcal/mole range (24). This mechanism would effectively increase the number of sites found in the uncatalyzed reaction.

REFERENCES

1. D. W. McKee, Chemistry & Physics of Carbon, 16 (1981) 1.
2. C. M. Tessi du Montay and C. R. Marechal Brit. Pat. 2548 (1867).
3. H. S. Taylor and H. A. Neville, J. Am. Chem. Soc., 43 (1921) 2055.
4. C. Kroger, Z. Angew Chem. 52 (1939) 129.
5. Wen-Yang Wen, Catal. Rev. Sci. Eng. 22 (1980).
6. H. Harker, "Proc. 4th Conf. on Carbon" Buffalo, NY 1959, Permagon Press, NY (1960) pp. 124-139.
7. F. J. Long and K. W. Sykes; J. Chem. Phys. 47 (1950) 361.
8. J. L. Johnson, Catalytic Rev. Sci. Eng. 14 (1976) 131.
9. C. A. Mims and J. K. Pabst, Fuel 62 (1983) 178.
10. C. A. Mims, K. D Rose, M. T. Melchior and J. K. Pabst, J. Am. Chem. Soc. 104 (1982) 6886.
11. S. Yokoyama, K. Miyahara, K. Tanaka, I. Takakwua and J. Tashior, Fuel 58 (1979) 510.
12. C. A. Mims, and J. K. Pabst, Am. Chem. Soc. Dev. Fuel Chem. Preprints 25(3) (1980) 258.
13. S. R. Kelemen and C. A. Mims, Surface Science 136 (1984) L35.
14. S. R. Kelemen, H. Freund and C. A. Mims J. Vac. Sci and Technol A(2) (1984) 987.
15. S. R. Kelemen and C. A. Mims, Surface Science 133 (1983) 71.
16. H. Freund, unpublished results.
17. K. Kishi and S. Ikeda, Bull. Chem. Soc. Japan 46 (1973) 342.
18. I. L. C. Freiks, H. M. H. van Wechem, J. C. M. Striver and R. Bouwman Fuel 60 (1981) 463.
19. B. Neumann, C. Kroger and E. Z. Fingas Anorg. Chem. 197 (1931) 321.
20. H. Amariglio and X. Duval Carbon 4 (1966) 423.
21. D. W. McKee Fuel 62 (1983) 170.
22. C. L. Spiro, D. W. McKee, P. G. Kosky, E. J. Lamby, Fuel 63 (1984) 686.
23. C. A. Mims, R. T. K. Baker, J. J. Chludzinski, and J. K. Pabst, Am. Chem. Soc. Div. Fuel Chem., Preprints 28(1) (1983), 71.
24. S. R. Kelemen and H. Freund, Carbon submitted.

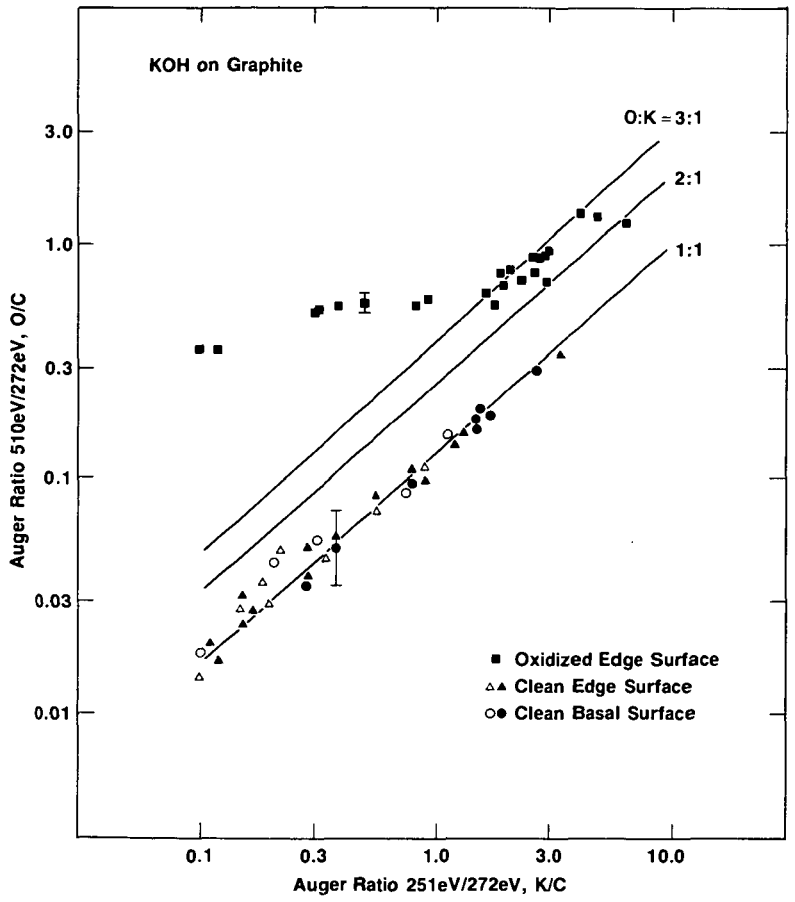

Figure 1: Solid triangles are obtained from the prism surface following KOH deposition at room temperature. Open triangles are a result of heating a KOH overlayer on the prism surface. Solid circles are obtained from the basal surface following KOH deposition at room temperature. Open circles are a result of heating the KOH overlayer on the basal surface. Solid squares are a result of heating KOH added to an oxidized edge graphite surface.

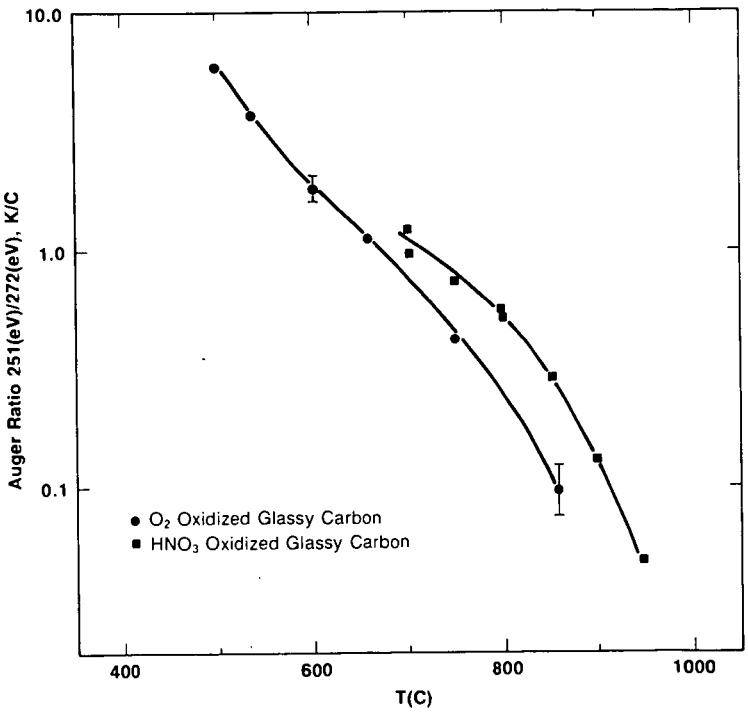

Figure 2: A comparison of the decrease in the K/C Auger ratio as a function of temperature after KOH addition to glassy carbon surfaces oxidized by O_2 at 300°C and by HNO_3.

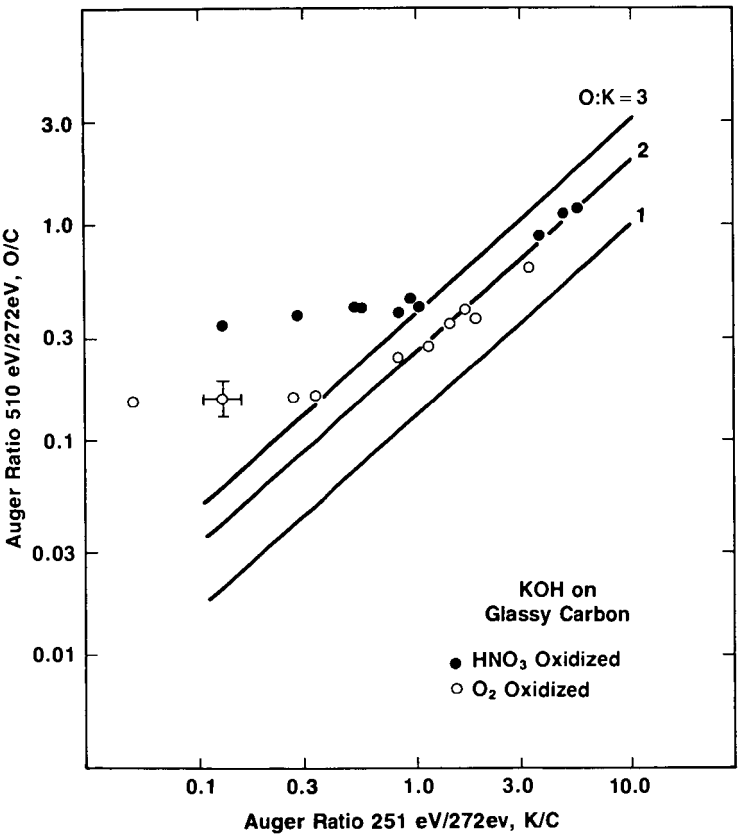

Figure 3: Change in the potassium and oxygen AES signals normalized to carbon following KOH addition to oxidized glassy carbon surfaces and subsequent heating in UHV.

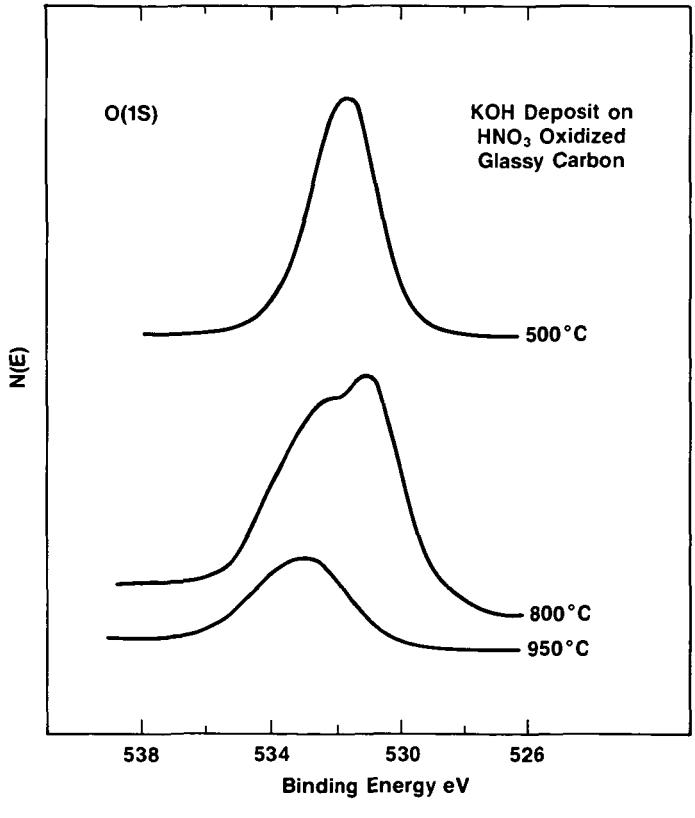

Figure 4: O(1S) XPS signal after KOH addition to a HNO_3 oxidized glassy carbon sample and heating for 300 sec in UHV at each temperature.